NACA

RESEARCH MEMORANDUM

EFFECT OF LEADING-EDGE HIGH-LIFT DEVICES AND SPLIT FLAPS

ON THE MAXIMUM-LIFT AND LATERAL CHARACTERISTICS OF A

RECTANGULAR WING OF ASPECT RATIO 3.4 WITH

CIRCULAR-ARC AIRFOIL SECTIONS AT REYNOLDS

NUMBERS FROM 2.9 × 10^6 TO 8.4 × 10^6

By

Roy H. Lange and Ralph W. May, Jr.

Langley Aeronautical Laboratory
Langley Field, Va.

CLASSIFICATION CANCELLED

NATIONAL ADVISORY COMMITTEE
FOR AERONAUTICS

WASHINGTON

November 10, 1948

UNCLASSIFIED

RESTRICTED

UNCLASSIFIED

NATIONAL ADVISORY COMMITTEE FOR AERONAUTICS

RESEARCH MEMORANDUM

EFFECT OF LEADING-EDGE HIGH-LIFT DEVICES AND SPLIT FLAPS

ON THE MAXIMUM-LIFT AND LATERAL CHARACTERISTICS OF A

RECTANGULAR WING OF ASPECT RATIO 3.4 WITH

CIRCULAR-ARC AIRFOIL SECTIONS AT REYNOLDS

NUMBERS FROM 2.9×10^6 TO 8.4×10^6

By Roy H. Lange and Ralph W. May, Jr.

SUMMARY

The results of an investigation at high Reynolds numbers and low
Mach numbers in the Langley full-scale tunnel to determine the effect
of leading-edge high-lift devices and split flaps on the maximum-lift
and lateral characteristics of a rectangular wing of aspect ratio 3.4
with circular-arc airfoil sections are presented in this report. The
investigation included measurements of the aerodynamic characteristics
in pitch and in yaw of the basic wing and of the wing with several
leading-edge high-lift devices and 0.20-chord split flaps deflected
alone and in combination with one another. Scale effects were investi-
gated at Reynolds numbers ranging from 2.9×10^6 to 8.4×10^6. In
addition to the force measurements, the stalling characteristics of the
wing were determined.

The maximum lift coefficient of the basic wing is 0.58. The
addition of half-span and full-span split flaps deflected 60° increases
this value to 1.00 and 1.24, respectively. The agreement between the
experimental values of the maximum lift coefficient and lift-curve slope
of the basic wing and the increments in lift coefficients due to flap
deflection and those calculated by the best available methods is good.
Maximum lift coefficients of 0.89, 1.20, and 1.21 are obtained for the
wing with the drooped-nose flap deflected 20°, with the extensible
leading-edge flap, and with the combination of drooped-nose flap deflected
10° with 0.032-chord round leading edge, respectively. These values were
increased to 1.26, 1.58, and 1.47, respectively, with the addition of
half-span split flaps deflected 60°. The drag of the wing is high
throughout the moderate to high angle-of-attack range. The addition of
split flaps causes a large drag increase; however, an appreciable
reduction in the drag in this range is obtained by deflecting either the
drooped-nose flap or by the installation of the extensible leading-edge
flap. The pitching-moment characteristics of the basic wing and of the
wing with the leading-edge high-lift devices giving highest maximum lift
indicate that below the stall the center-of-pressure location is slightly
forward of the quarter chord. A stable pitching-moment break is shown
at the stall for all configurations except those with the extensible

leading-edge flap and with the combination of the drooped-nose flap deflected 10° with the 0.032-chord round leading edge, which have marginal stability. In general, the addition of split flaps to all configurations causes a slightly rearward shift of the center-of-pressure location. For the basic wing the dihedral effect increases parabolically with lift coefficient and the directional stability increases essentially linearly with lift coefficient and the respective parameters attain values of 0.0023 per degree and -0.00050 per degree near maximum lift. Values of the side-force parameter are low. All the leading-edge high-lift devices investigated on this wing with circular-arc section produce almost linear dihedral-effect variations with lift coefficient, which is consistent with the characteristics of conventional blunt-nose airfoils and with theory; the directional stability and lateral-force characteristics are not materially affected. The split flaps decrease the dihedral effect of the basic wing at a given lift coefficient, but they generally do not materially affect the lateral characteristics of the wing when installed in combination with the leading-edge high-lift devices.

INTRODUCTION

In order to provide large-scale data on the high-angle-of-attack characteristics of wings having airfoil sections with sharp leading edges, an investigation is being conducted in the Langley full-scale tunnel at high Reynolds numbers and low Mach numbers of several typical transonic and supersonic swept and unswept wing plan forms having 10-percent-thick, circular-arc airfoil sections. One of the wings investigated was a trapezoidal wing of aspect ratio 4, and the maximum-lift and stalling characteristics have been reported in reference 1. The results of reference 1 show that the inherently low maximum lift and high drag of the wing were appreciably improved when a drooped-nose flap was deflected. Inasmuch as this type of high-lift device was found to be effective, a more complete study was made of several leading-edge high-lift devices as a part of a general investigation conducted on a rectangular wing of aspect ratio 3.4 with 10-percent-thick circular-arc airfoil sections. This wing is identical to the wing tested in reference 1 except that the tips were modified so as to form a rectangular plan form.

The investigation included measurements at high Reynolds numbers and low Mach numbers of the aerodynamic characteristics in pitch and in yaw of the basic wing and of the wing with several leading-edge high-lift devices and 0.20-chord split flaps deflected both alone and in combination with one another. The leading-edge high-lift devices investigated included a 0.20-chord drooped-nose flap, a 0.10-chord extensible leading-edge flap, and several simulated round leading edges. The scale effect on the aerodynamic characteristics was determined for a range of Reynolds numbers from about 2.9×10^6 to 8.4×10^6. In addition to the force measurements, the stalling characteristics of the wing with and without high-lift devices were determined by means of tuft observations.

COEFFICIENTS AND SYMBOLS

The test data are presented as standard NACA coefficients of forces and moments referred to the standard stability axes. The Y-axis is assumed to lie along the quarter-chord line of the wing and in the plane of the wing geometric chord lines.

C_L lift coefficient $\left(\dfrac{\text{Lift}}{qS}\right)$

C_D drag coefficient $\left(\dfrac{\text{Drag}}{qS}\right)$

C_m pitching-moment coefficient $\left(\dfrac{M}{qSc}\right)$

C_l rolling-moment coefficient $\left(\dfrac{L}{qSb}\right)$

C_n yawing-moment coefficient $\left(\dfrac{N}{qSb}\right)$

C_Y lateral-force coefficient $\left(\dfrac{Y}{qS}\right)$

$C_{L_{max}}$ maximum lift coefficient

c_l section lift coefficient

$c_{l_{max}}$ maximum section lift coefficient

P pressure coefficient $\left(\dfrac{p - p_0}{q}\right)$

P_{cr} critical pressure coefficient; pressure coefficient at a local Mach number of 1.00

R Reynolds number $\left(\dfrac{\rho V c}{\mu}\right)$

M_0 free-stream Mach number

M pitching moment

L rolling moment

N   yawing moment

Y   lateral force

α angle of attack, degrees

q   free-stream dynamic pressure

S   wing area (286.0 sq ft)

c   wing chord (9.23 ft)

b   wing span (31.29 ft)

V   free-stream velocity

ρ mass density of air

μ coefficient of viscosity

A   aspect ratio $\left(\dfrac{b^2}{S}\right)$

y   distance along semispan from plane of symmetry

λ taper ratio; ratio of tip chord to root chord

$\alpha_{C_{L_{max}}}$ angle of attack for maximum lift, degrees

p   local static pressure

p_o free-stream static pressure

δ_n drooped-nose-flap deflection, degrees

δ_f split-flap deflection, degrees

ψ angle of yaw, degrees

Subscripts:

ψ denotes partial derivative of a coefficient with respect to
           yaw in degrees $\left(\text{example:}\quad C_{l_\psi} = \dfrac{\partial C_l}{\partial \psi}\right)$

C_L denotes partial derivative of a coefficient with respect to C_L
           $\left(\text{example:}\quad C_{l_{\psi C_L}} = \dfrac{\partial C_{l_\psi}}{\partial C_L}\right)$

MODEL

The geometric characteristics of the wing and the arrangement of the high-lift devices are given in figures 1 and 2. Photographs of the wing mounted on the airfoil supports and on the yaw supports are given as figure 3. The airfoil section of the wing is the NACA 2S-(50)(05)-(50)(05), the ordinates of which may be found in reference 2. The wing-tip shape is one-half of a body of revolution of the airfoil section. The wing has no geometric dihedral or twist.

The wing construction consisted of a simple framework of $\frac{1}{4}$-inch steel channel spars covered with a $\frac{1}{4}$-inch skin of aluminum sheet rolled to the correct airfoil contour. The wing surfaces were about the equivalent in roughness to conventional thin dural sheet construction with dimpled skin and unfilled flush rivets. The wing construction was extremely rigid and it is believed that no deflections of an appreciable magnitude occurred during the tests. The 0.20c drooped-nose flap was pivoted on piano hinges mounted flush with the lower wing surface, and with the flap deflected the gap on the upper wing surface was sealed with a faired cover plate. Drooped-nose-flap deflections up to 40° could be obtained. The extensible leading-edge-flap configuration tested (see fig. 2) was selected from considerations of high maximum lift and was determined from the results of two-dimensional tests reported in reference 3. The extensible leading-edge flap had an area of 9.9 percent of the wing area measured in a plane along the angle of flap deflection. The round-leading-edge modifications consisted of cylinders attached to the under surface of the leading edge with diameters selected in the range of the nose diameter of a 0012 airfoil (0.032c). The split flaps were made of sheet metal attached to the wing under surface at a flap deflection of 60° measured as shown in figure 2. The half-span and full-span split flaps used in the zero-yaw tests were actually 48 and 97.5 percent of the wing span. When the wing was mounted on the yaw supports (see figs. 1 and 3(b)) a 12-inch cut-out in the split-flap center section was provided to give clearance for the sting.

TESTS

In order to determine the longitudinal and lateral characteristics of the wing, all the tests were made through an angle-of-attack range from about -2° through the stall in increments of 2° except near maximum lift, where 1° increments were used. The scale effect on the aerodynamic characteristics of the wing was determined from tests made at various tunnel airspeeds to give a Reynolds number range of from about 2.9×10^6 to 8.4×10^6. The highest Mach number obtained in the tests was 0.14, at a Reynolds number of 8.4×10^6.

The investigation of the maximum-lift characteristics of the wing made at 0° yaw included measurements of the lift, the drag, and the pitching moment of the basic wing and of the wing with several leading-edge high-lift devices and 0.20c split flaps deflected. The various high-lift devices were tested both alone and in combination with one another. Tests were made with the drooped-nose flap deflected from 10° to 40° in 10° increments except in the region of $\delta_n = 20°$, where 5° increments were used inasmuch as this deflection appeared optimum for maximum lift in the tests reported in reference 1. The tests of the wing with the round leading edges installed were made with the nose drooped through a range of δ_n from 10° to 20°. In addition, the 0.032c round–leading-edge installation was tested without the nose drooped. The scale effect was investigated for all configurations except those with the basic sharp leading edge, which were tested at a Reynolds number of about 4.1×10^6 inasmuch as the results of reference 1 showed no appreciable scale effect on the lift, the drag, and the pitching-moment coefficients in the Reynolds number range from about 3.27×10^6 to 7.67×10^6. Due to structural limitation, the extensible leading-edge flap could not be tested at a tunnel airspeed higher than that corresponding to a Reynolds number of about 5.90×10^6.

The stalling characteristics were determined by observing the action of wool tufts attached to the upper wing surface. These tuft studies were made of the basic wing and of the wing with the more effective high-lift arrangements. The tuft studies were made at a Reynolds number of about 4.1×10^6 for the wing with the sharp leading edge and at about 4.1×10^6 and 6.0×10^6 for the round–leading-edge configurations.

Surface static-pressure measurements were made at several chordwise points along the upper surface of the nose at the wing center line for the configuration with the drooped-nose flap deflected 10° with the 0.032c round leading edge and half-span split flap installed. These measurements were made at the angle of attack for maximum lift at a Reynolds number of about 7.2×10^6.

The investigation in yaw included measurements of the lift, lateral force, rolling moment, and yawing moment of eight configurations at approximately 6° increments of yaw through a range of from approximately -6° to 18°. The configurations tested in yaw were the basic wing and the wing with half-span and full-span split flaps installed. Also tested were the more promising high-lift arrangements involving the drooped-nose flap, the 0.032c round leading edge, and the extensible leading-edge flap. The basic wing and the wing with the split flaps installed were tested throughout the complete yaw range, whereas the other configurations were investigated only from about -6° to 6° yaw angles, which was considered a sufficient range of yaw to obtain the stability parameters.

RESULTS AND DISCUSSION

The results have been corrected for the stream alinement, the blocking effects, the jet-boundary effects, and the tares caused by the wing supports.

The discussion of the test results is grouped into two main sections. The first section presents the results of tests made to determine the maximum-lift and stalling characteristics of the wing and the second section gives the lateral characteristics as determined from the tests in yaw. The data are presented for a Reynolds number of about 4.1×10^6 except where noted.

MAXIMUM-LIFT AND STALLING CHARACTERISTICS

The figures covering the maximum-lift results are outlined below to facilitate the discussion of the results. The results for the basic wing and the wing with split flaps installed are given in figure 4. The determination of the calculated C_L at which stalling begins for the basic wing is given in figure 5. The effects of the leading-edge high-lift devices on the aerodynamic characteristics are presented in figures 6 to 13. The stalling characteristics of the basic wing and of the wing with the leading-edge high-lift devices are shown in tuft diagrams of figure 14 and are discussed in each of the subsections of the results and discussion. The results of tests of the wing with several leading-edge high-lift devices deflected in combination with split flaps are presented in figures 15 to 20. The stalling characteristics of the wing with the combined deflections of the high-lift devices are presented in figure 21. For convenience, a summary of the variation of maximum lift coefficient with Reynolds number for the more pertinent configurations is presented in figure 22. The power-off landing-approach speed characteristics of the wing are given in figure 23, which shows lines of constant gliding speed and constant sinking speed for a wing loading of 40 pounds per square foot superimposed on the lift-drag polars of several wing-flap configurations. The critical compressibility speed of the wing with the 0.032c round leading edge installed, with the drooped-nose flap deflected 10°, and with half-span split flaps installed is given in figure 24.

Basic Wing

Force measurements.- The maximum lift coefficient of the basic wing is 0.58 at an angle of attack of 15.9° (fig. 4). This value of maximum lift coefficient is 0.09 lower than that obtained in two-dimensional tests

of the airfoil section (reference 2). The influence of the low aspect
ratio can be seen in the shape of the lift curve which is nonlinear and
has a well-rounded peak. The lift-curve slope (measured at $C_L = 0.2$ to
avoid the slight discontinuity at lower lift coefficients). is about 0.050
per degree. Although this value of lift-curve slope is lower than the
value of 0.061 calculated by the methods of reference 4 based on a section
lift-curve slope of 0.090, it is in good agreement with the value of
0.053 calculated by the methods of reference 5.

An estimation of the maximum lift coefficient of the wing was
made based on the methods outlined in reference 4. The lift coefficient
at which each section along the semispan stalls was obtained from the
two-dimensional data of reference 2 and is shown by the dashed curve
in figure 5. The curves of the span-lift distribution for three values
of wing C_L were determined by the methods of reference 4. As soon as
the span-lift-distribution curve becomes tangent to the stalling $c_{l_{max}}$
curve, the section at that point reaches its maximum lift coefficient
and stalling should soon spread over a considerable part of the wing.
The stalling C_L obtained by this method is usually within a few percent
of the measured $C_{L_{max}}$. As shown in figure 5, the calculated stalling C_L
is 0.549. Inasmuch as the measured value of $C_{L_{max}}$ is 0.58, the agreement
between the measured and calculated values is considered good, and thus
the method in this case appears to be applicable to low-aspect-ratio,
rectangular wings having airfoil sections with sharp leading edges.

The variation of the pitching-moment coefficient with lift coefficient
indicates a slightly forward location of the center of pressure with
respect to the quarter chord up to about $C_L = 0.45$ above which the
center of pressure moves rearward with increase in lift coefficient showing
a large degree of longitudinal stability through the stall. The drag
coefficient of the wing is high at the moderate and high angles of attack
as compared with the drag of wings with conventional, round-nose airfoil
sections.

Stalling characteristics.- Tuft studies of the basic wing (fig. 14(a))
show early separation at the leading edge of the wing center section
which spreads rapidly toward the tips up to an angle of attack of about 6°.
At this angle of attack the flow over the wing resembles the flow over the
airfoil section in two-dimensional flow where a bubble of separation at
the nose of the airfoil followed by smooth flow has been observed at low
angles of attack (reference 6). With further increases in the angle of
attack the wing exhibits the usual flow characteristics of a rectangular

wing inasmuch as the center section stalls first and the stalled area
spreads toward the tips. This stall progression results from the higher
effective angle of attack of the root sections caused by the induced flow.

Effect of Split-Flap Deflection

Maximum lift coefficients of 1.00 and 1.24, respectively, are
obtained for the wing with the half-span and full-span split flaps
deflected 60°. These values of lift coefficient are 0.42 and 0.66 higher
than those obtained for the basic wing (fig. 4). Calculations were made
using the methods of reference 7 and the two-dimensional section data of
reference 2 to determine the increments in lift coefficient due to split-
flap deflection. The measured and calculated values are in good agree-
ment, thus indicating that the sharp leading-edge wing is affected by the
simple high-lift devices in the same manner as conventional wings.

The pitching-moment curves show the usual change in trim with flap
deflection and show a center-of-pressure location below the stall slightly
to the rear of that obtained for the basic wing. The variations of the
pitching-moment coefficient with lift coefficient indicate a slightly
forward center-of-pressure location with respect to the quarter chord up
to lift coefficients of 0.75 and 1.05 for half-span and full-span split
flaps, respectively, beyond which the center of pressure moves rearward
with increasing lift coefficient and produces a stable break at the stall.
Tuft studies of the wing with half-span split flaps installed (fig. 21(a))
show the early leading-edge stalling and other characteristics that are
typical of the basic wing. (See fig. 14(a).)

An evaluation of the lift and drag coefficients of the wing in terms
of power-off landing-approach characteristics is made possible by use of
figure 23. The increase in lift due to half-span split-flap deflection
is shown here to be in part, at least, offset by a large increase in drag
with the result that the sinking speeds considerably exceed the criterion
set forth in reference 8 that a sinking speed should not exceed 25 feet
per second at about $0.85C_{L_{max}}$. (See fig. 23(b).)

Effect of Leading-Edge High-Lift Devices

Drooped-nose flap.- The maximum lift coefficient of the wing with
the drooped-nose flap deflected 20° is 0.89. (See fig. 6.) This value
is 0.31 higher than that obtained for the basic wing. Although a maxi-
mum lift coefficient of 0.92 is obtained with the drooped-nose flap
deflected 25°, it is obtained at a higher angle of attack and with consid-
erably more drag than for the case with $\delta_n = 20^\circ$. (See figs. 6 and 17.)

The increases in maximum lift coefficient and angle of attack for maximum

lift with the drooped-nose flap deflected result primarily from the
improved flow conditions at the leading edge by more nearly alining the
wing contour with the air stream and thereby delaying stall to higher
angles of attack. This alinement of the leading edge tends to alleviate
the negative pressure peaks and thereby to decrease the adverse pressure
gradient that causes leading-edge separation. Although the leading-edge
separation has not been eliminated with the drooped-nose flap deflected
20°, as shown in the tuft studies (see fig. 14(b)), the initial separation
has been delayed to a considerably higher angle of attack than that for
the basic wing. (See fig. 14(a).) It is interesting to note that the
optimum drooped-nose-flap deflection for maximum lift found in these
tests is lower than the value found in the two-dimensional tests of the
section (reference 2).

Deflecting the drooped-nose flap causes an appreciable reduction in
the drag of the wing at the moderate and high angles of attack. This
reduction in drag increases with increasing drooped-nose-flap deflection
up to $\delta_n = 25°$. At the low angles of attack the drooped-nose flap has
the effect of a spoiler causing an increase in drag with flap deflection
as compared with the basic wing. The beneficial effect of drooped-nose-
flap deflection on the drag at high lift coefficients results in lower
sinking speeds as shown in figure 23(a); however, the gliding speed of
about 145 miles per hour to obtain a sinking speed of 25 feet per second
is above the range of present practice. It should be realized that the
drag coefficients plotted in figure 23 are for the wing alone and, there-
fore, the sinking speeds of the complete airplane would be somewhat
greater. Power could be used for the landing approach and landing condi-
tions to offset the high drags shown in figure 23, but this practice could
lead to dangerous conditions for emergency landings with power off.

The pitching-moment curves show no significant change in the longi-
tudinal stability of the wing as compared with the basic wing (fig. 6).
A smaller change in trim due to drooped-nose-flap deflection is noted
than was measured with the split flaps deflected. (See fig. 4.)

Extensible leading-edge flap.- The maximum lift coefficient of the
wing with the extensible leading-edge flap installed is 1.20 at a Reynolds
number of about 5.90×10^6. (See fig. 7(a).) This value of maximum lift
coefficient is 0.62 higher than that obtained for the basic wing. The
increase is due not only to a delay of the stalling to higher angles of
attack as compared with the basic wing but also to an increase in wing
area which has not been taken into account in the calculation of the wing
coefficients. The delay in the stalling to higher angles of attack with
the extensible leading-edge flap installed is attributed mainly to the
favorable effects of the round leading edge rather than to the effect of
leading-edge-flap deflection. The section data (reference 2) show that
the increase in maximum lift coefficient over that for the basic wing due
to a 0.10c extensible leading-edge flap with sharp leading edges is only
about one-half the magnitude of that obtained with the drooped-nose flap
deflected. The higher slopes of the lift curves are primarily due to the

fact that the lift coefficients are based on the area of the original wing. The sharp peaks of the lift curves are considered undesirable inasmuch as a slight asymmetry near the stall may lead to serious rolling instability.

The maximum lift coefficient increases with increasing Reynolds number for the range of Reynolds numbers investigated. (See figs. 7(a) and 22(a).) Tuft studies of the wing (fig. 14(e)) show early separation over the nose flap, but as compared with the wing with $\delta_n = 20^{\circ}$ (fig. 14(b)) the root stalling at the wing trailing edge has been delayed to higher angles of attack and covers a smaller area of the wing near maximum lift.

The extensible leading-edge flap causes a considerable reduction in drag of the wing at the higher angles of attack as compared with the basic wing or the wing with $\delta_n = 20^{\circ}$. As shown in figure 23(a), the gliding speed required to maintain a sinking speed of 25 feet per second is reduced from 145 miles per hour to about 117 miles per hour.

The variations of the pitching-moment coefficient with lift coefficient (fig. 7(b)) show a center-of-pressure location which is slightly ahead of that for both the basic wing and the wing with $\delta_n = 20^{\circ}$ throughout the lift-coefficient range. The stability at the stall is not appreciably affected by increasing Reynolds number.

Round leading-edge modifications.- The highest maximum lift coefficients obtained in the tests of the wing with the drooped-nose flap deflected and with round leading edges installed are 1.21 for $\delta_n = 10^{\circ}$ with the 0.032c round leading edge and 1.22 for $\delta_n = 15^{\circ}$ with the 0.040c round leading edge. (See figs. 9(a) and 11(b).) The results with $\delta_n = 10^{\circ}$ and 15° and with the 0.032c and 0.040c round leading edges installed show considerable scale effect on $C_{L_{max}}$ and $\alpha_{C_{L_{max}}}$, although this scale effect on $C_{L_{max}}$ decreases with increasing drooped-nose-flap deflection (fig. 12). As shown in figure 22(a), the value of the maximum lift coefficient for the $\delta_n = 10^{\circ}$, 0.032c configuration is the same as that obtained for the extensible leading-edge-flap installation. It should also be noted that this value of maximum lift coefficient is obtained with no increase in wing area, as is the case with the extensible leading-edge flap. A comparison of the $\delta_n = 10^{\circ}$, 0.032c configuration with the $\delta_n = 15^{\circ}$, 0.040c configuration shows no apparent superiority of one over the other inasmuch as the maximum lift coefficients and the drag coefficients at high angles of attack are essentially the same; however, the $\delta_n = 10^{\circ}$, 0.032c configuration is chosen because of the practicability of the smaller diameter round leading-edge and the lower drooped-nose flap deflection.

The tuft studies of the wing with the $\delta_n = 10^\circ$, 0,032c round-leading-edge configuration at a Reynolds number of about 4.1×10^6 (fig. 14(d)) show a stall progression which resembles that obtained for the wing with $\delta_n = 20^\circ$ (fig. 14(b)) except that the initial leading-edge separation is confined to a region at about $0.5 \frac{b}{2}$ and that a smaller area of the wing is stalled in the region of $C_{L_{max}}$. The tuft studies at a Reynolds number of about 6.0×10^6 show no change in the stall progression and consequently are not presented.

Inspection of the gliding-speed and sinking-speed chart (fig. 23(a)) shows slightly lower drag coefficients in the moderate and high lift-coefficient range for the $\delta_n = 10^\circ$, 0.032c round-leading-edge configuration than for the extensible leading-edge flap; however, in the region of $C_{L_{max}}$ the gliding speed required to maintain a sinking speed of 25 feet per second is about the same (115 miles per hour) as for the extensible leading-edge flap.

As in the case of the extensible leading-edge flap the variations of the pitching-moment coefficient with lift coefficient indicate a center-of-pressure location which is slightly ahead of that for the basic wing and the wing with $\delta_n = 20^\circ$ throughout the lift-coefficient range for Reynolds numbers of 2.99×10^6 and 4.3×10^6 and for lift coefficients up to 0.60 for higher Reynolds numbers (fig. 9(b)). For the higher Reynolds numbers, the center-of-pressure location is moved rearward to a point slightly ahead of the quarter chord for lift coefficients greater than 0.60. In general, the break in the pitching-moment curves at the stall was in a stable direction throughout the range of Reynolds numbers investigated.

The results of tests made with the 0.032c round leading-edge installed and with the drooped-nose flap neutral (see figs. 13(a) and 22(a)) show an appreciable scale effect on the maximum lift coefficient but the values of maximum lift coefficient are considerably lower than those obtained for the combination with the drooped-nose flap deflected 10°. The maximum lift coefficient of 0.88 obtained at a Reynolds number of approximately 7.0×10^6 is slightly lower than that obtained with the round leading edge removed and the drooped-nose flap deflected 20° (fig. 22(a)). The tuft studies (fig. 14(c)) show that the initial leading-edge stalling is delayed to higher angles of attack as compared with the basic wing (fig. 14(a)) and that the stall progression is about the same as that for the basic wing except for the rough flow along the trailing edge at the moderate angles of attack. The pitching-moment curves (fig. 13(b)) indicate the same static longitudinal instability as that for the basic wing at Reynolds numbers up to 4.28×10^6, but above this Reynolds number the stability is somewhat reduced.

EFFECT OF LEADING-EDGE DEVICES IN COMBINATION WITH SPLIT FLAPS

Force Measurements and Stalling Characteristics

Drooped-nose flap.- The wing with the drooped-nose flap deflected in combination with half-span and full-span split flaps gives $C_{L_{max}}$ values of 1.26 and 1.48 at angles of attack of 17.8° and 17.0°, respectively. (See figs. 15(a), 16(a), and 17.) These highest $C_{L_{max}}$ values occur with a nose deflection of 30°, which will hereinafter be discussed as the optimum deflection for the combination, instead of 20° as for the drooped-nose-alone configuration. These $C_{L_{max}}$ values at the optimum deflection are 0.26 and 0.24 higher, respectively, for the half-span and full-span split-flap configurations with the basic leading edge (sharp leading edge with $\delta_n = 0°$). Deflecting the drooped-nose flap 30° produces pitching-moment characteristics which are decidedly different than for the half-span and full-span split-flap-alone configurations in that rearward center-of-pressure positions with respect to the quarter chord are indicated up to lift coefficients of about 0.70 and 1.05, respectively, beyond which the center of pressure moves forward giving instability at the stall (figs. 15(b) and 16(b)). Tuft studies (figs. 21(a) and 21(b)) show that drooping the nose with the half-span split flap installed delays the trailing-edge separation until $C_{L_{max}}$ is reached and also reduces the area of separation over the center section. Deflecting the the drooped-nose flap in conjunction with the split flap affects the drag in about the same manner as previously noted for the drooped-nose-alone configuration. However, as shown in the gliding and sinking-speed chart of figure 23(b), the high drag coefficients developed by the $\delta_n = 30°$, half-span split-flap configuration results in a minimum sinking speed of about 34 feet per second, which is probably prohibitive according to present landing techniques.

Extensible leading-edge flap.- At a Reynolds number of about 4.1×10^6 the extensible leading-edge flap in combination with half-span and full-span split flaps gives $C_{L_{max}}$ values of 1.58 and 1.71 (fig. 18), which are 0.58 and 0.47 greater, respectively, than those shown for the split-flap installations alone. Practically no scale effect on maximum lift is indicated for the half-span and full-span split-flap combinations. The pitching-moment characteristics are practically the same for both split-flap combinations as for the extensible leading-edge nose flap, alone in that the center of pressure remains at a constant forward position with reference to the quarter-chord line throughout the lift-coefficient range until the stall, where it moves rearward giving marginal stability. The addition of the half-span split flap to the wing with the extensible leading-edge flap produces higher negative pressures over the rear of the wing and thereby provides a more favorable pressure gradient which tends

to eliminate the separation behind the leading edge (fig. 21(d)) that is
inherent in all the other configurations tested. The drag characteristics
of the split-flap combinations are essentially the same as for the case
with the extensible leading-edge flap alone except that the absolute values
of drag coefficient are higher. As shown in figure 23(b), the half-span
split flap and the extensible leading-edge-flap combination has a high
minimum sinking speed of 32 feet per second at $0.85C_{L_{max}}$.

The 0.032c round leading edge with $\delta_n = 10°$.- For the combination
having the drooped nose deflected 10°, the 0.032c round leading edge,
and the half-span split flap installed, the maximum lift coefficient
increases abruptly between Reynolds numbers of 4.0×10^6 and 5.8×10^6
(see figs. 19(a) and 22(b)) and attains its highest value of 1.47 at a
Reynolds number of 8.0×10^6. This value of $C_{L_{max}}$ is 0.26 above that
for the configuration without the split flap, but 0.11 below that for the
extensible leading-edge flap in combination with only the half-span split
flap. The effect on the pitching-moment characteristics of adding the
half-span split flap (fig. 19(b)) is to give slightly more stability below
the stall but considerably less stability at $C_{L_{max}}$ than for the $\delta_n = 10°$
round-leading-edge configuration. The destabilizing effect at high lift
coefficients becomes more pronounced with increases in Reynolds number so
that at a Reynolds number of 8.0×10^6 the wing is unstable at stall. The
tuft studies of figure 21(c) (taken at a Reynolds number of about 4.1×10^6
where the pitching-moment break is stable at the stall) show that the split
flap reduces the trailing-edge separation that occurred for the wing with
the split flap removed (fig. 14(d)). As for the other combination config-
urations already discussed, the half-span split flap increases the drag of
the $\delta_n = 10°$, 0.032c round leading-edge condition so that a minimum
sinking speed of 31 feet per second is obtained at a gliding speed of
113 miles per hour (fig. 23(b)).

The 0.032c round leading edge with $\delta_n = 0$.- With the 0.032c round-
leading-edge configuration with half-span split flaps installed, a $C_{L_{max}}$
of 1.25 is obtained (fig. 20). This value of $C_{L_{max}}$ is 0.37 higher than
that for the round leading edge alone but is slightly lower than that for
the drooped-nose, half-span, split-flap configuration. The scale effect
on maximum lift is similar to that for the other round-leading-edge config-
urations previously discussed (see fig. 22) in that a marked increase in
$C_{L_{max}}$ occurs between Reynolds numbers of 4.2×10^6 and 6.2×10^6. Gener-
ally marginal stability is shown at low and moderate lift coefficients and
the stabilizing trend at high lift coefficients occurs at increasing
values of C_L as the Reynolds number is increased.

Leading-Edge Pressure Measurements

The maximum observed negative pressure coefficient for the config-
uration of $\delta_n = 10^o$ with the 0.032c round leading edge and the half-
span split flap installed was -3.69 with the wing at $C_{L_{max}}$ and at a
Reynolds number of 7.2×10^6 and a Mach number of 0.11. This pressure
coefficient, when extrapolated by the Glauert-Prandtl method, corresponds
to a critical Mach number of 0.37 (fig. 24) which is much greater than
the free-stream Mach number that would be attained in flight with flaps
deflected.

LATERAL CHARACTERISTICS

The lateral characteristics of this rectangular wing with and with-
out high-lift devices are presented as variations of C_l, C_n, and C_Y
with angle of yaw in figures 25 to 30. From these basic data the static-
lateral-stability parameters C_{l_ψ}, C_{n_ψ}, and C_{Y_ψ} are determined as a
function of C_L and are presented in figures 31 to 34. The 12-inch cut-
out in the split flaps and the rear support sting used in the yaw tests
are believed to have no first-order effects on the lateral characteristics.

Basic Leading Edge

The lift-curve slope of the basic wing is not affected materially
by yaw. Figure 25 shows an average value of lift-curve slope (measured
at $C_L = 0.2$ to avoid discontinuities at lower lift coefficients) of
about 0.051 for all yaw angles investigated. The maximum lift coef-
ficient is increased, however, from 0.56 to 0.61 as the wing is yawed
from 0° to 18.25^o.

The dihedral-effect parameter C_{l_ψ} of the basic wing increases
parabolically with lift coefficient from 0.0002 at low values of C_L
to 0.0023 at $0.95C_{L_{max}}$ (fig. 31). This variation, which is unlike
the generally linear variation shown in references 9 and 10 for wings
with conventional round-leading-edge airfoils, can probably be attributed
to the sharp leading edge of the circular-arc airfoil section inasmuch as
swept wings with conventional airfoil sections have been found to have
decidedly different dihedral-effect characteristics than geometrically
identical wings with circular-arc sections. Data from tests of a trape-
zoidal wing with the same cross section as the rectangular wing of the
present tests (reference 11) show the same general variation of C_{l_ψ}
with C_L although the C_{l_ψ} values are somewhat lower because of the

higher aspect ratio of the trapezoidal wing. Weissinger derives in reference 12 a theoretical formula for determining dihedral effect in the low and moderate lift-coefficient range which, corrected to apply to the total wing span, is

$$57.3 C_{l_{\psi C_L}} = \frac{K}{A} \left[\frac{\lambda + 0.29(1 - \lambda)}{\lambda + 1} \right] - 0.10$$

where K is an empirical constant. This relation predicts a uniform slope and consequently does not agree with the test results.

The basic wing possesses a small amount of directional stability with $C_{n_{\psi}}$ increasing linearly with C_L up to the stall and breaking more stable near the stall to give a $C_{n_{\psi}}$ value of -0.00050 at $0.95 C_{L_{max}}$. The side-force parameter $C_{Y_{\psi}}$ is small and increases uniformly from 0 at low lift coefficients to -0.0010 at $0.95 C_{L_{max}}$. As shown in the basic data of figure 26(a), the $C_{n_{\psi}}$ and $C_{Y_{\psi}}$ slopes at zero yaw generally hold throughout the yaw range investigated, whereas $C_{l_{\psi}}$ decreases negatively at the highest positive yaw angles tested.

Deflecting the half-span split flap 60° reduces the dihedral effect and produces a more nearly linear variation with lift coefficient (fig. 31). The directional stability and lateral-force characteristics are essentially unaltered by the half-span split-flap deflection. The $C_{l_{\psi}}$, $C_{n_{\psi}}$, and $C_{Y_{\psi}}$ slopes measured at zero yaw are generally consistent throughout the yaw range investigated. (See fig. 26(b).)

Deflection of the full-span split flap produces practically a linear dihedral-effect variation which gives a $C_{l_{\psi}}$ value of 0.0019 at $C_{L_{max}}$ (fig. 31). The directional stability is greater than for the basic wing $\left(C_{n_{\psi}} = -0.0011 \text{ at } C_{L_{max}} \right)$, but the $C_{Y_{\psi}}$ characteristics are practically the same.

Drooped-Nose Flap

The effect of deflecting the 0.20c drooped-nose flap 20° is to produce a $C_{l_{\psi C_L}}$ slope that is almost linear throughout the C_L range, except near the stall where a strong positive break occurs (fig. 32(a)). A $C_{l_{\psi}}$ of 0.0040 is obtained at the stall. This variation is similar to that given in references 9 and 10 for similar wings with conventional round-leading-edge airfoils and probably results from the pressure distribution over the forward part of the biconvex airfoil being more like that

for conventional airfoils. The same effect was noted in reference 11 when a drooped-nose flap was deflected on a similar wing with trapezoidal plan form and circular-arc airfoil sections. Calculations using Weissinger's relation previously noted with a K value of 1.56, as determined experimentally in reference 10, give a $C_{l_\psi C_L}$ slope of 0.0023, which agrees closely with the measured slope at low and moderate lift coefficients. The directional stability of the drooped-nose configuration is greater than that for the basic wing in the high-lift-coefficient range. The C_{Y_ψ} characteristics are not changed materially by deflecting the nose flap.

Deflecting the half-span split flap 60° in conjunction with the drooped-nose flap 30° reduces the dihedral effect in the high-lift range below that for the drooped-nose-flap-alone configuration (fig. 32(b)) and produces a constant small positive dihedral effect in the moderate lift-coefficient range. The directional stability and lateral-force characteristics are not materially affected by deflecting the half-span split flap.

Drooped-Nose Flap With 0.032c Round-Leading-Edge Modification

The dihedral effect of the drooped-nose configuration is not altered appreciably by the installation of the 0.032c round leading edge (fig. 33(a)). The data for the drooped-nose flap deflected 10° with the round leading edge show no consistent variation with Reynolds number and, except for the irregularities at Reynolds numbers of about 3.0×10^6 and 6.0×10^6, the $C_{l_\psi C_L}$ slopes check the calculated value of 0.0023 very well. The directional stability is not affected materially by the addition of the round leading edge or by Reynolds number for the Reynolds number range investigated. The lateral-force characteristics are similar to those for the sharp-leading-edge drooped-nose configuration except that the C_{Y_ψ} values are about double (-0.0025) at the stall for the highest Reynolds number investigated.

Deflecting the half-span split flap generally decreases the dihedral effect at any given lift coefficient (fig. 33(b)) and decreases the $C_{l_\psi C_L}$ slope to about 0.0020 or 13 percent below the calculated value. The directional stability and side-force characteristics are essentially unaffected by the deflection of the split flap and also have no significant variation with Reynolds number.

Extensible Leading-Edge Flap

The dihedral effect with the extensible leading-edge flap installed has a fairly normal variation with lift coefficient (fig. 34) and an

average $C_{l_{\psi_{C_L}}}$ slope that agrees well with theory. Actually, however,

the $C_{l_{\psi_{C_L}}}$ slope is smaller at moderate lift coefficients and greater
than the calculated value of 0.0023 at low and high lift coefficients.
The directional stability is somewhat different than for any other config-
uration tested in that it is zero at a C_L of 0.25 and increases rapidly
for both higher and lower lift coefficients. Of course, this difference
at low lift coefficients is relatively unimportant because the flap would
probably not be deflected at such lift coefficients corresponding to high
flight speeds. The C_{Y_ψ} variation is quite similar to that for the
drooped-nose configuration with the 0.032c round leading edge installed
in that it increases about linearly to -0.0025 at $C_{L_{max}}$. No consistent
scale effects on the lateral-characteristic parameters are shown for the
Reynolds number range investigated.

SUMMARY OF RESULTS

The results of an investigation at high Reynolds numbers and low
Mach numbers in the Langley full-scale tunnel of the maximum-lift and
lateral characteristics of a rectangular wing of aspect ratio 3.4 with
circular-arc airfoil section are summarized as follows:

1. The maximum lift coefficient of the basic wing is 0.58. The
addition of half-span and full-span split flaps deflected 60° increases
this value to 1.00 and 1.24, respectively. The agreement between the
experimental values of the maximum lift coefficient and lift-curve slope
of the basic wing and the increments in lift coefficient due to flap
deflection with those calculated by the best available methods is good.

2. Maximum lift coefficients of 0.89, 1.20, and 1.21 are obtained
for the wing with the drooped-nose flap deflected 20°, for the wing with
the extensible leading-edge flap, and for the wing with the combination
of drooped-nose flap deflected 10° and the 0.032c round leading edge,
respectively. These values are increased to 1.26, 1.58, and 1.47,
respectively, with the addition of half-span split flaps deflected 60°.

3. The drag of the wing is high throughout the moderate to high
angle-of-attack range. The addition of split flaps causes a large drag
increase; however, an appreciable reduction in the drag in this range is
obtained by deflecting either the drooped-nose flap, or by the installa-
tion of the extensible leading-edge flap, or by deflecting the drooped-
nose flap in combination with a rounded leading edge.

4. The pitching-moment characteristics of the basic wing and of the wing with the leading-edge high-lift devices giving highest maximum lift indicate a slightly forward center-of-pressure location with respect to the quarter chord below the stall. A stable pitching-moment break is shown at the stall for all configurations except those with the extensible leading-edge flap and with the $\delta_n = 10^\circ$, 0.032c round-leading-edge configuration, which have breaks showing marginal stability.

5. Except for the wing with the extensible leading-edge flap, where the center-of-pressure shift with split-flap installation is negligible, the addition of split flaps moves the center-of-pressure location slightly rearward at high lift coefficients from the positions shown for the wing configurations without the split flaps. The only significant changes in the pitching-moment characteristics at the stall caused by the split flaps are an unstable break for drooped-nose-flap deflections greater than 20° and an unstable break for the $\delta_n = 10^\circ$, 0.032c round-leading-edge configuration at the highest Reynolds numbers investigated.

6. For the basic wing the dihedral effect increases parabolically with lift coefficient and the directional stability increases about linearly with lift coefficient and attain values for the respective parameters of 0.0023 per degree and -0.00050 per degree near maximum lift. The values for side-force parameter C_{Y_ψ} are low.

7. All the leading-edge high-lift devices investigated do not affect materially C_{n_ψ} or C_{Y_ψ}, but do produce almost linear C_{l_ψ} variations with C_L which, in general, agree well with those for conventional round-nose airfoils and with theory.

8. The split flaps decrease, at a given lift coefficient, the dihedral effect of the wing with the basic leading edge but generally do not produce any significant changes in the lateral characteristics when installed in combination with the leading-edge high-lift devices.

9. The separation behind the leading edge that is inherent for all other configurations investigated is eliminated when the extensible leading-edge nose flap is installed in conjunction with the half-span split flap.

10. An appreciable scale effect on the maximum lift coefficient is shown for the configurations with the round leading edges installed. The pitching-moment and lateral characteristics are not appreciably affected by changes in Reynolds number.

Langley Aeronautical Laboratory
    National Advisory Committee for Aeronautics
        Langley Field, Va.

REFERENCES

1. Lange, Roy H.: Langley Full-Scale-Tunnel Investigation of the
   Maximum Lift and Stalling Characteristics of a Trapezoidal Wing of
   Aspect Ratio 4 with Circular-Arc Airfoil Sections. NACA RM
   No. L7H19, 1947.

2. Underwood, William J., and Nuber, Robert J.: Two-Dimensional Wind-
   Tunnel Investigation at High Reynolds Numbers of Two Symmetrical
   Circular-Arc Airfoil Sections with High-Lift Devices. NACA RM
   No. L6K22, 1947.

3. Krueger, W.: Systematic Wind-Tunnel Measurements on a Laminar Wing
   with Nose Flap. NACA TM No. 1119, 1947.

4. Anderson, Raymond F.: Determination of the Characteristics of
   Tapered Wings. NACA Rep. No. 572, 1936.

5. Swanson, Robert S., and Crandall, Stewart M.: Lifting-Surface-Theory
   Aspect-Ratio Corrections to the Lift and Hinge-Moment Parameters
   for Full-Span Elevators on Horizontal Tail Surfaces. NACA TN
   No. 1175, 1947.

6. Underwood, William J., and Nuber, Robert J.: Aerodynamic Load
   Measurements over Leading-Edge and Trailing-Edge Plain Flaps on
   a 6-Percent-Thick Symmetrical Circular-Arc Airfoil Section.
   NACA RM No. L7H04, 1947.

7. Silverstein, Abe, and Katzoff, S.: Design Charts for Predicting
   Downwash Angles and Wake Characteristics behind Plain and Flapped
   Wings. NACA Rep. No. 648, 1939.

8. Gustafson, F. B., and O'Sullivan, William J., Jr.: The Effect of
   High Wing Loading on Landing Technique and Distance, with Experi-
   mental Data for the B-26 Airplane. NACA ARR No. L4K07, 1945.

9. Zimmerman, C. H.: Characteristics of Clark Y Airfoils of Small
   Aspect Ratios. NACA Rep. No. 431, 1932.

10. Purser, Paul E., and Spearman, M. Leroy: Wind-Tunnel Tests at Low
    Speed of Swept and Yawed Wings Having Various Plan Forms. NACA RM
    No. L7D23, 1947.

11. May, Ralph W., Jr., and Stevens, George L.: Langley Full-Scale Tunnel
    Investigation of the Characteristics in Yaw of a Trapezoidal Wing
    of Aspect Ratio 4 with Circular-Arc Airfoil Sections. NACA RM
    No. L8C15, 1948.

12. Weissinger, J.: Der schiebende Tragflügel bei gesunder Strömung.
    Bericht S 2 der Lilienthal-Gesellschaft für Luftfahrtforschung,
    1938-39, pp. 13-51.

375.48

110.80

0.25c

Center-of-gravity
location

A

A

Arrangement of split flaps

6.00

85.40

182.80

Flap cut-out
for yaw tests

Wing area, 286.0 sq ft
Aspect ratio, 3.4

NACA

Section A-A
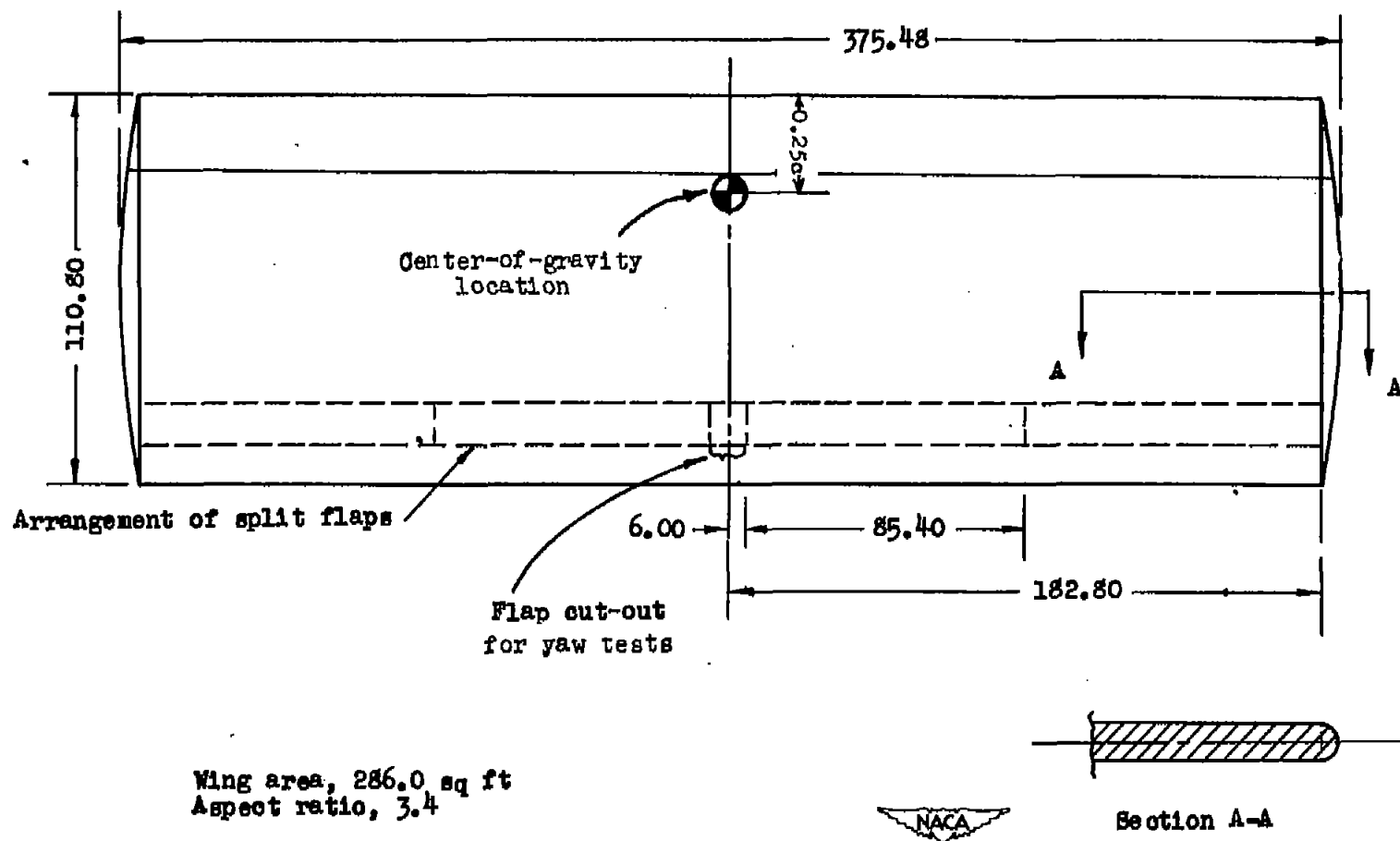
Figure 1.- Geometric characteristics of the rectangular wing. All dimensions are given
in inches.
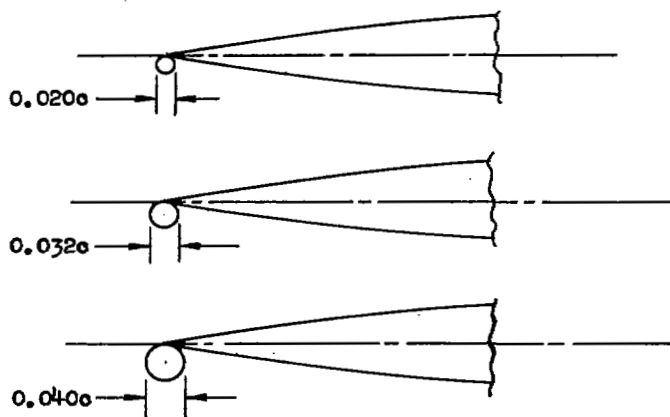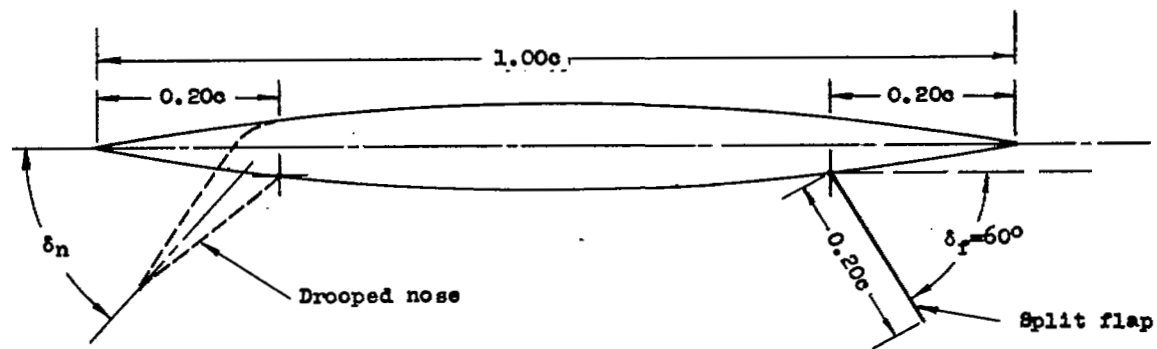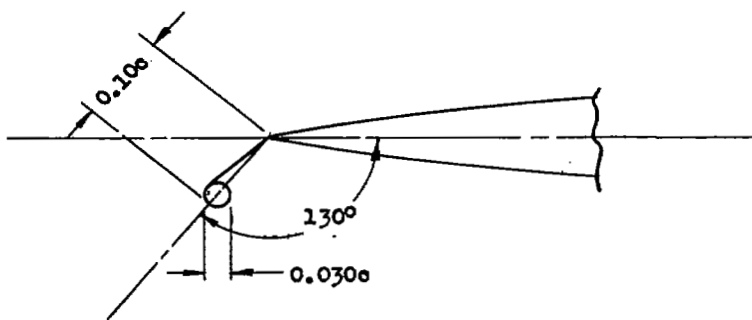
Figure 2.- Arrangement of high-lift devices investigated.
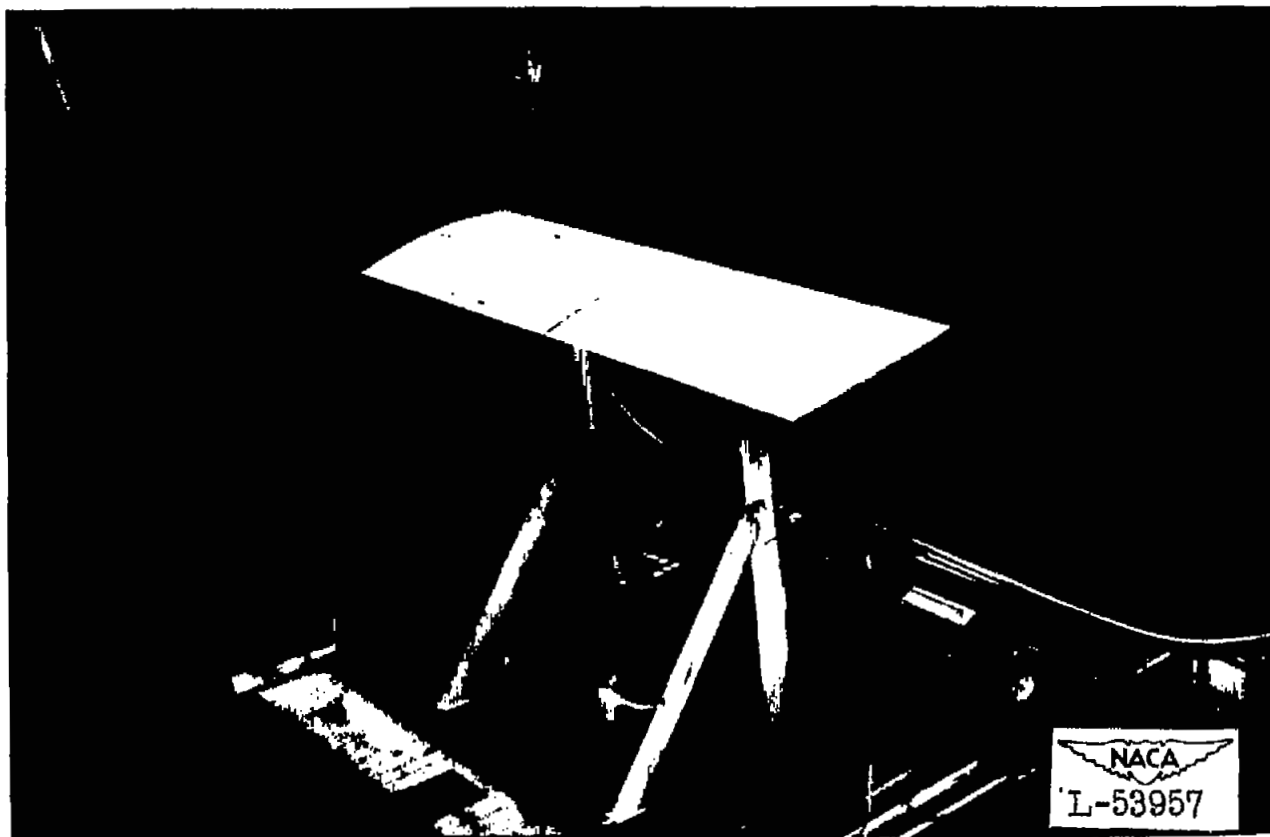
(a) Wing mounted on airfoil supports.

Figure 3.- Photographs of rectangular wing mounted in the Langley full-scale tunnel.
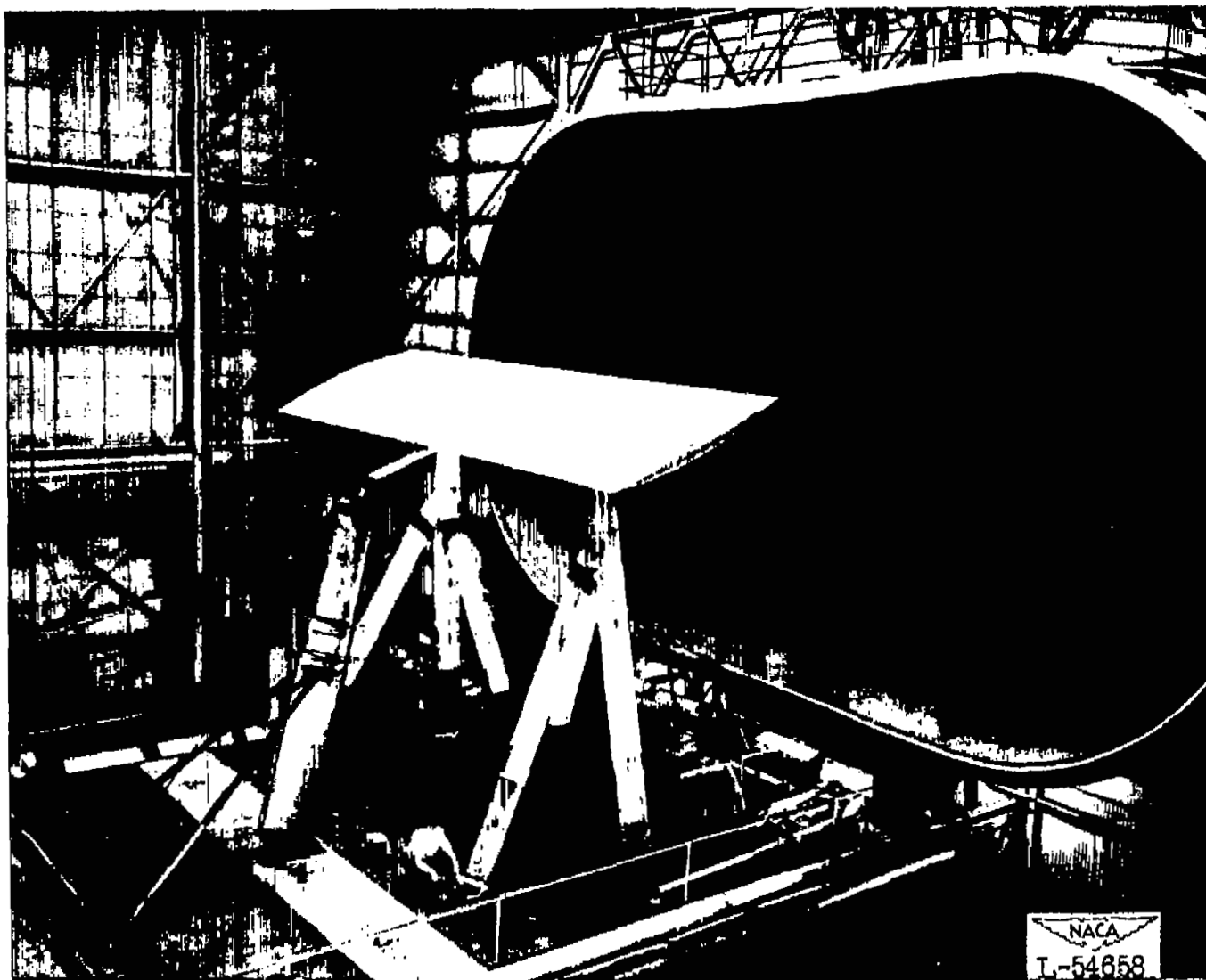
(b) Wing mounted on yaw supports.

Figure 3.- Concluded.
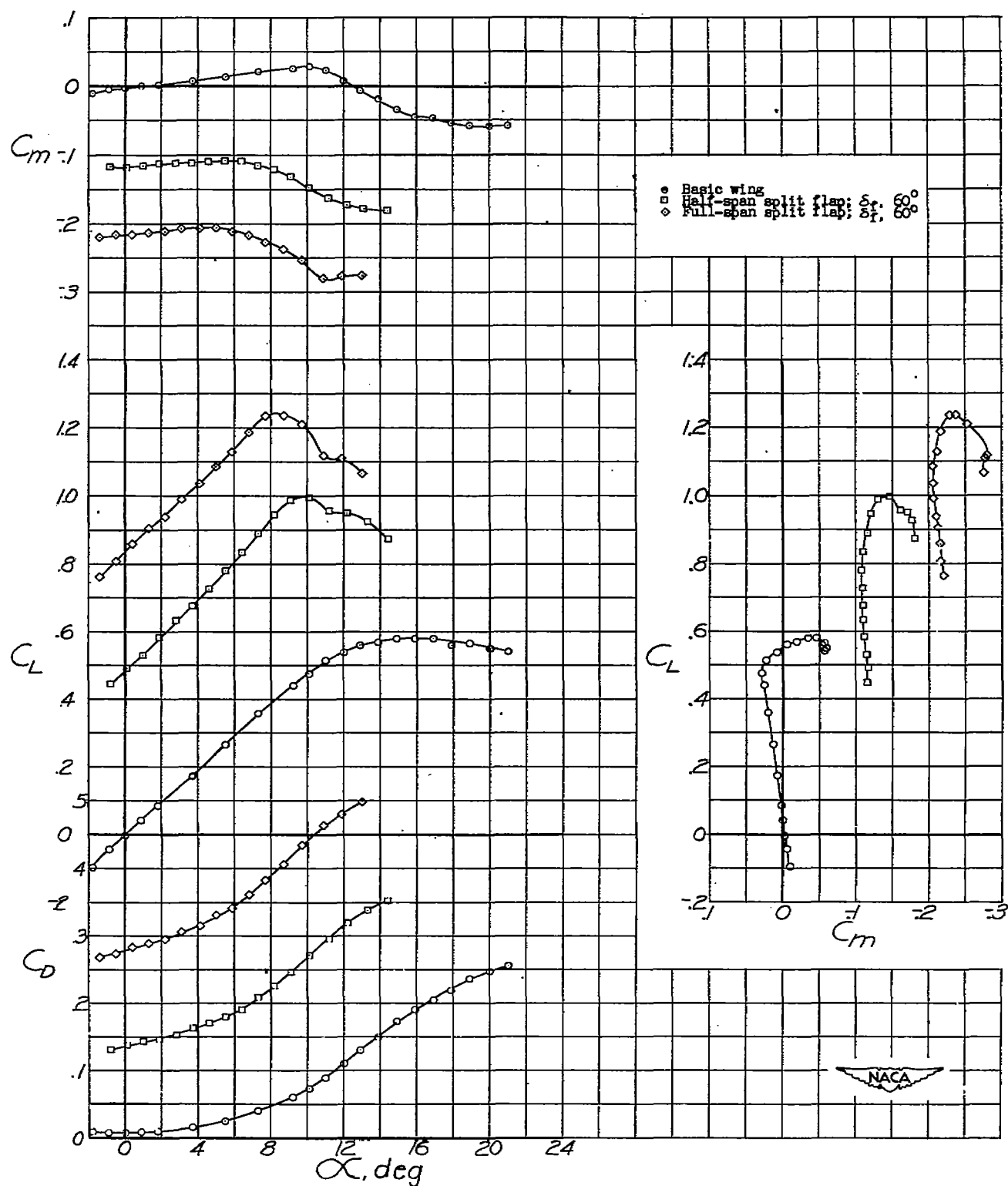
Figure 4.-   Effect of split-flap deflection on C_L, C_D,   and C_m of a
rectangular wing.
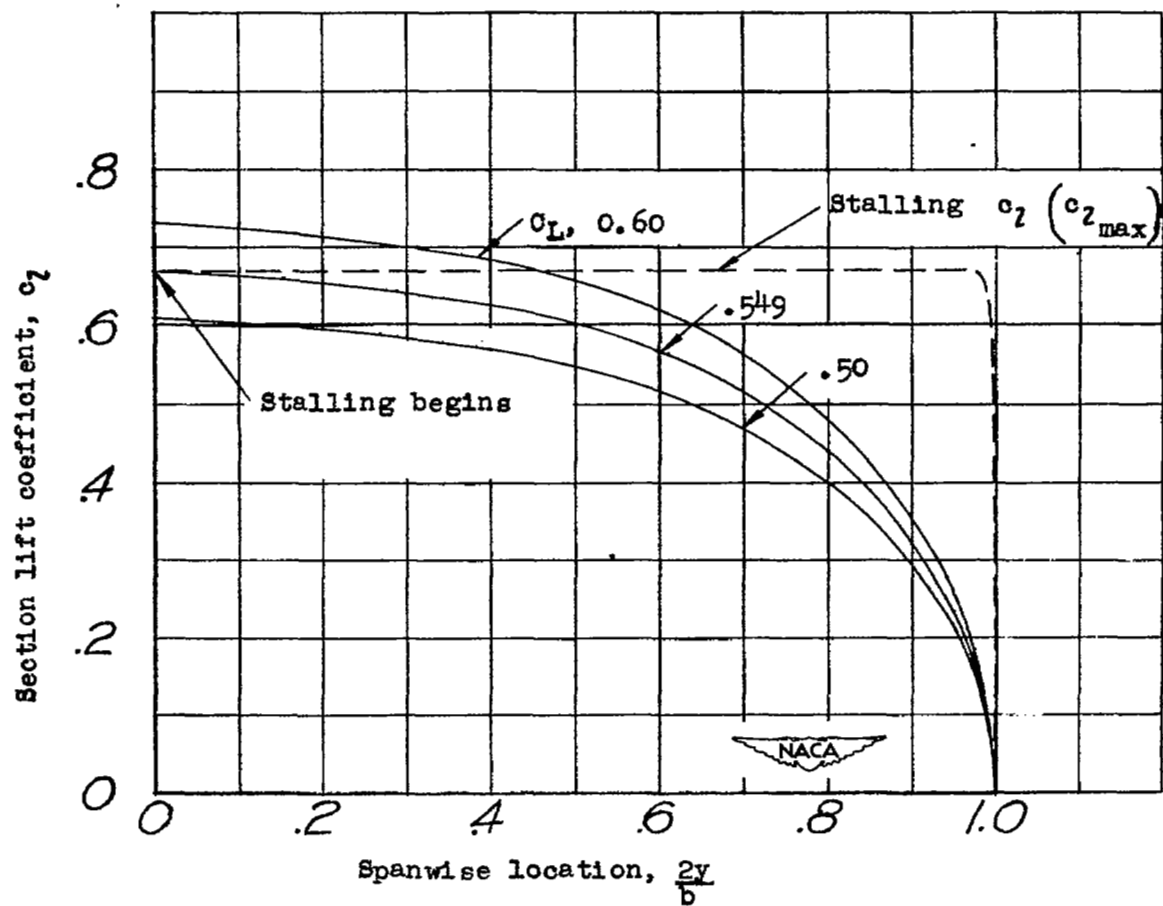
Figure 5.- Determination of C_L at which basic wing begins to stall.
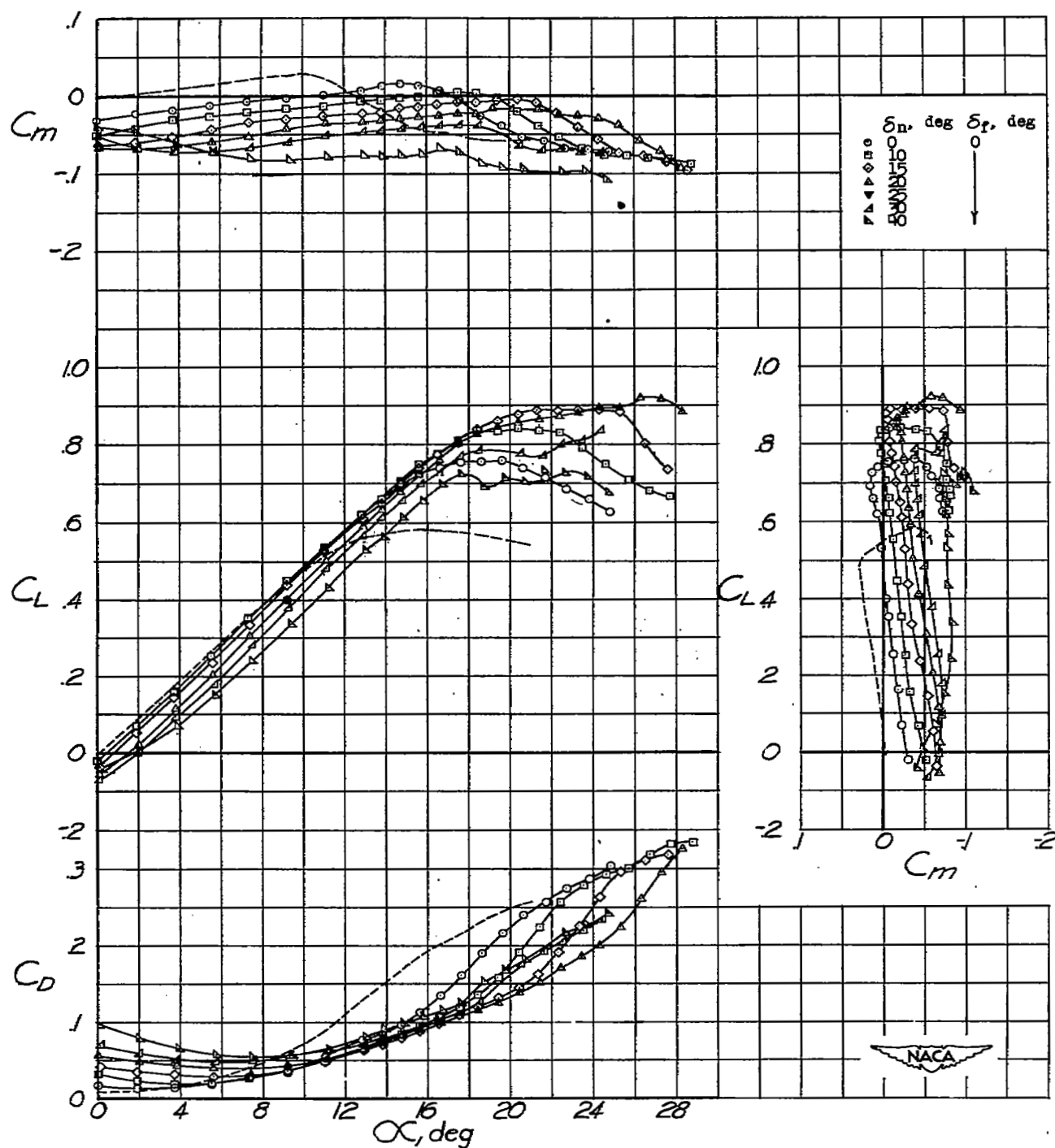
Figure 6.- Effect of drooped-nose-flap deflection on C_L, C_D, and C_m of a rectangular wing. $\delta_f = 0°$.
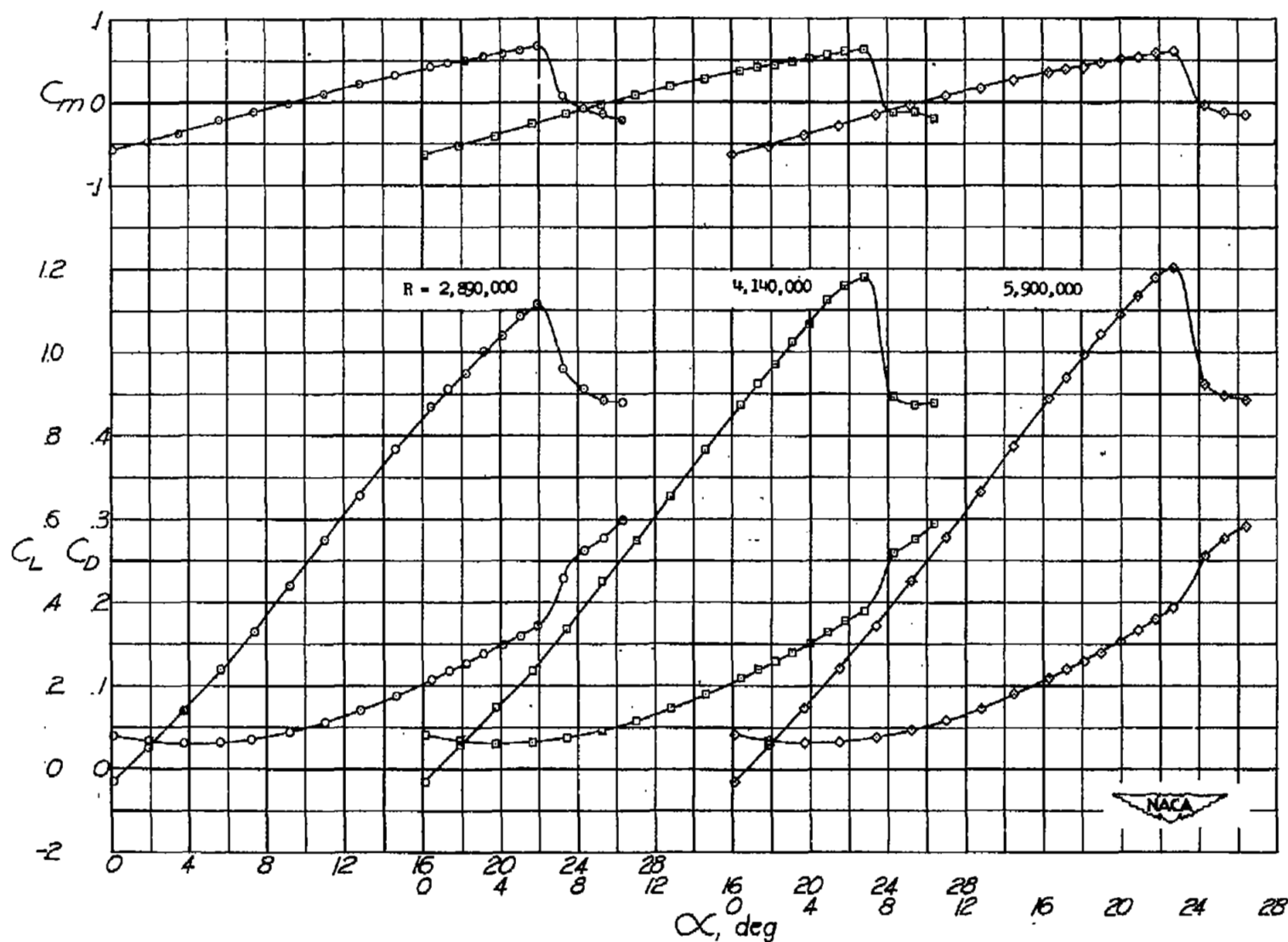
(a) Variation of C_L, C_D and C_m with α.

Figure 7.- Effect of Reynolds number on C_L, C_D, and C_m of wing with extensible leading-edge flap installed. $\delta_f = 0^O$.
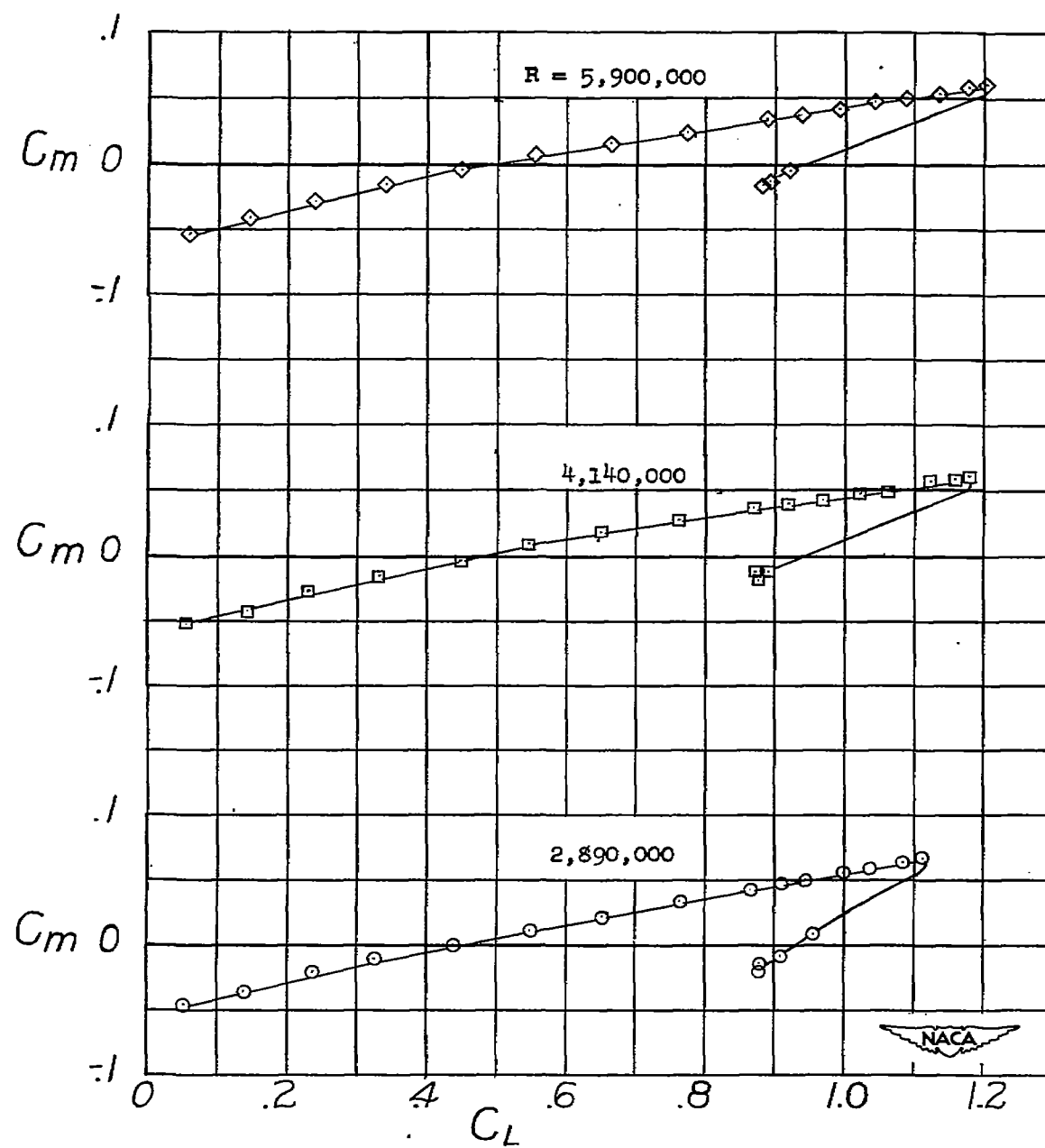
(b)   Variation of C_m with C_L.

Figure 7.- Concluded.
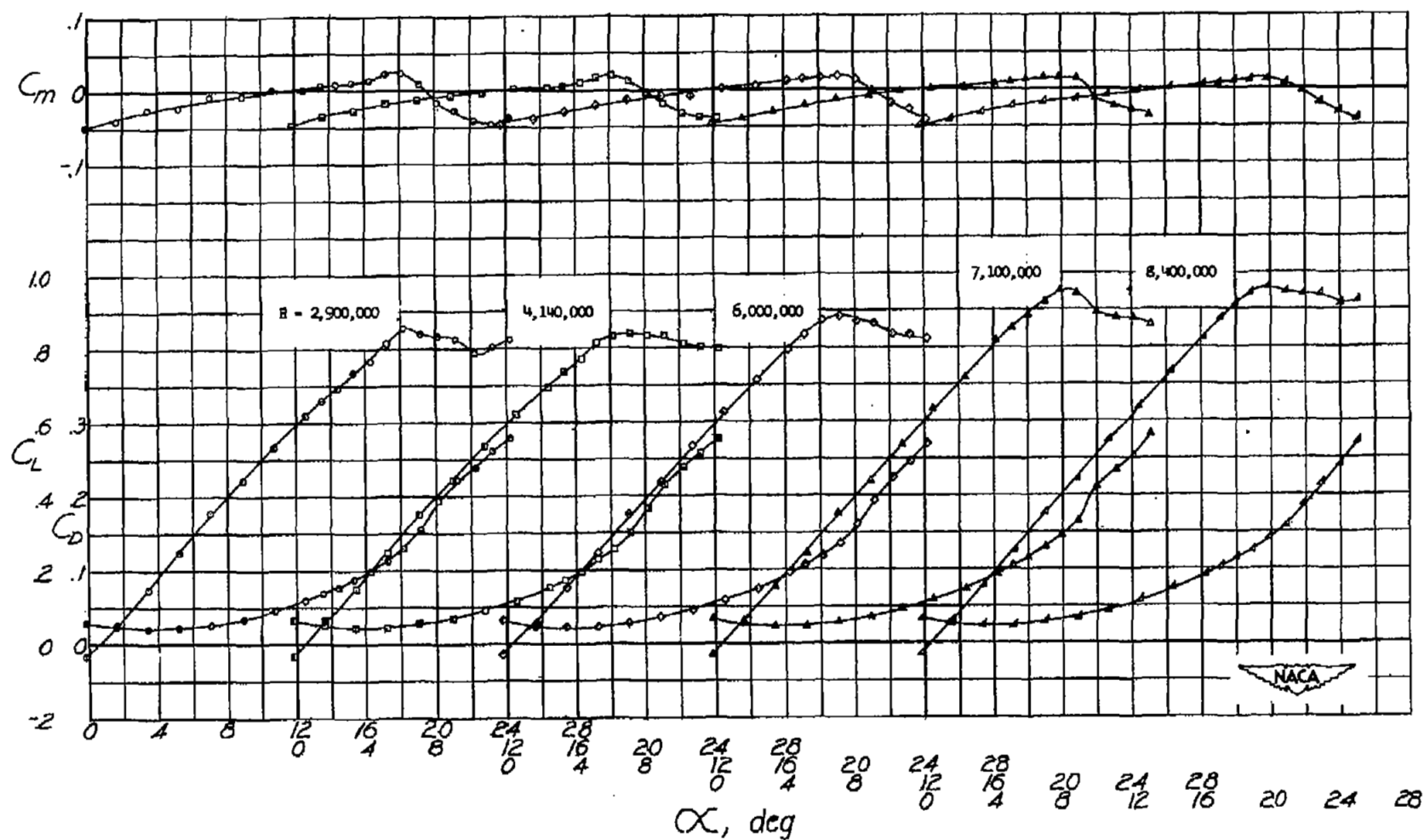
(a) $\delta_n = 10°$.

Figure 8.- Effect of Reynolds number on C_L, C_D, and C_m of wing with 0.020c round leading edge installed. $\delta_f = 0°$.

C_m

C_L

C_D

R = 2,960,000   4,200,000   6,030,000   7,250,000   8,340,000

NACA

$\propto$, deg

(b) $\delta_n = 15^o$.
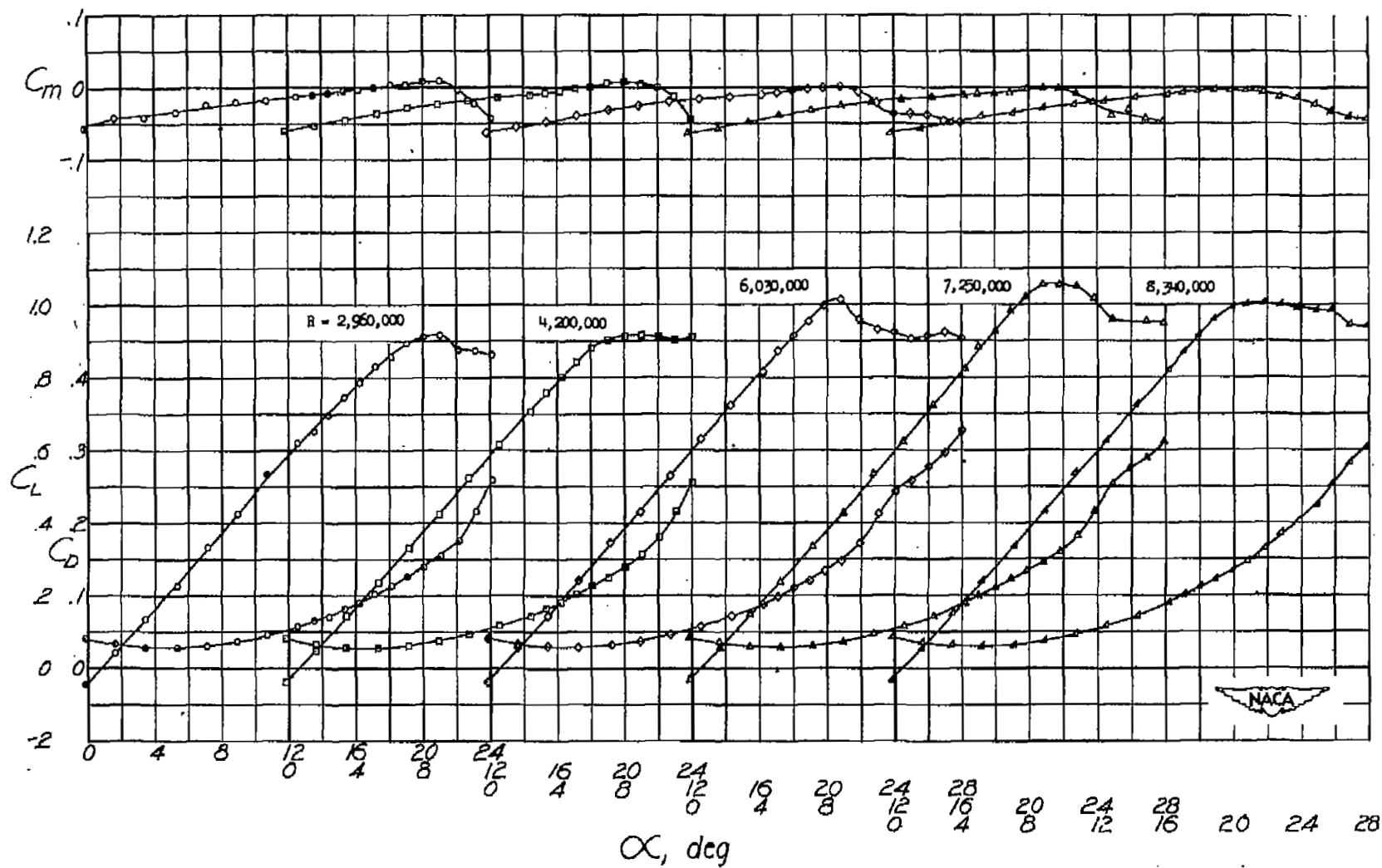
Figure 8.- Concluded.
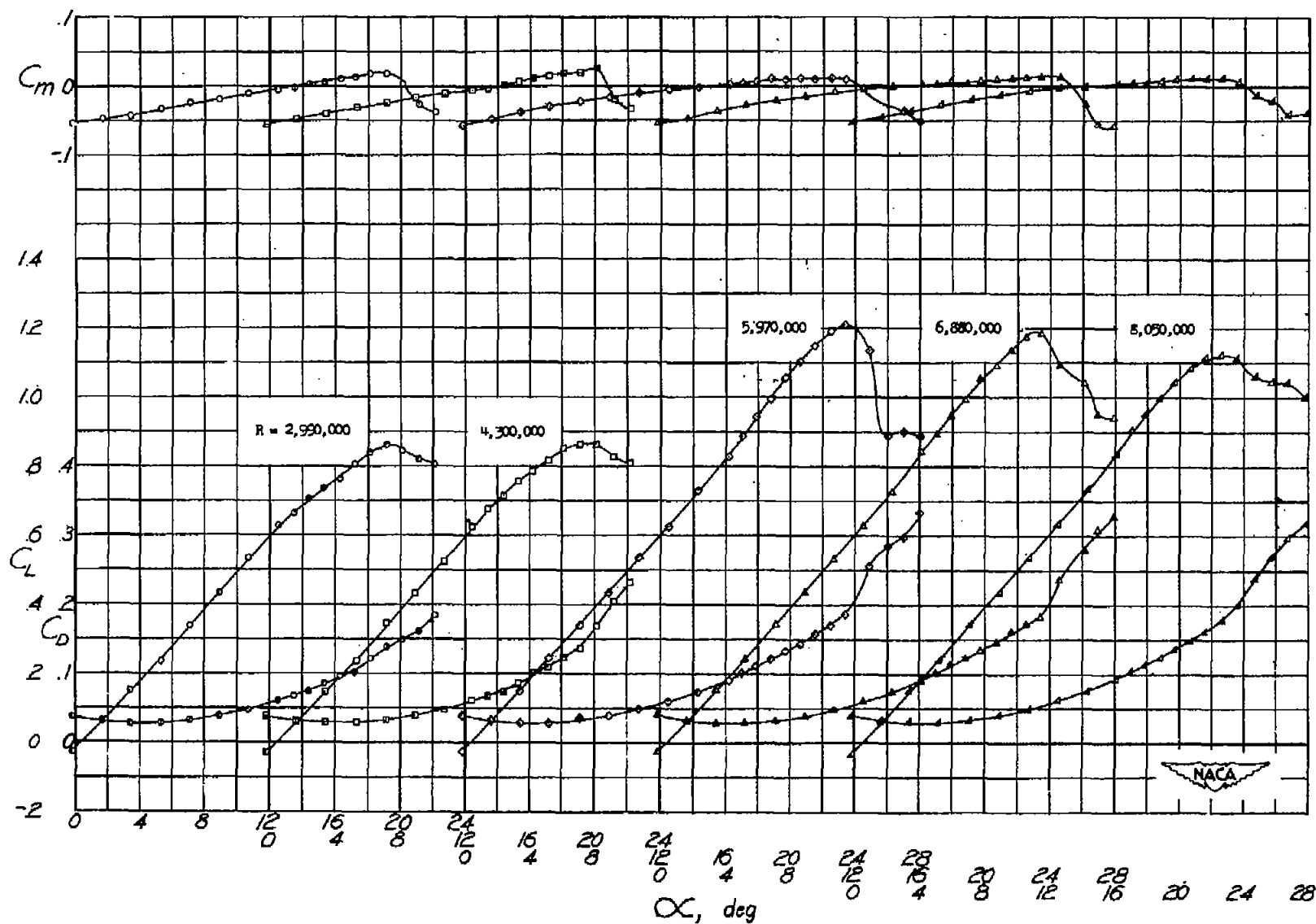
(a) Variation of C_L, C_D, and C_m with α.

Figure 9.- Effect of Reynolds number on C_L, C_D, and C_m of wing with 0.032c round leading edge installed. $\delta_n = 10^O$; $\delta_f = 0^O$.
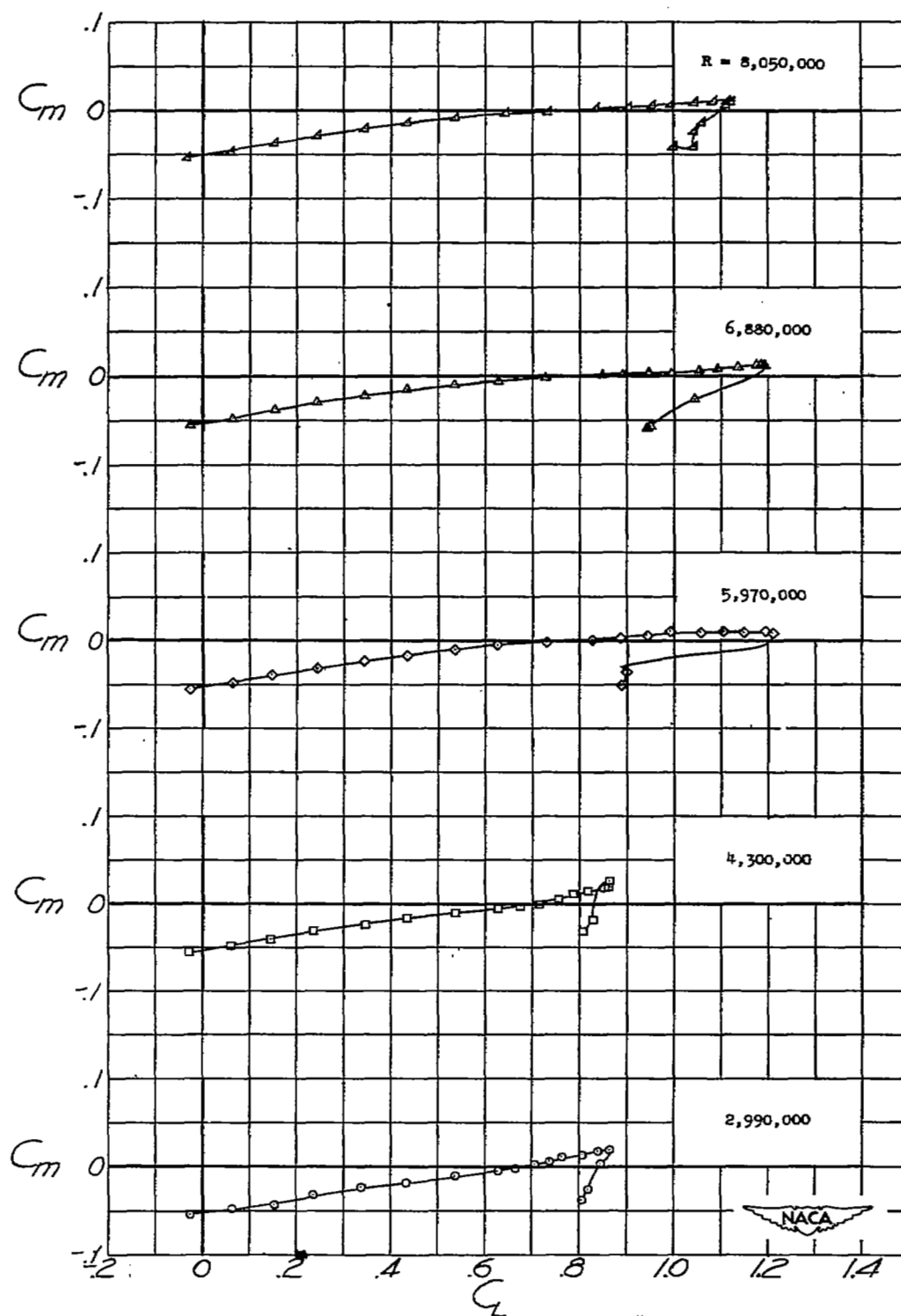
(b) Variation of C_m with C_L.

Figure 9.- Concluded.

(a) $\delta_n = 15^O$.
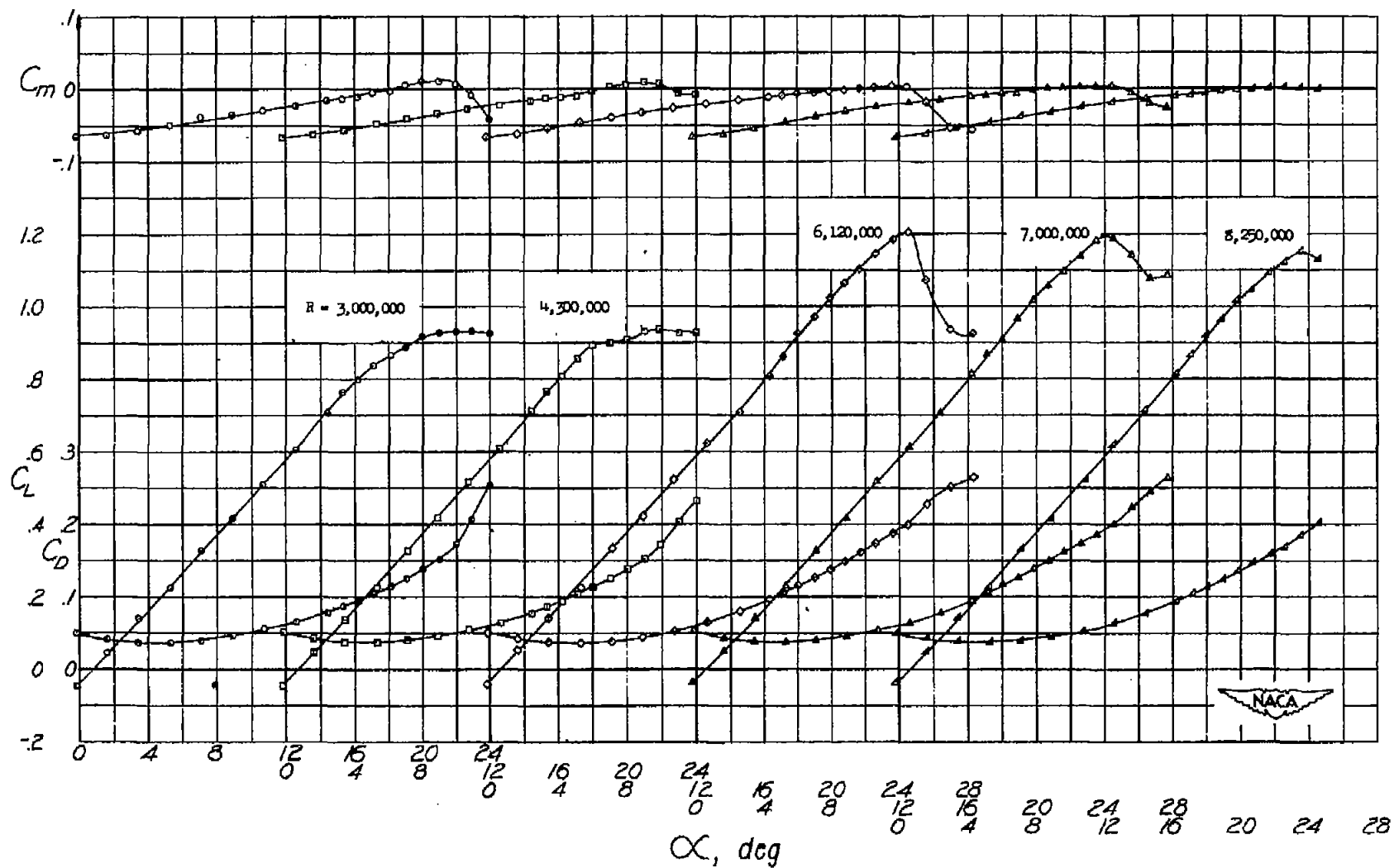
Figure 10.- Effect of Reynolds number on C_L, C_D, and C_m of wing with 0.032c round
leading edge installed. $\delta_f = 0^O$.
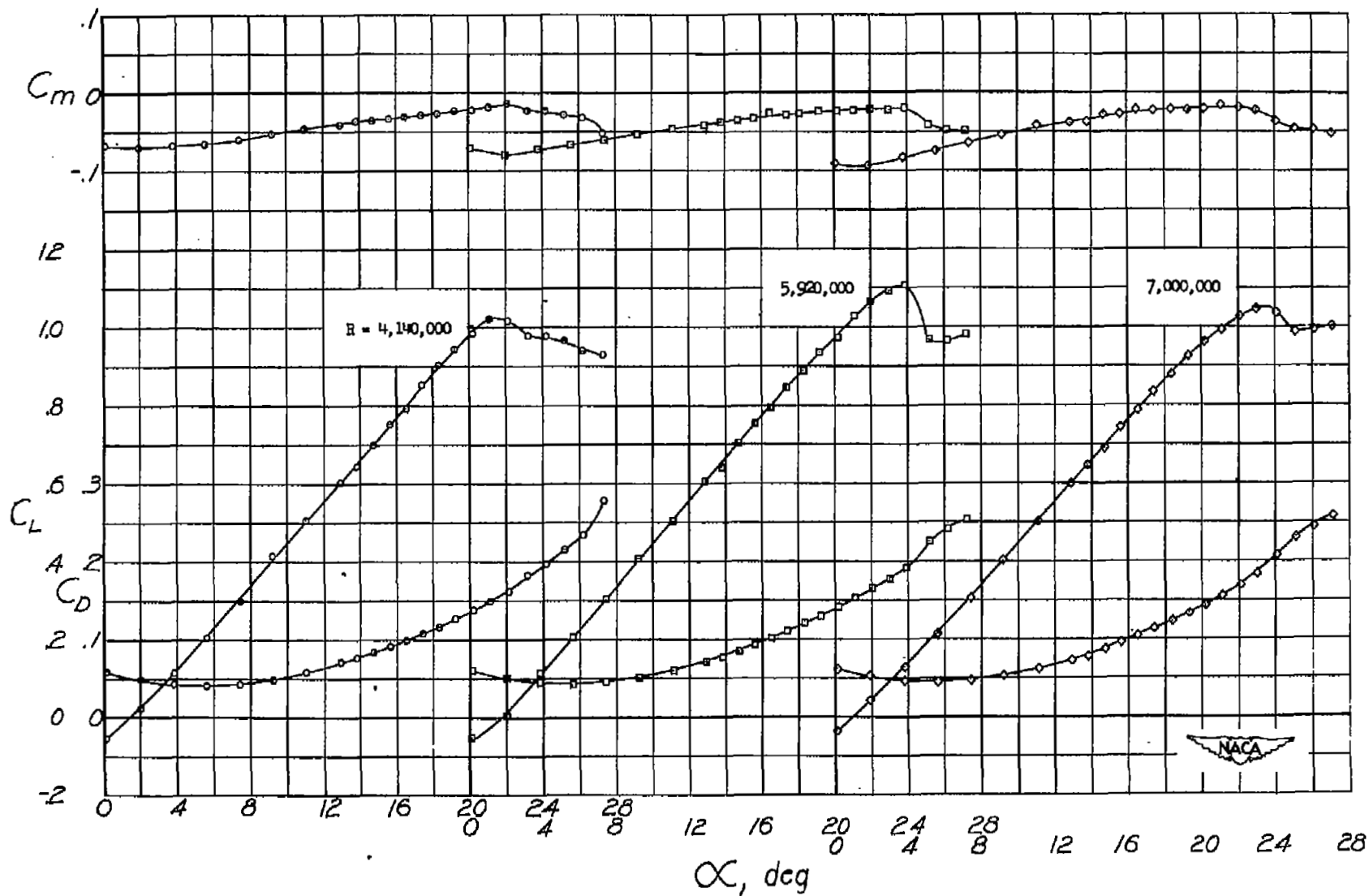
(b) $\delta_n = 20°$.

Figure 10.- Concluded.

(a) $\delta_n = 10^O$.
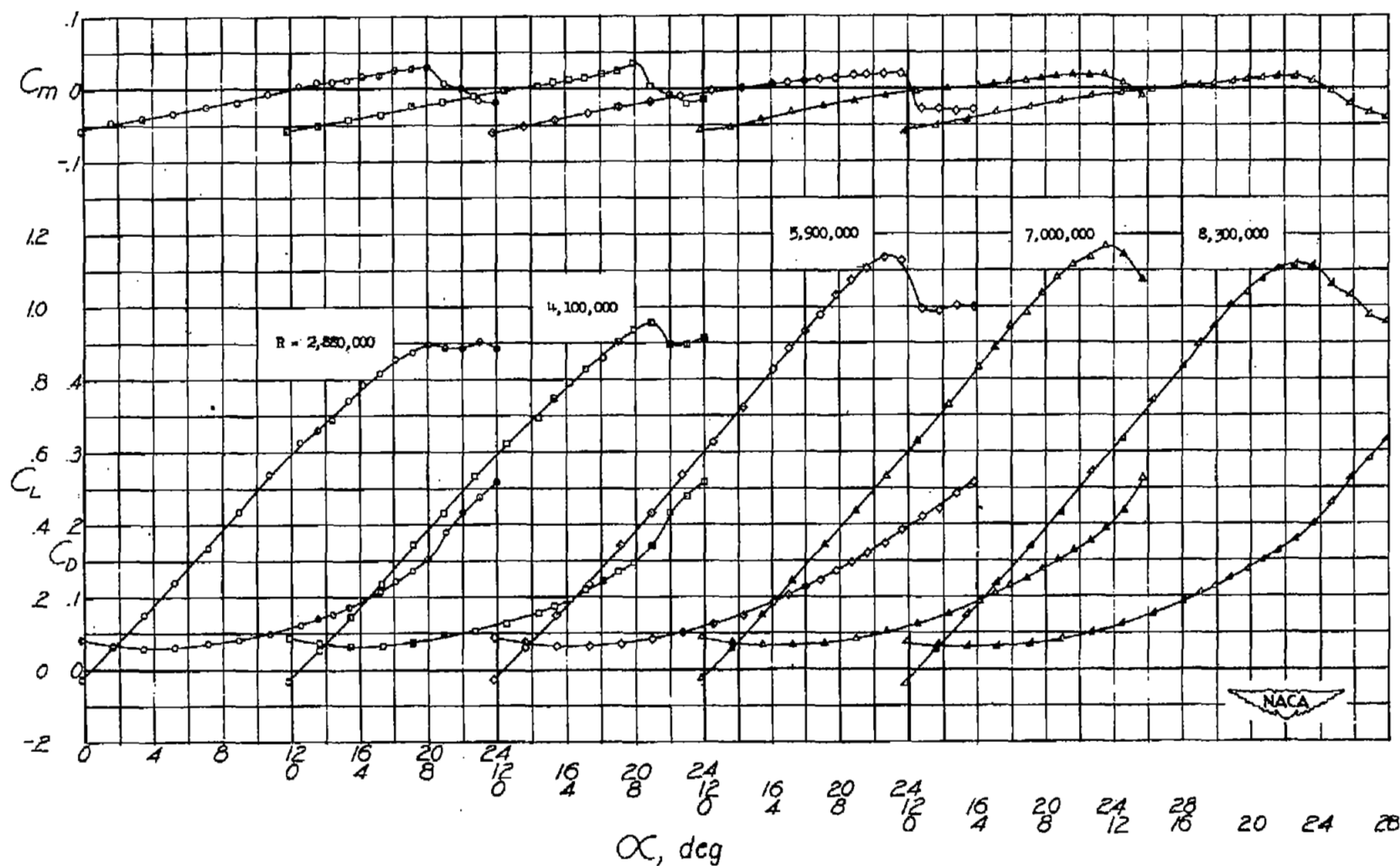
Figure 11.- Effect of Reynolds number on C_L, C_D, and C_m of wing with 0.040c round leading edge installed. $\delta_f = 0^O$.

(b) $\delta_n = 15^o$.
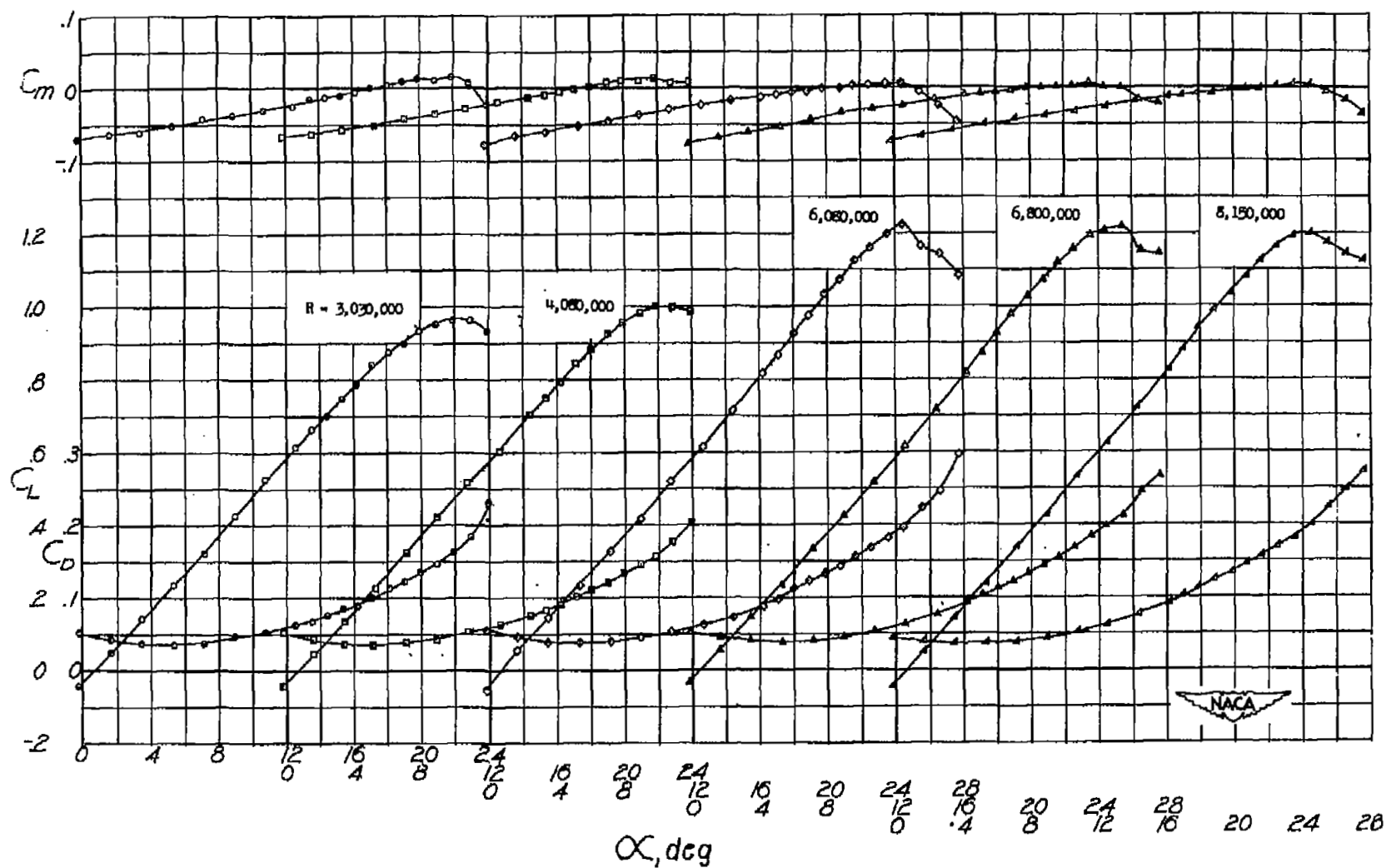
Figure 11.- Concluded.
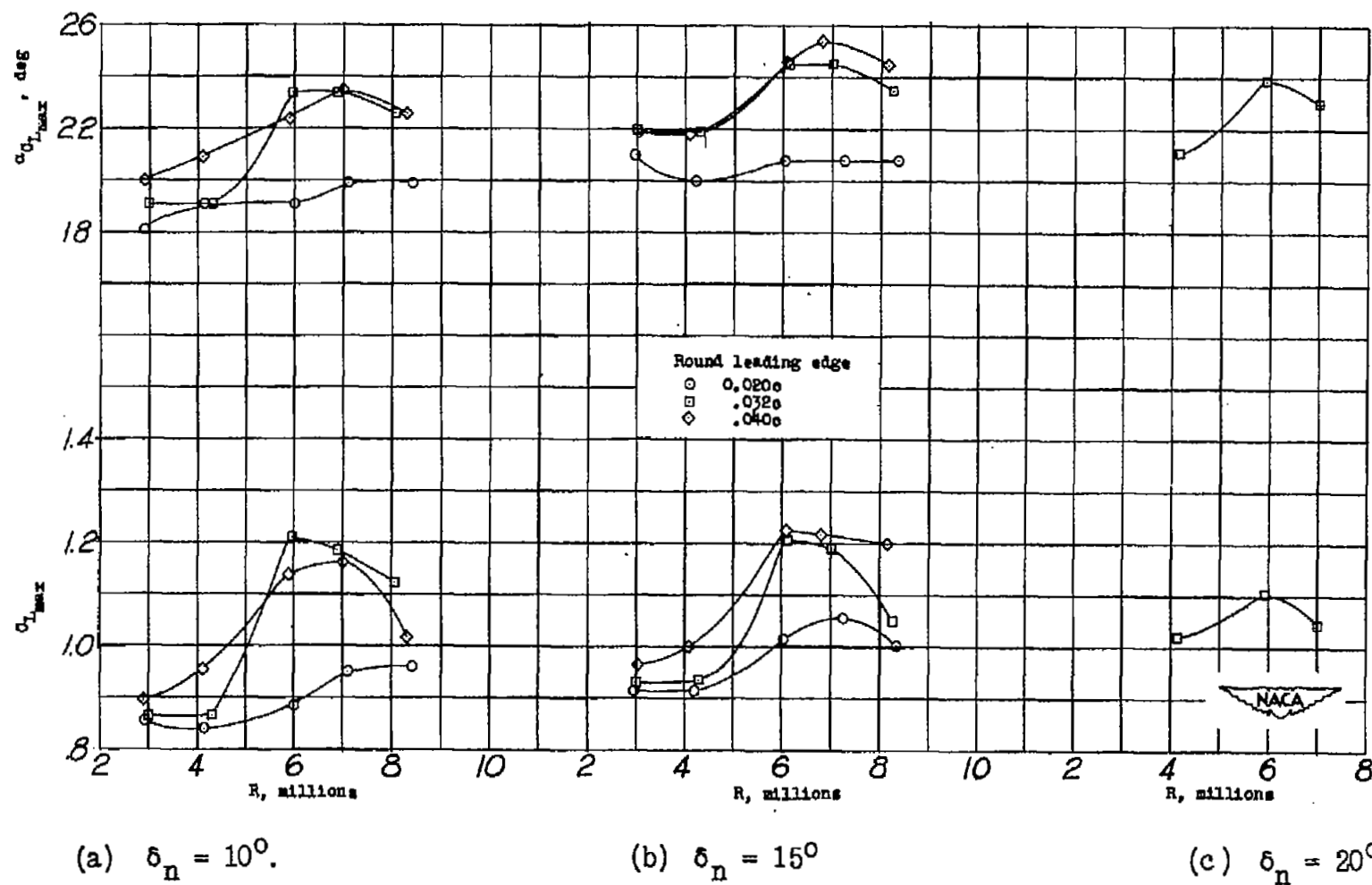
Figure 12.- Summary of maximum-lift results of round leading-edge configurations with several drooped-nose deflections. $\delta_f = 0°$.

(a) $\delta_n = 10°$.

(b) $\delta_n = 15°$

(c) $\delta_n = 20°$.
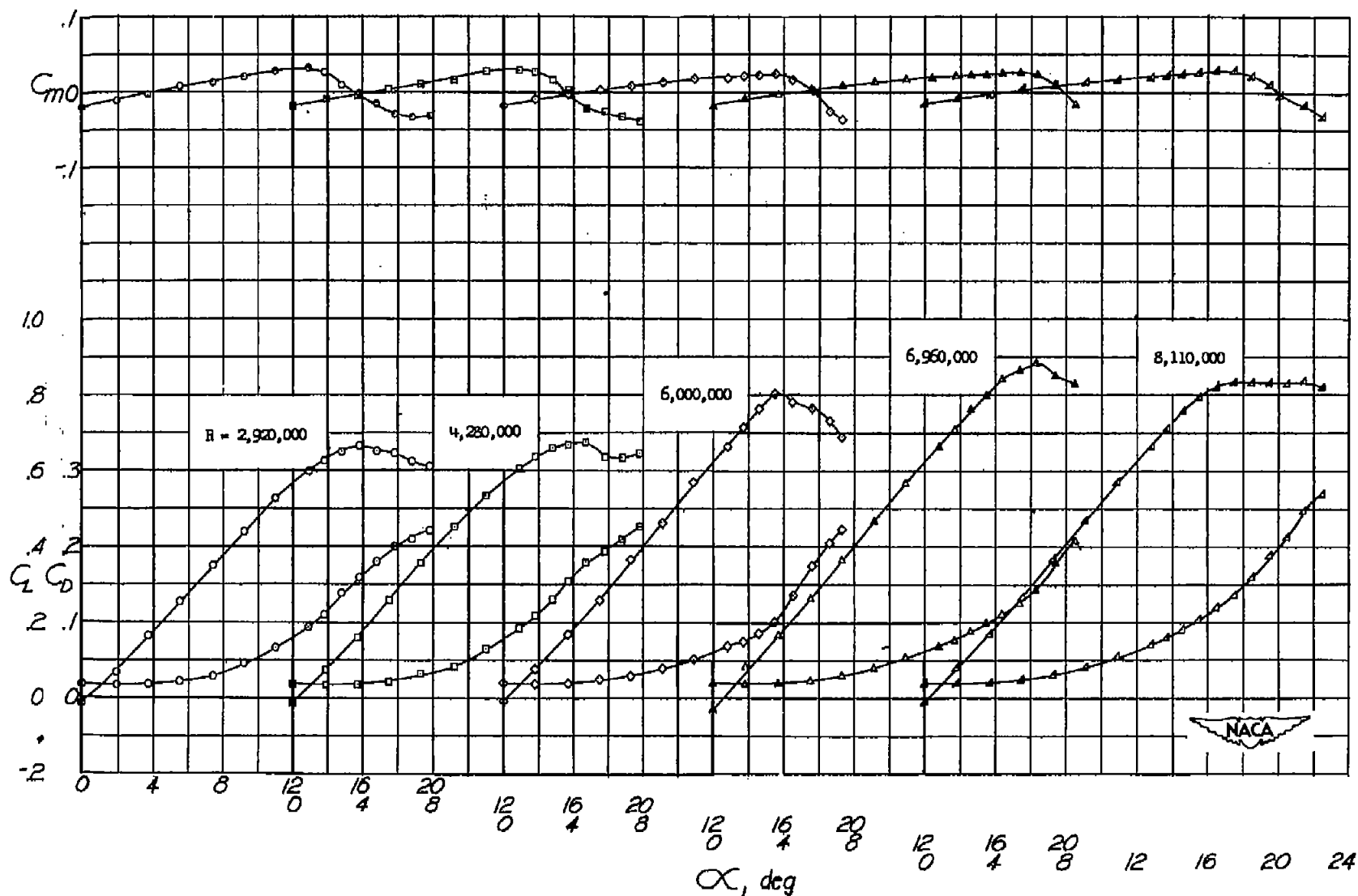
(a) Variation of C_L, C_D, and C_m with α.

Figure 13.-   Effect of Reynolds number on C_L, C_D, and C_m of wing with 0.032c round
leading edge installed. $\delta_n = 0^\circ$; $\delta_f = 0^\circ$.
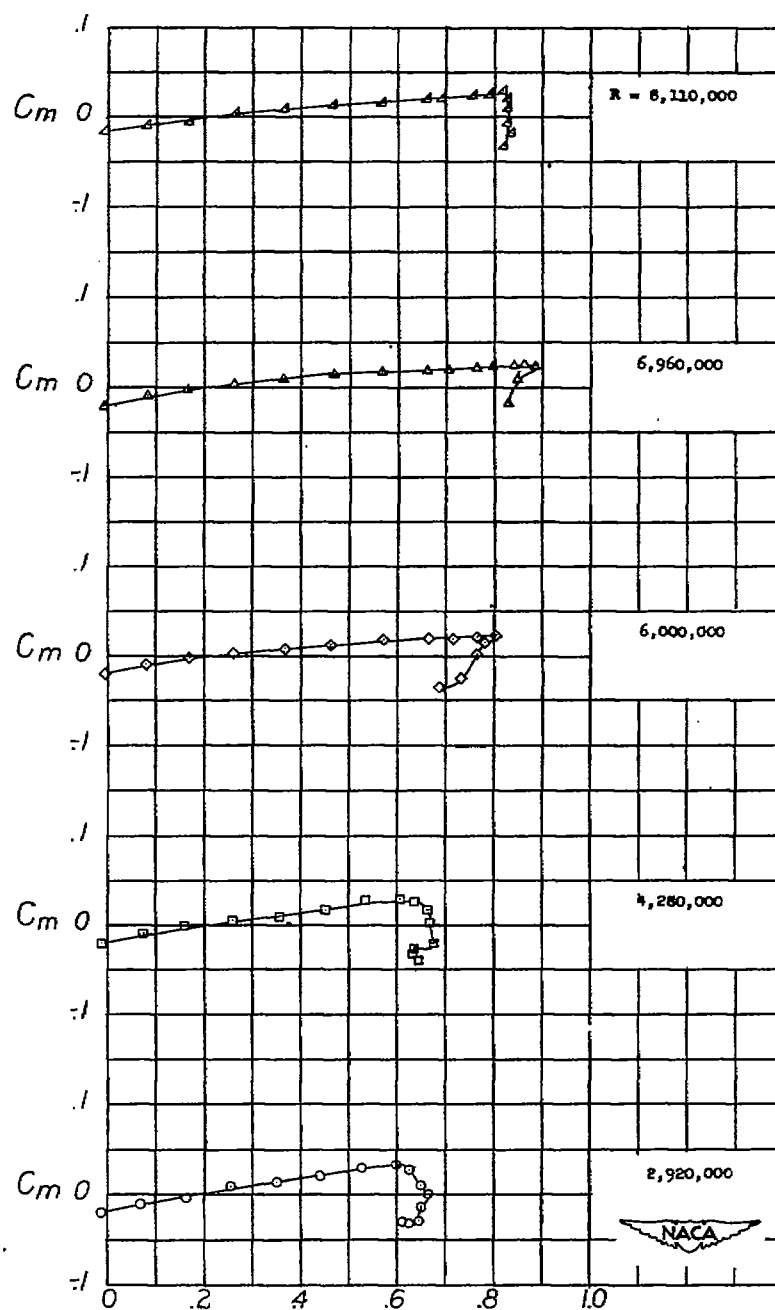
(b) Variation of C_m with C_L.

Figure 13.- Concluded.
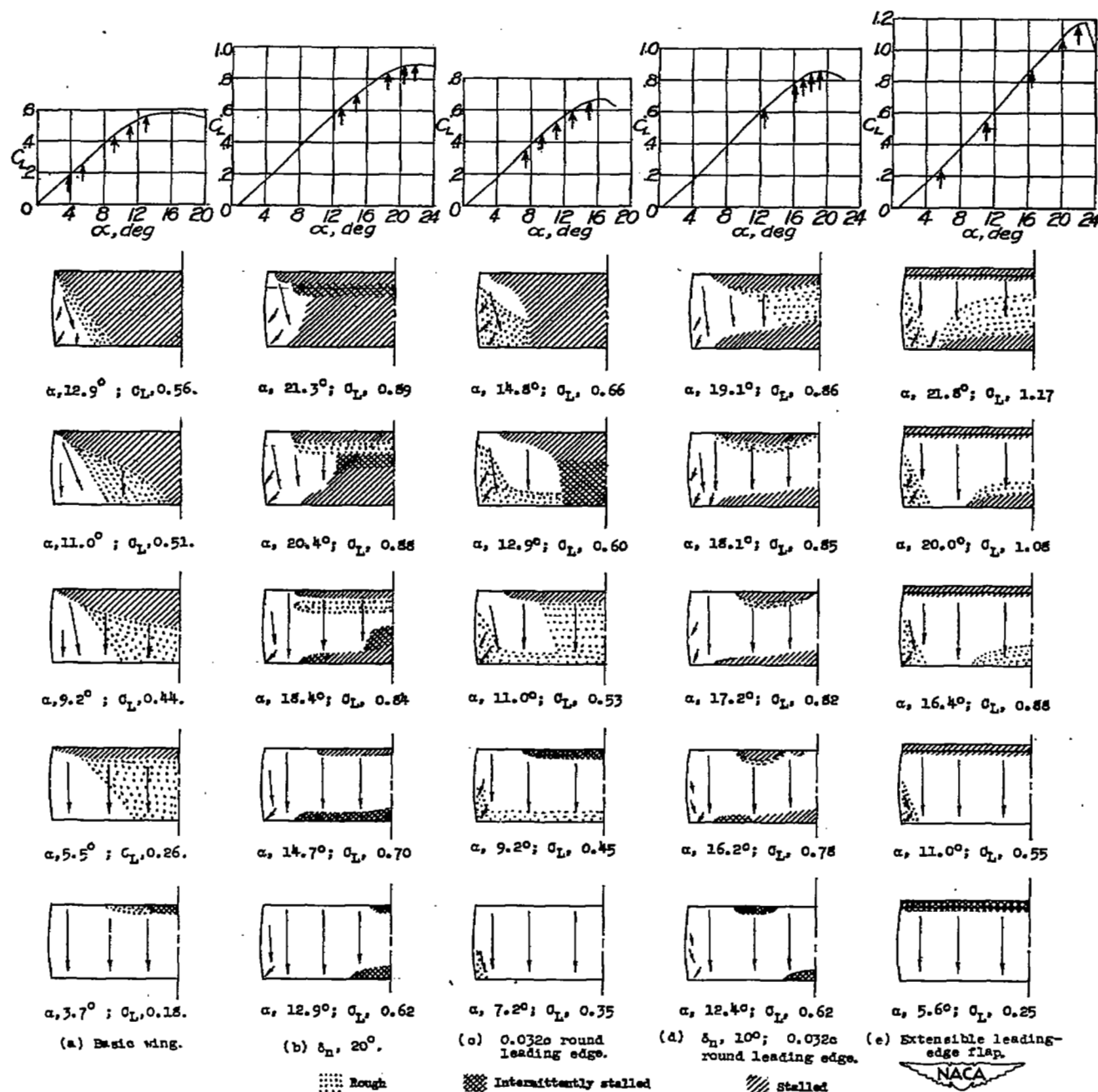
Figure 14.- Stalling characteristics of basic wing and of wing with
several leading-edge high-lift devices installed. Arrows indicate
direction of flow; R ≈ 4.1 × 10^6; δ_f = 0°.
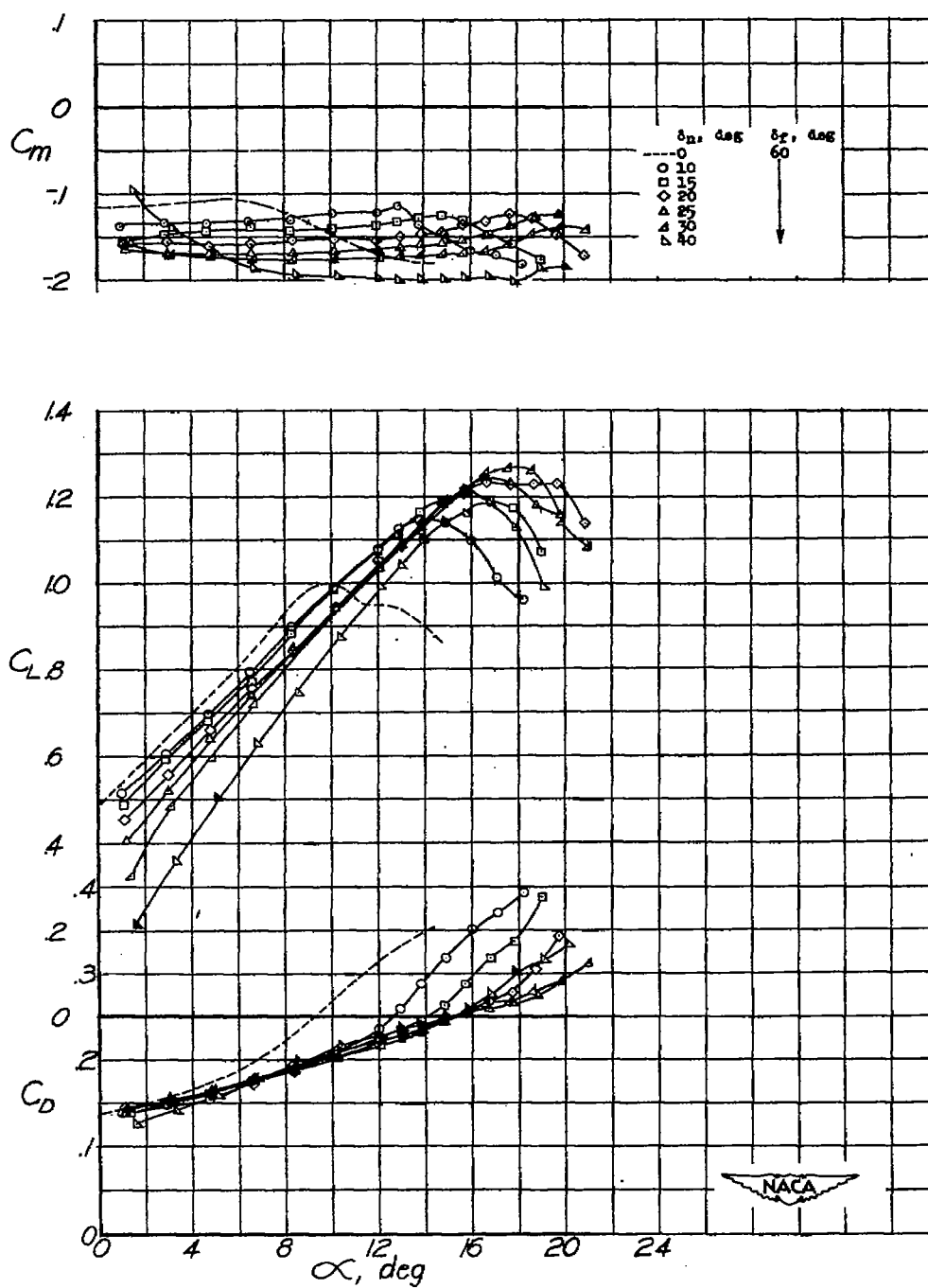
(a) Variation of C_L, C_D, and C_m with α.

Figure 15.- Effect of drooped-nose-flap deflection on C_L, C_D, and
C_m of wing with half-span split flaps installed. $\delta_f = 60°$.
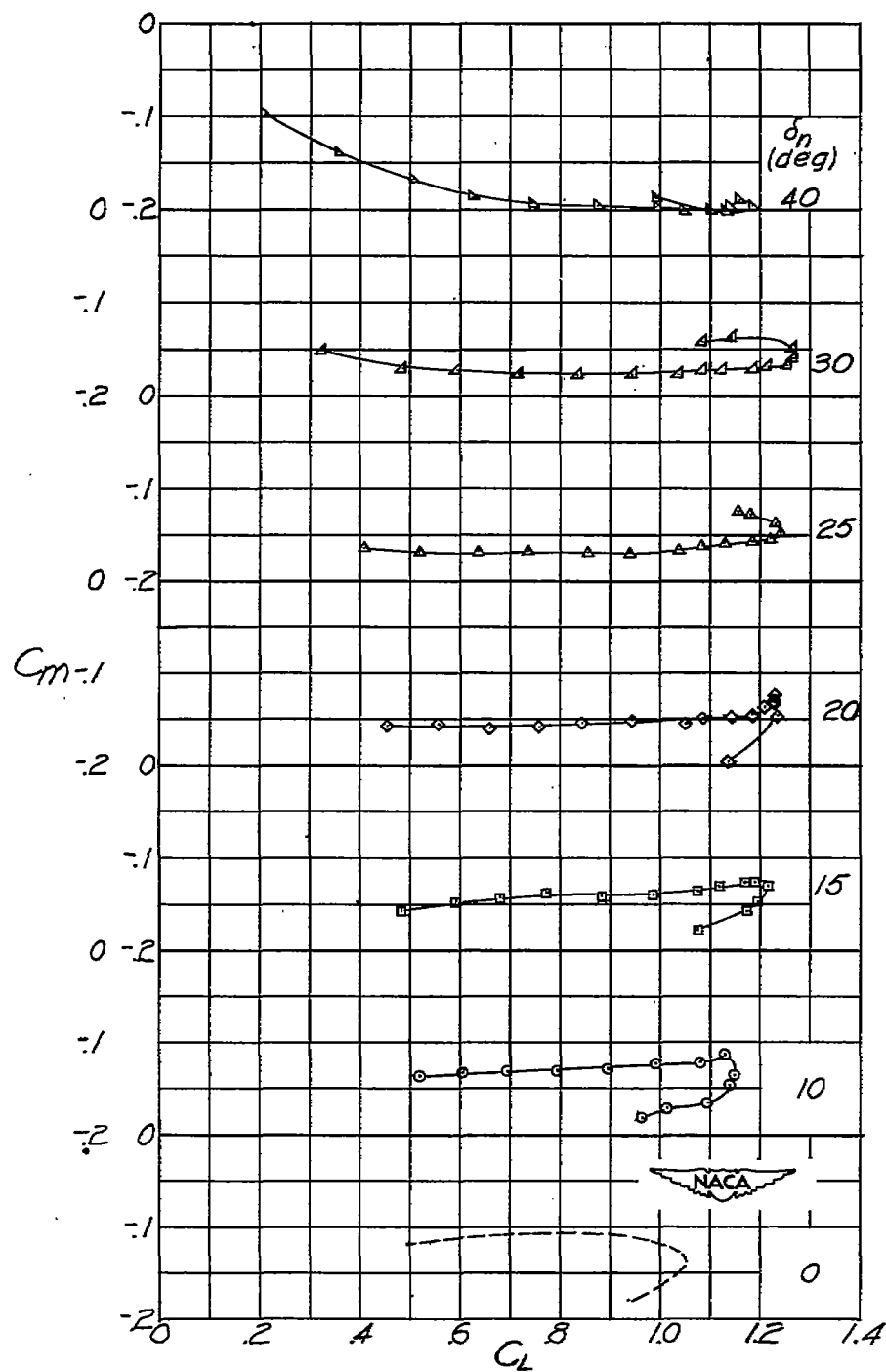
(b) Variation of C_m with C_L.

Figure 15.- Concluded.
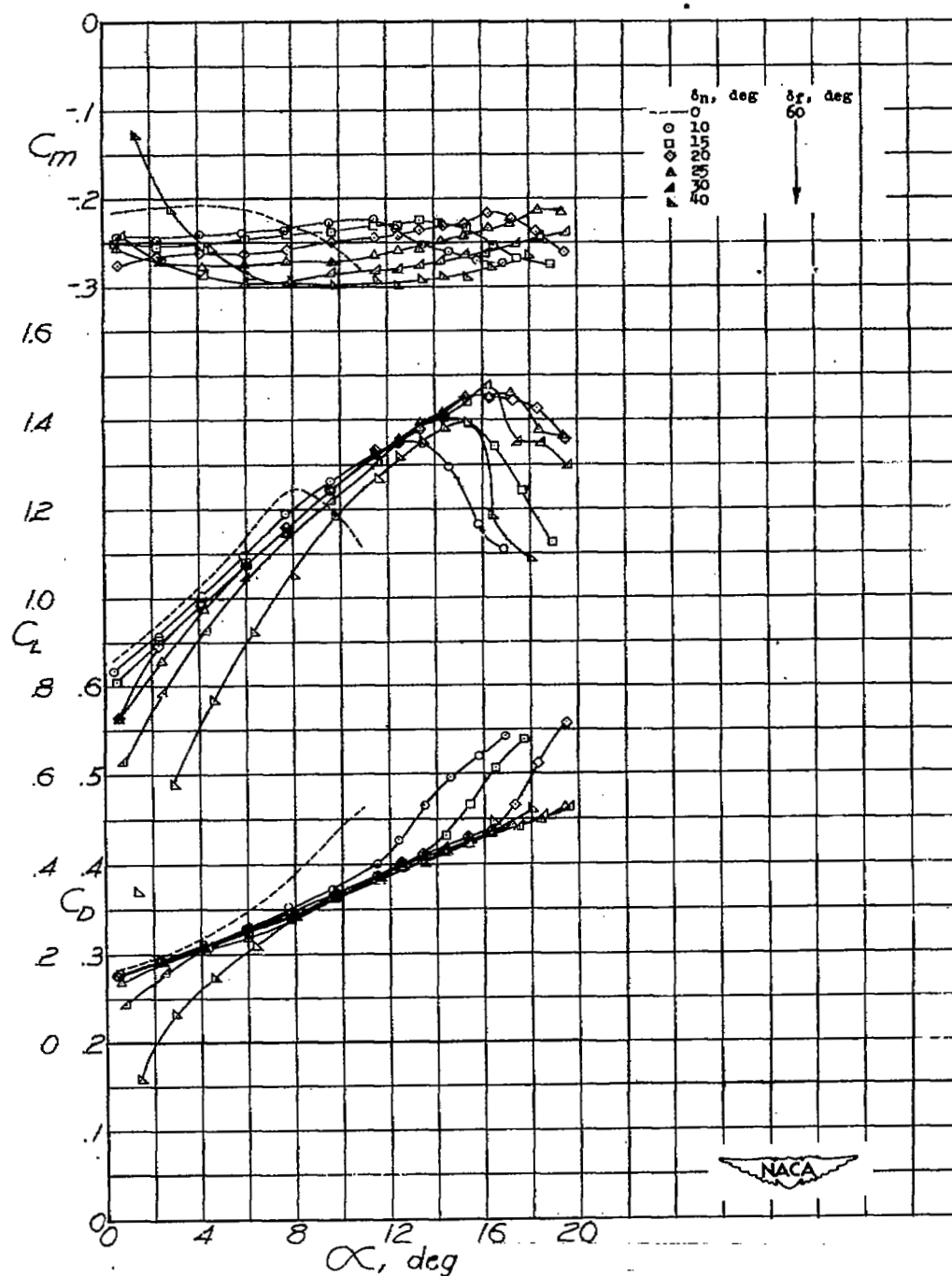
(a) Variation of C_L, C_D, and C_m with α.

Figure 16.- Effect of drooped-nose-flap deflection on C_L, C_D, and
C_m of wing with full-span split flaps installed. δ_f = 60°.
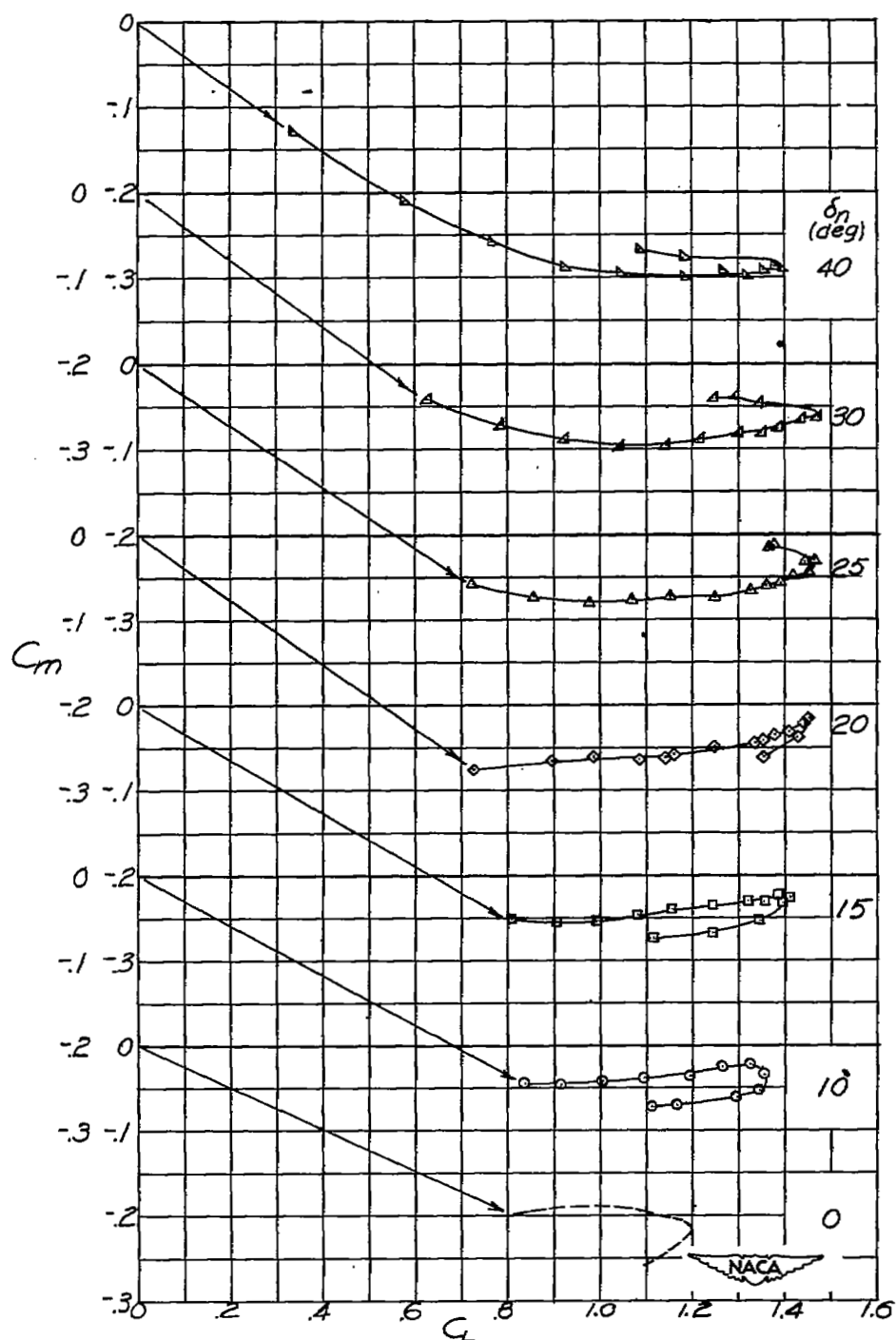
(b) Variation of C_m with C_L.

Figure 16.- Concluded.
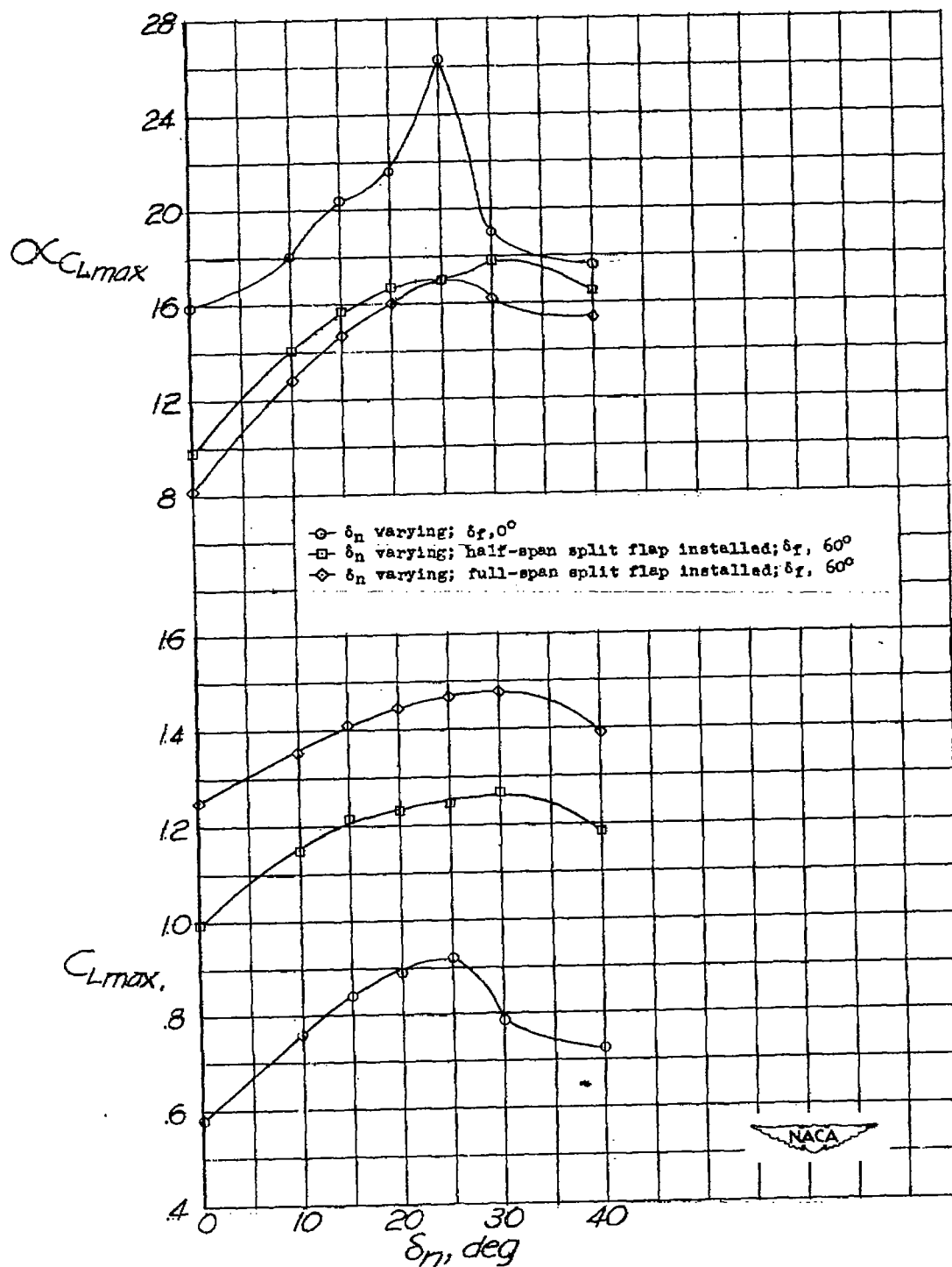
Figure 17.- Summary of maximum-lift results as affected by drooped-nose-flap deflection.
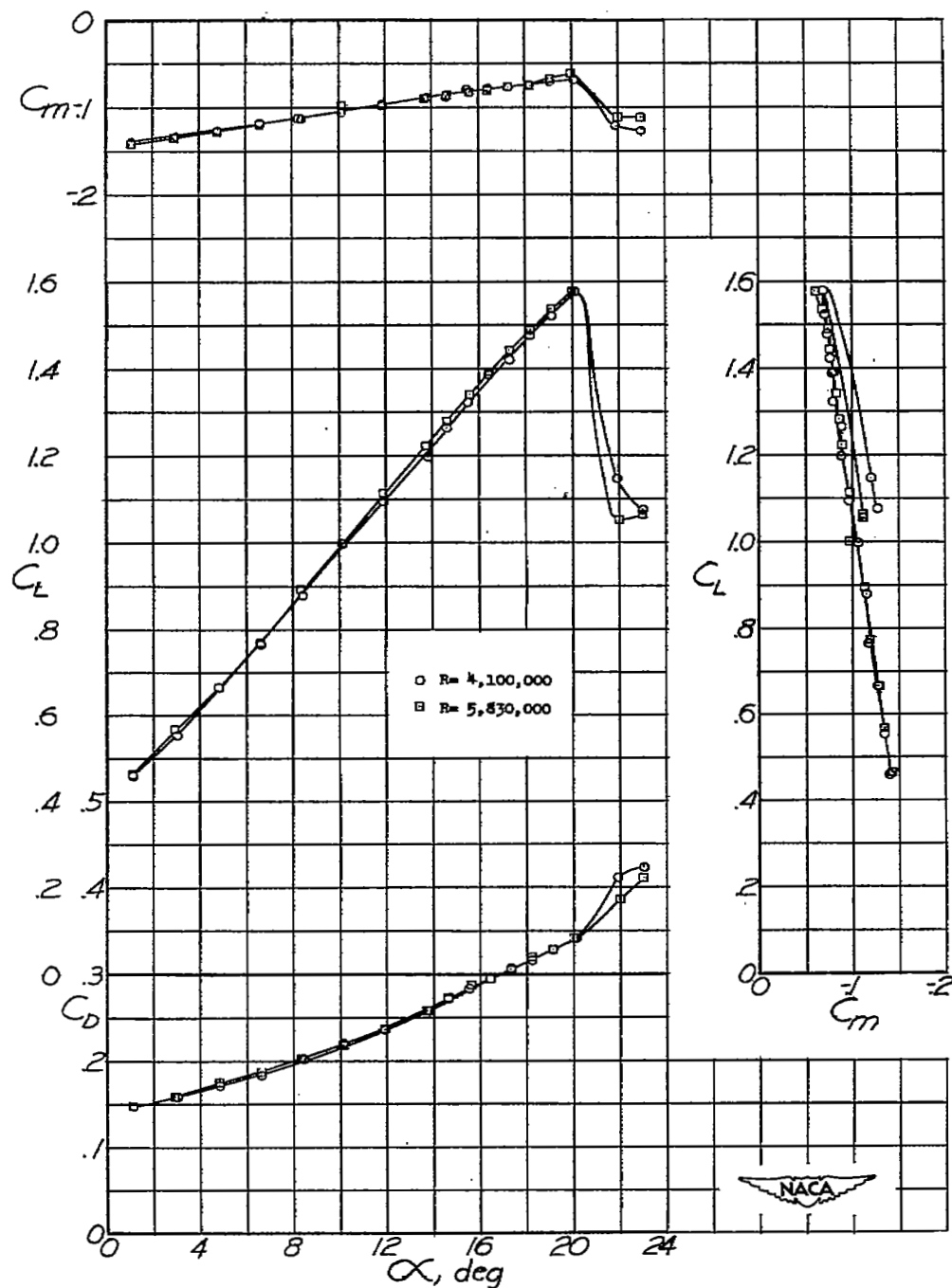
(a) Half-span rear flaps deflected 60°.

Figure 18.- Effect of Reynolds number on C_L, C_D, and C_m of wing
with extensible leading-edge flap installed in combination with split
flaps.
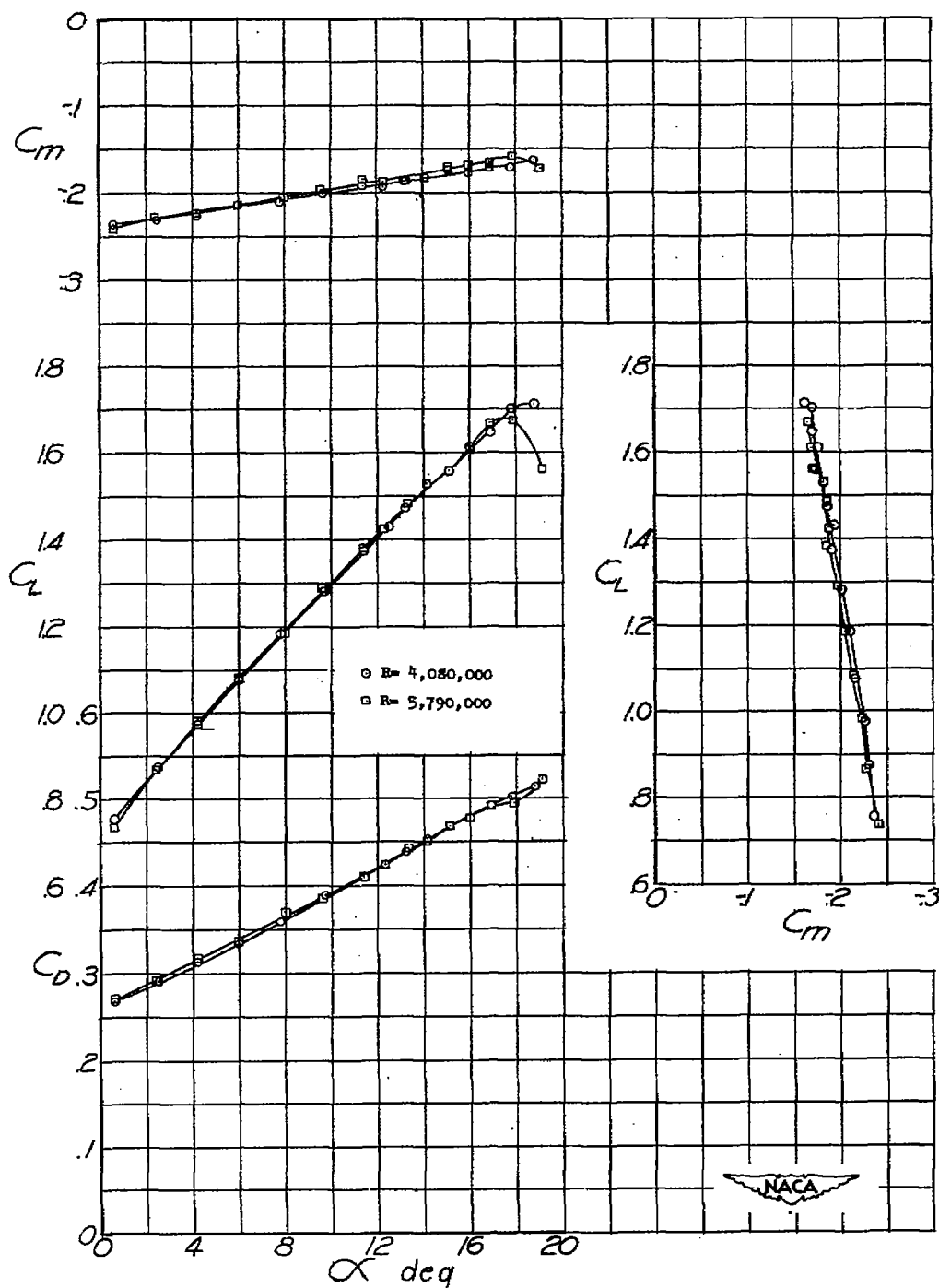
(b)   Full-span rear flaps deflected 60°.

Figure 18.- Concluded.
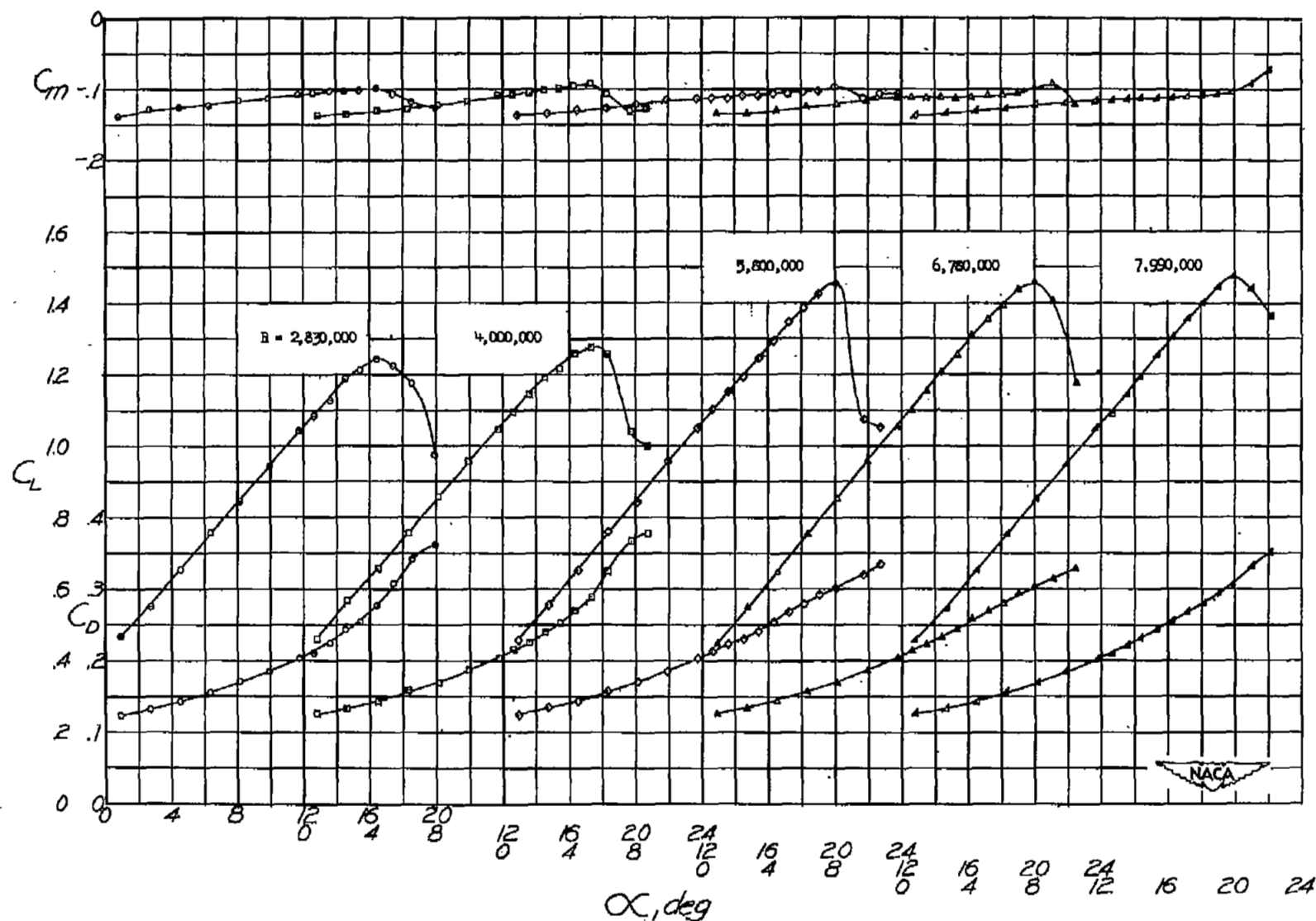
(a) Variation of C_L, C_D, and C_m with α.

Figure 19.- Effect of Reynolds number on C_L, C_D, and C_m of wing with 0.032c round leading edge installed in combination with half-span split flaps. $\delta_n = 10^\circ$; $\delta_f = 60^\circ$.
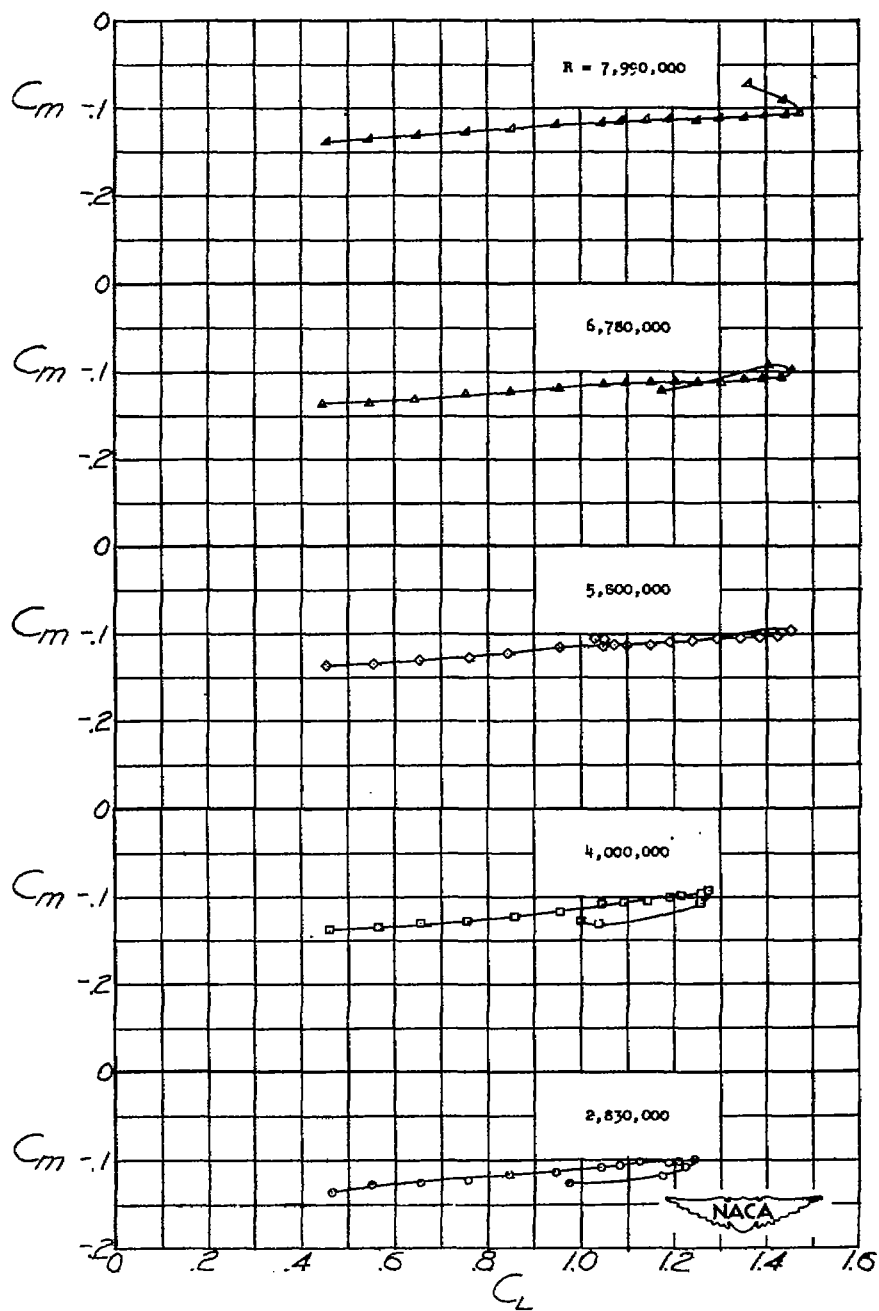
(b) Variation of C_m with C_L.

Figure 19.- Concluded.
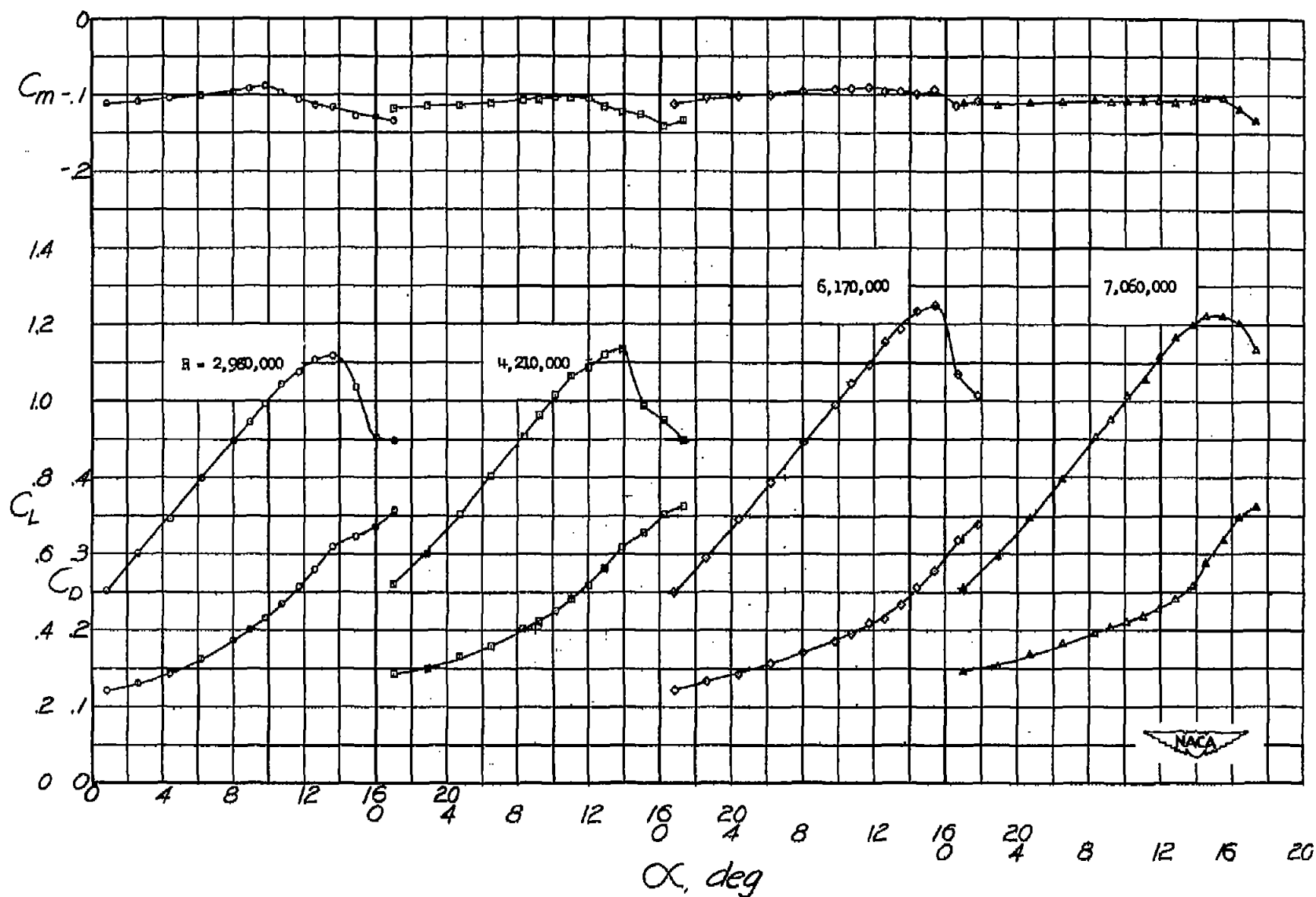
Figure 20.- Effect of Reynolds number on C_L, C_D, and C_m of wing with 0.032c round leading edge installed in combination with half-span split flaps. $\delta_n = 0^0$; $\delta_f = 60^0$.
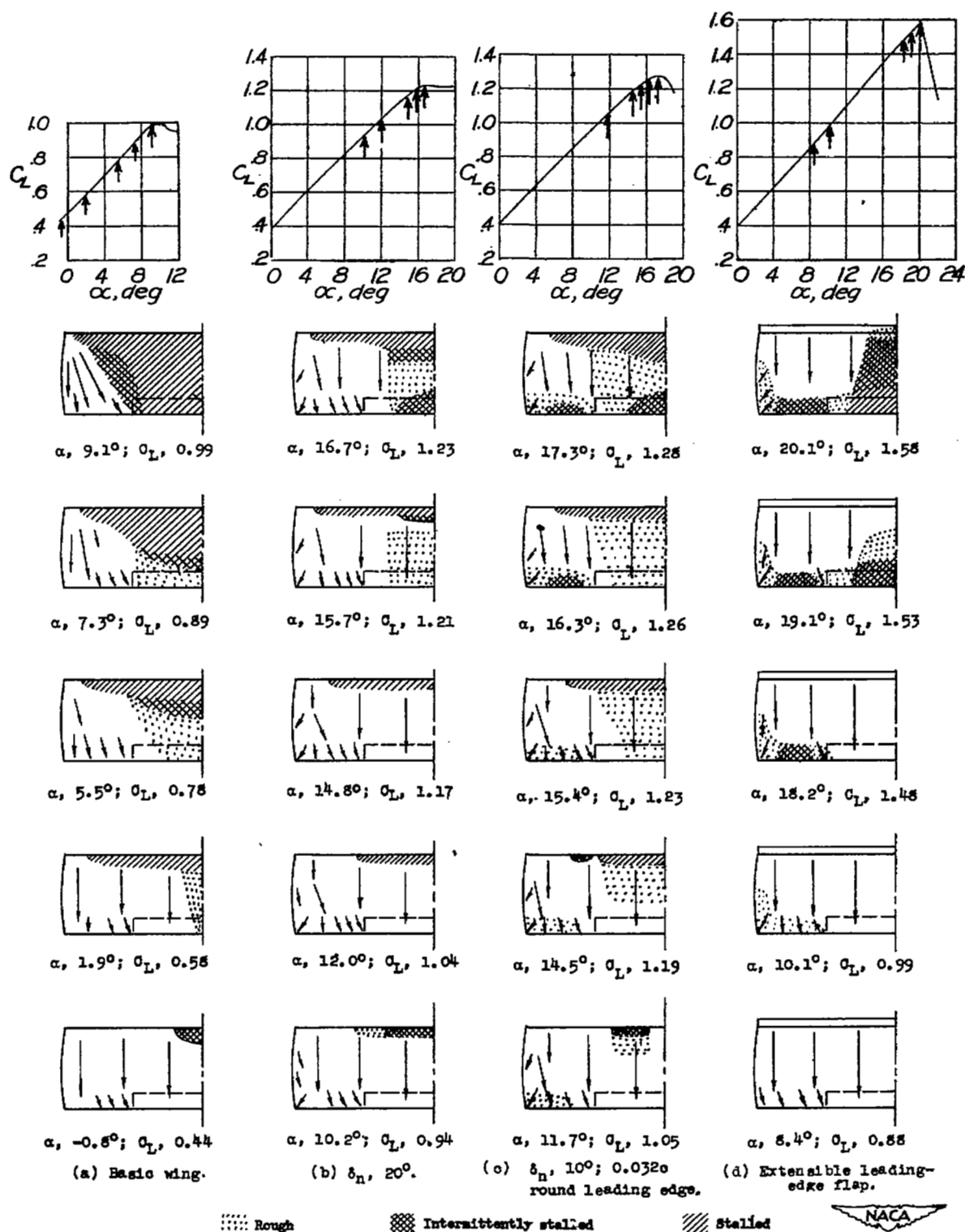
Figure 21.- Stalling characteristics of wing with half-span split flaps
  installed and of wing with several leading-edge high-lift devices in
  combination with half-span split flaps installed.   Arrows indicate
  direction of flow;   R ≈ 4.1 × 10^6; δ_f = 60°.
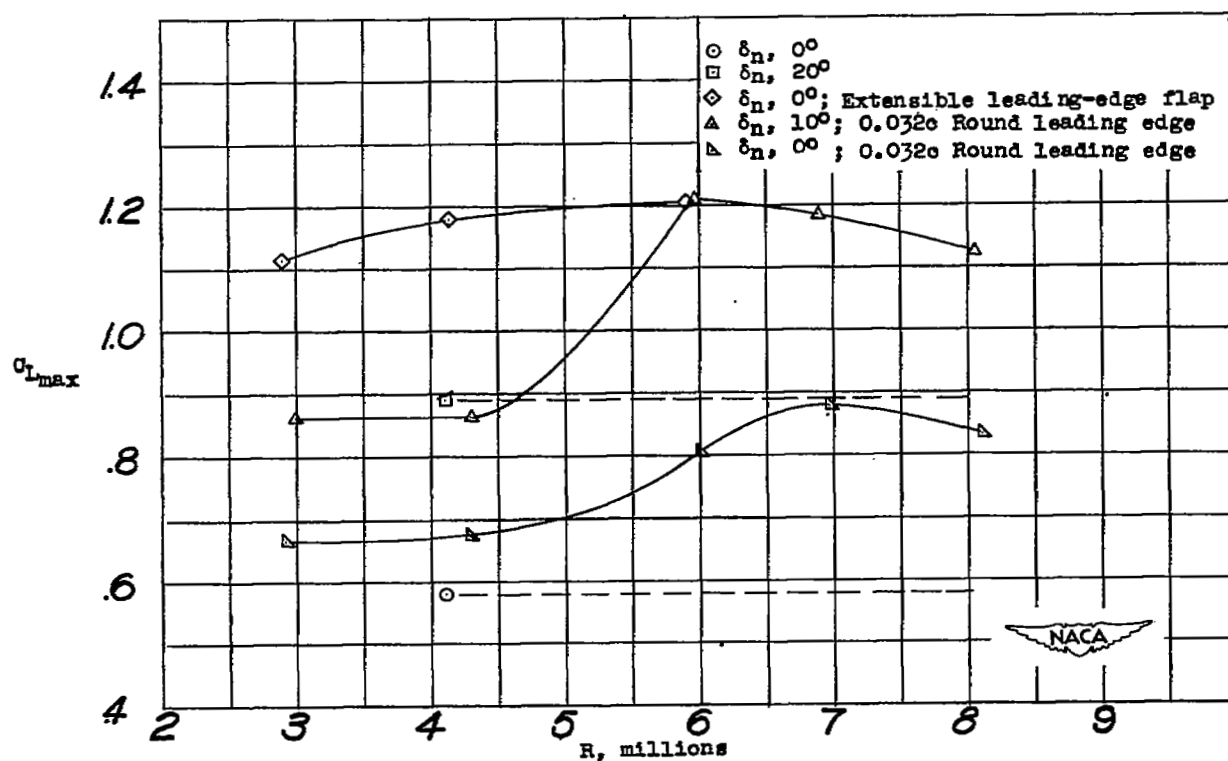
(a)   Split flaps removed.
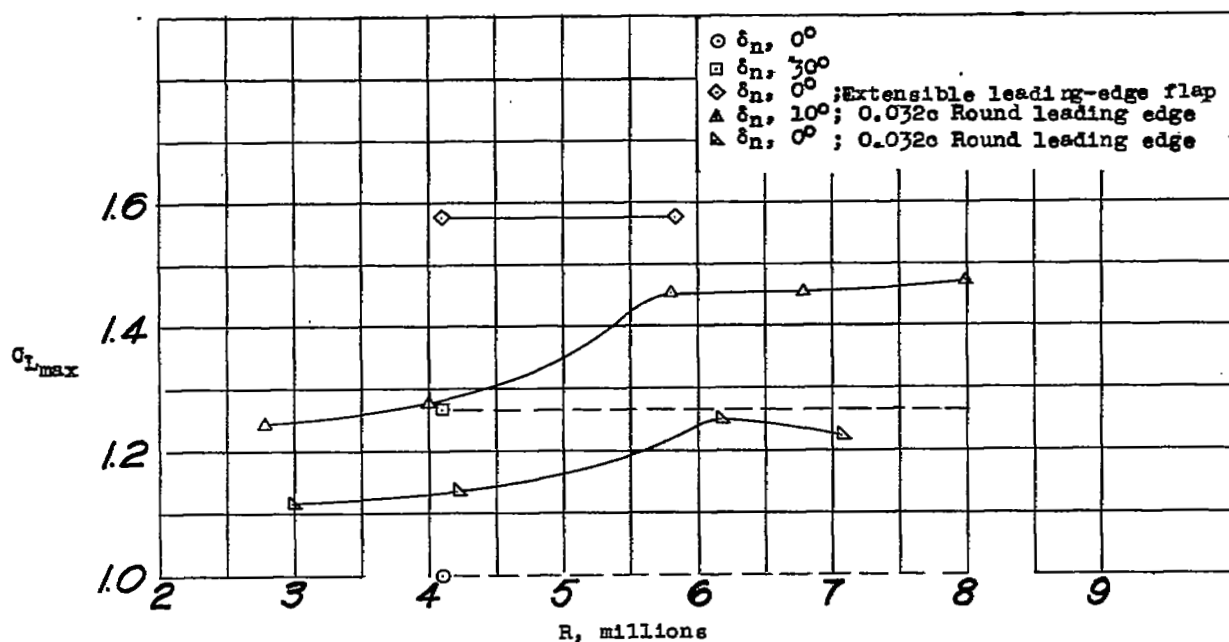
(b)   Half-span split flaps installed; $\delta_f = 60^\circ$.

Figure 22.-   Summary of maximum lift coefficients as affected by
Reynolds number.
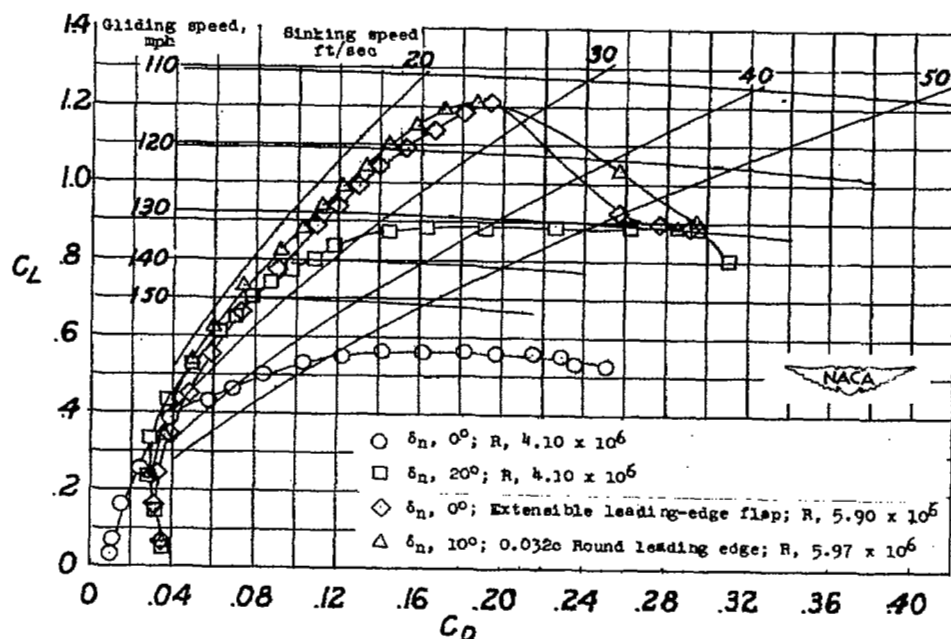
(a)   Split flaps removed.
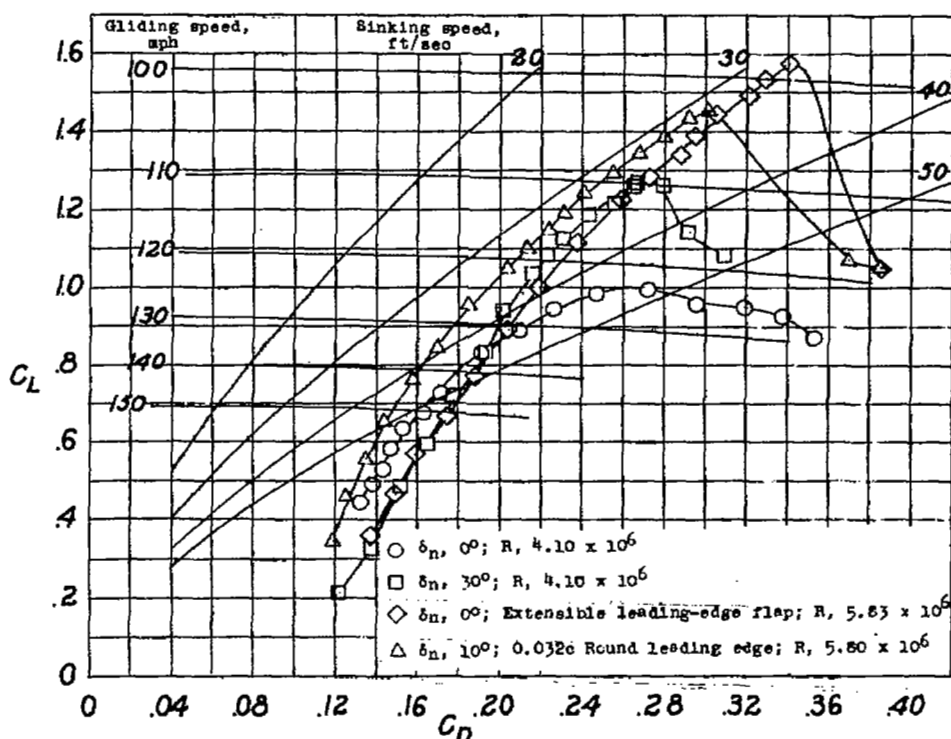
(b)   Half-span split flaps installed; $\delta_f = 60^{\circ}$.

Figure 23.-   Summary of landing-approach-speed characteristics of
rectangular wing. Wing loading, 40 lb/sq ft.
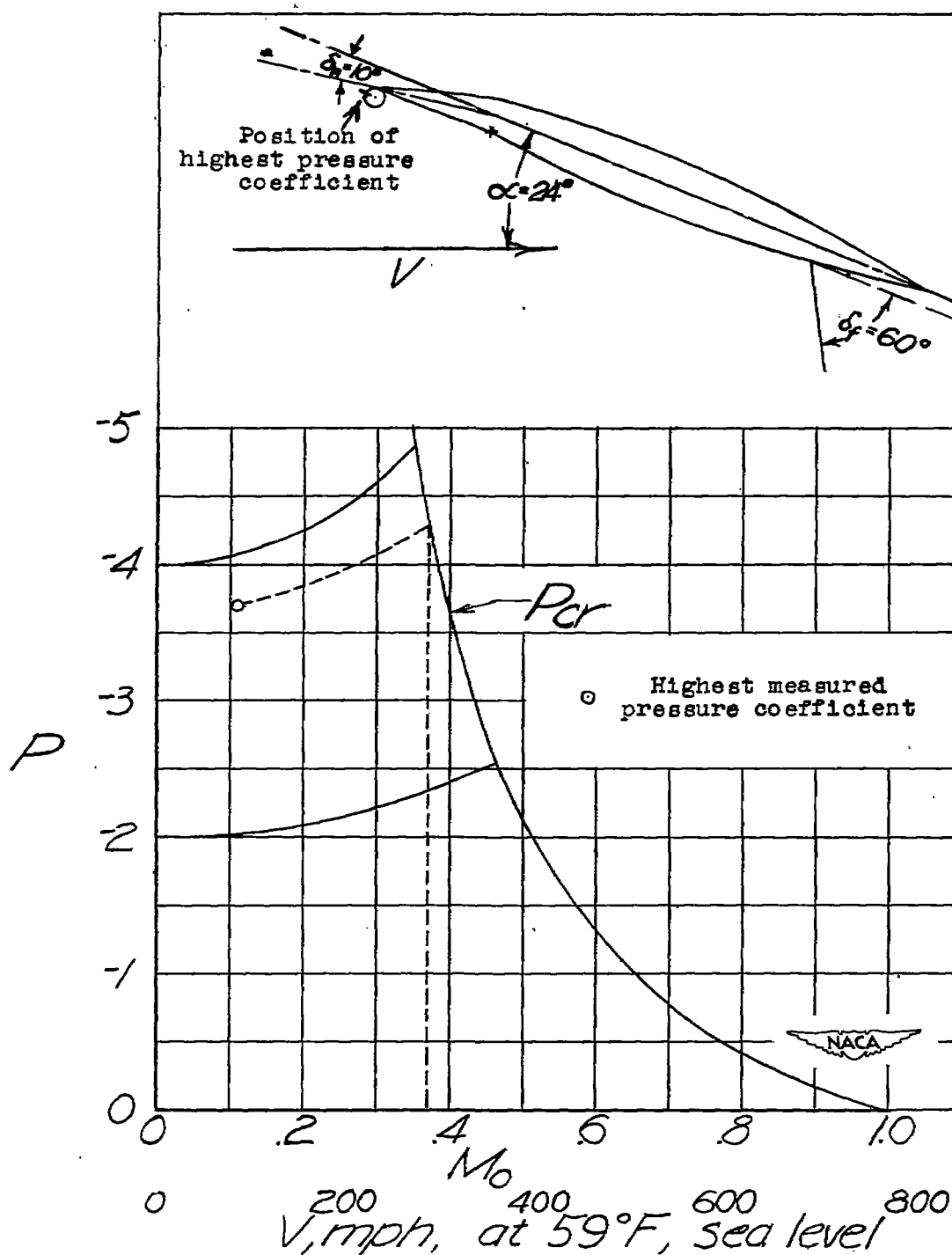
Figure 24.- Determination of critical Mach number of wing with 0.032c round leading edge and half-span split flaps installed. $\delta_n = 10^\circ$; $\delta_f = 60^\circ$.
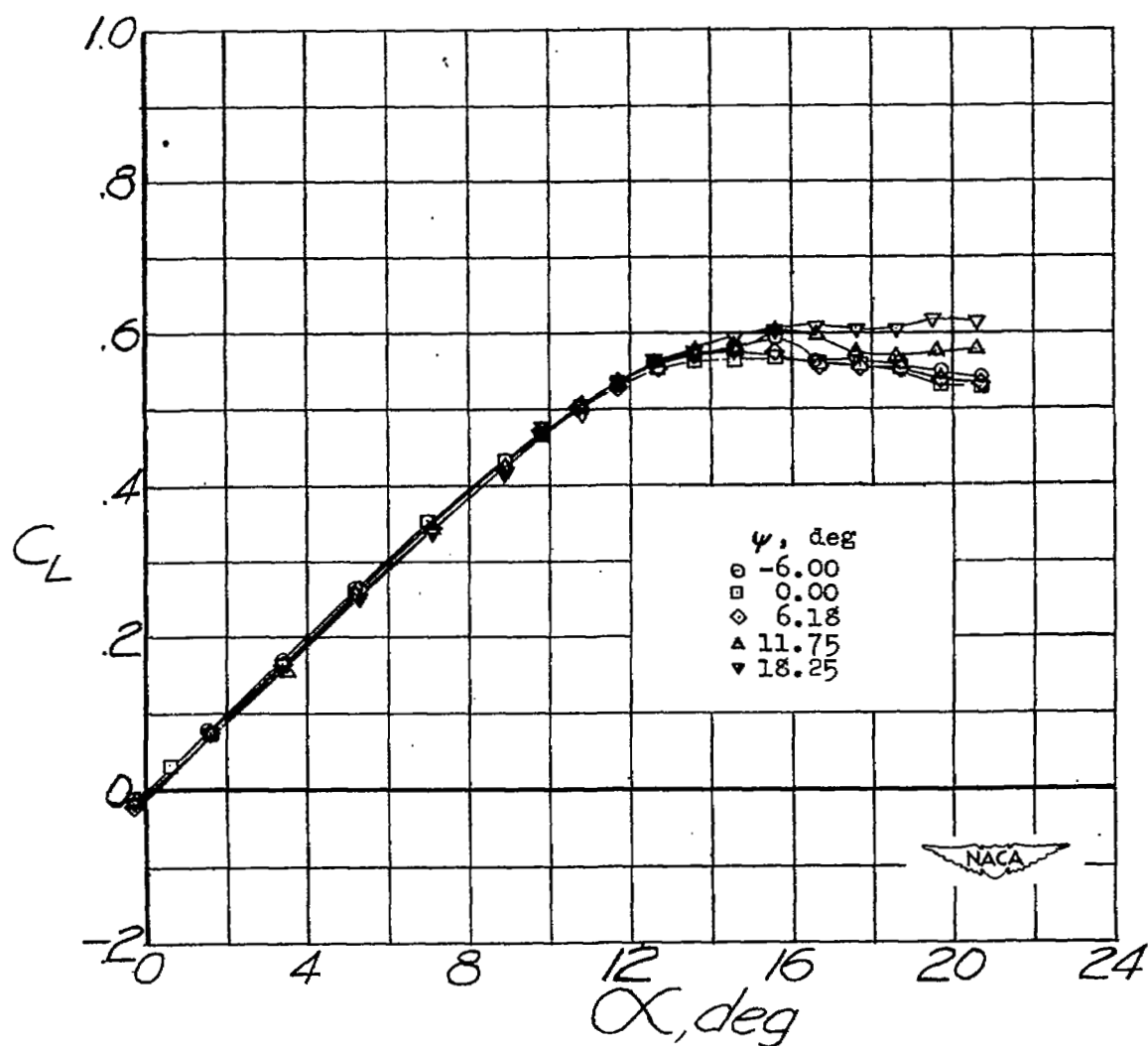
Figure 25.- Effect of yaw on the lift of the basic wing.
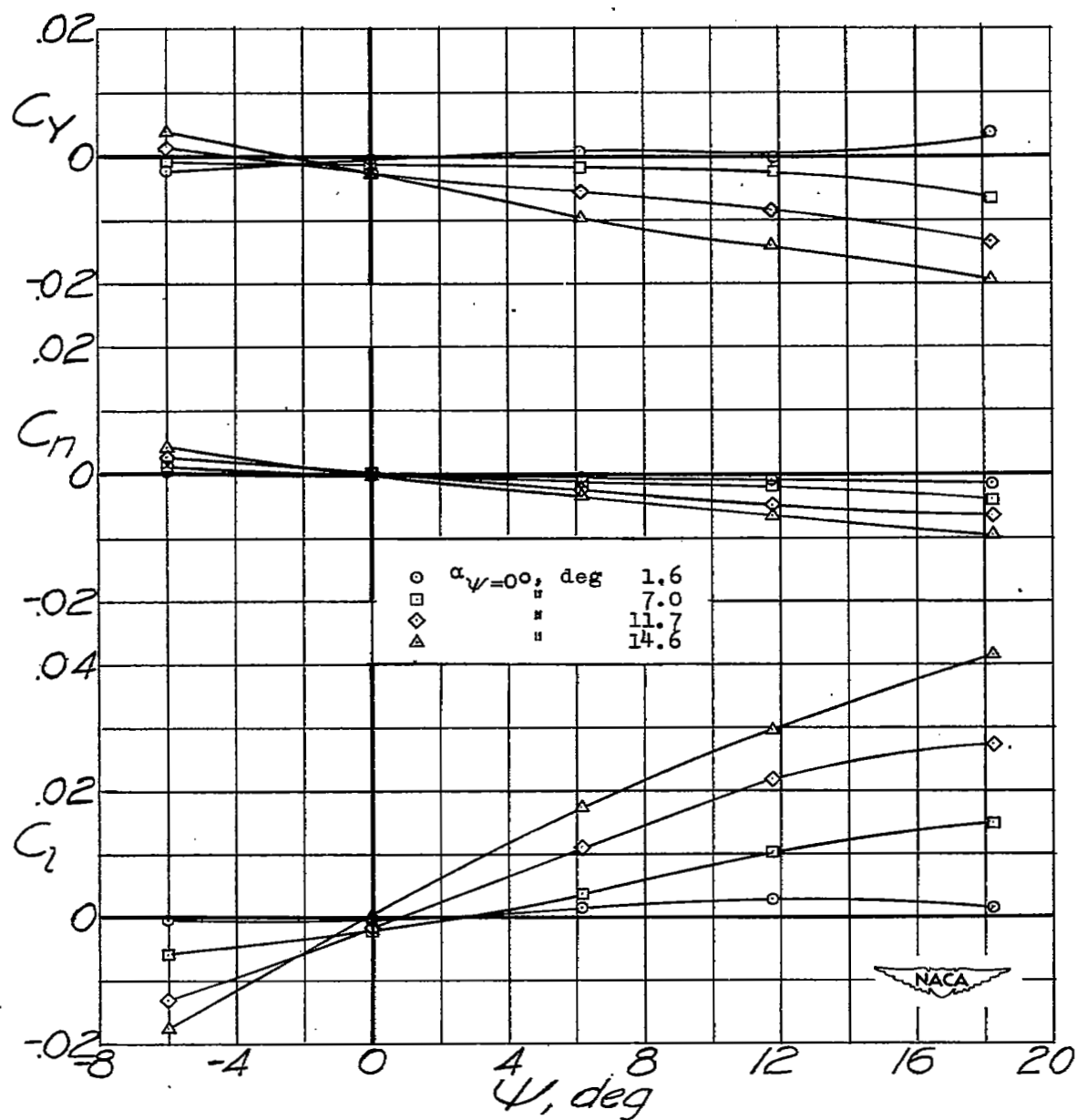
(a)   Basic wing.

Figure 26.-   Variation of C_l , C_n , and C_Y with ψ of wing for
several angles of attack.
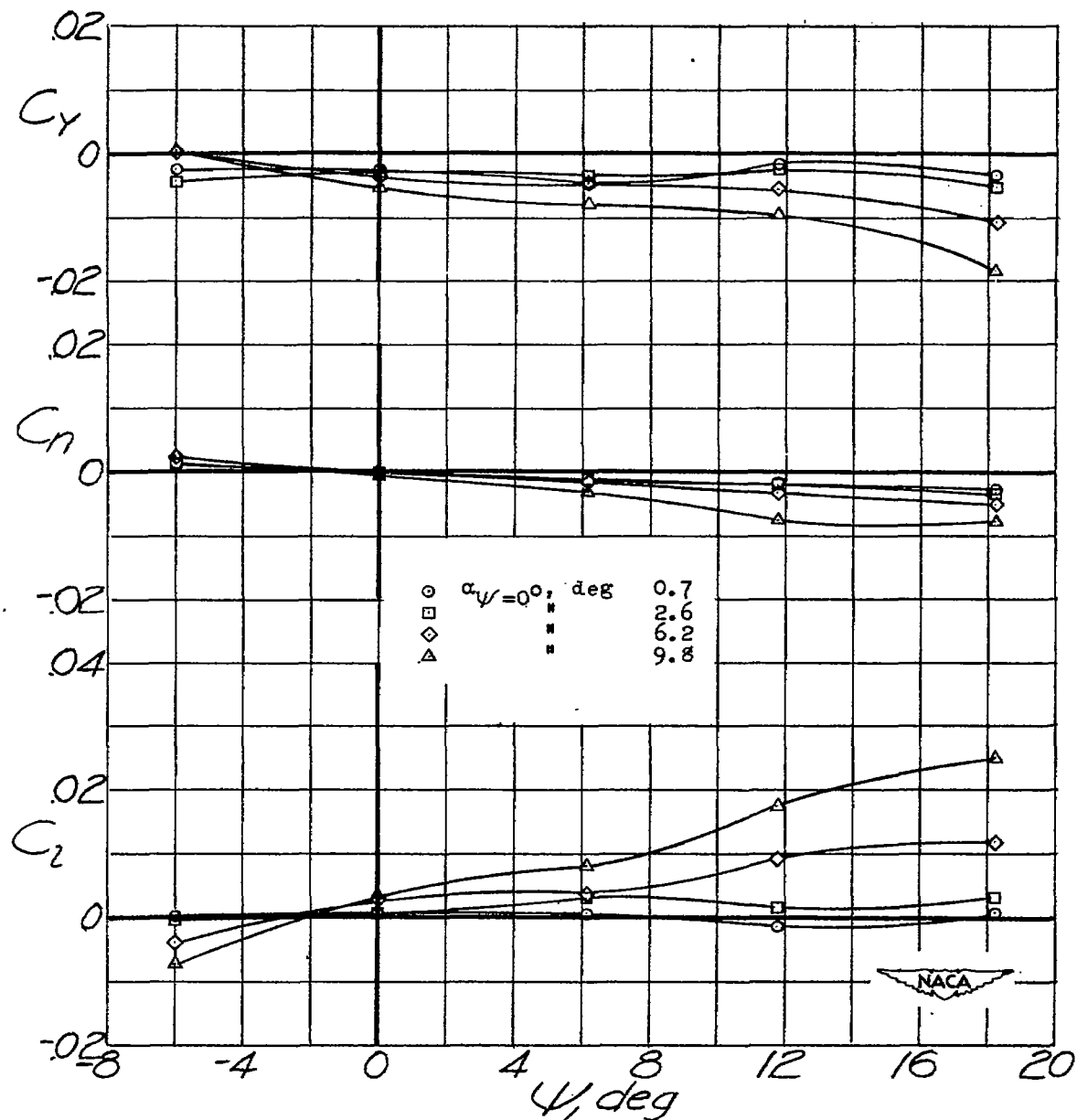
(b)   Half-span split flaps installed. $\delta_f = 60^0$.

Figure 26.- Continued.
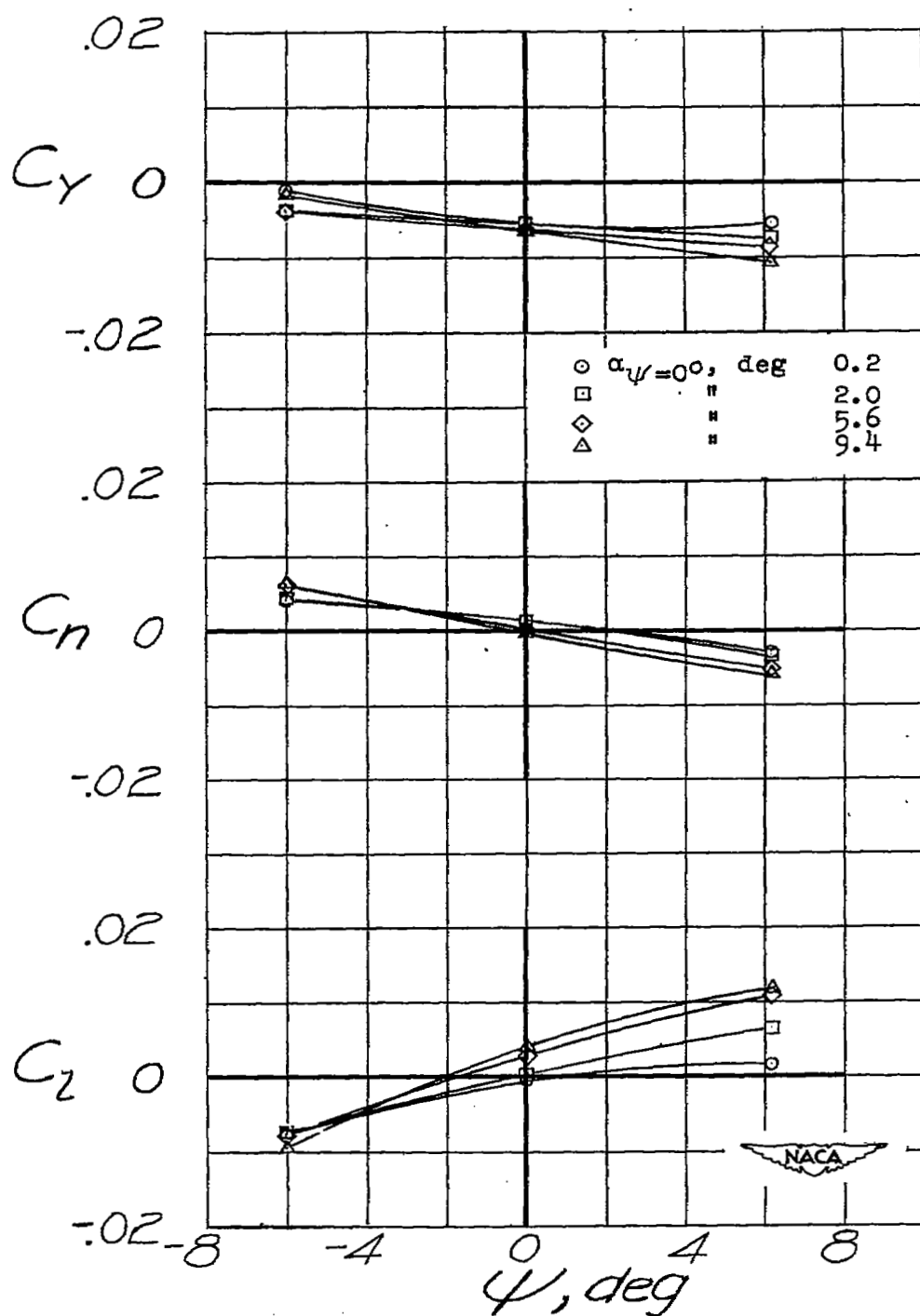
(c)   Full-span split flaps installed. $\delta_f = 60^\circ$.

Figure 26.-   Concluded.

(a) $\delta_n = 20^\circ$; $\delta_f = 0^\circ$.

(b) $\delta_n = 20^\circ$; $\delta_f = 60^\circ$.
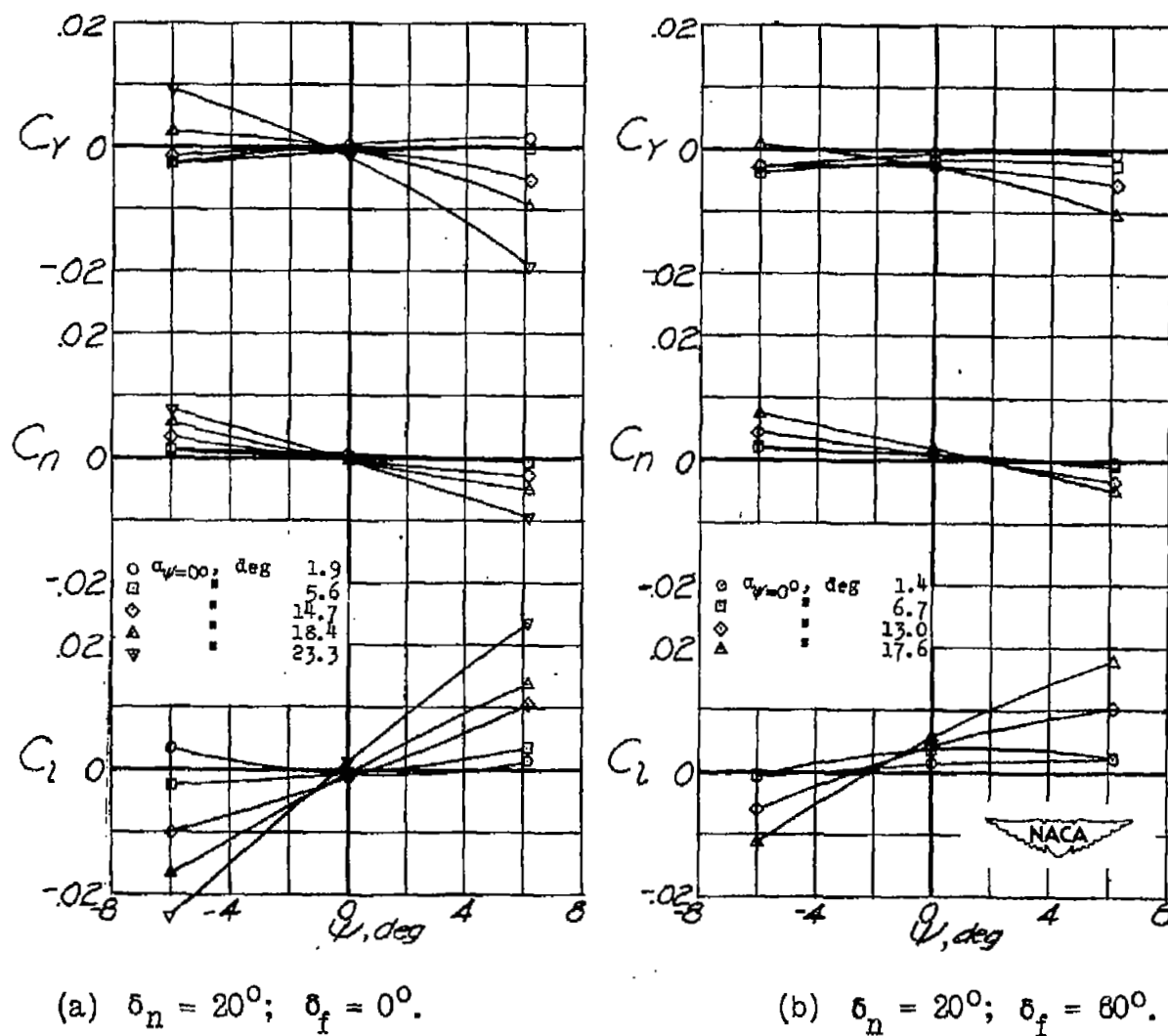
Figure 27.- Effect of half-span split-flap deflection on the variation of C_l, C_n, and C_Y of wing with drooped-nose flap deflected.
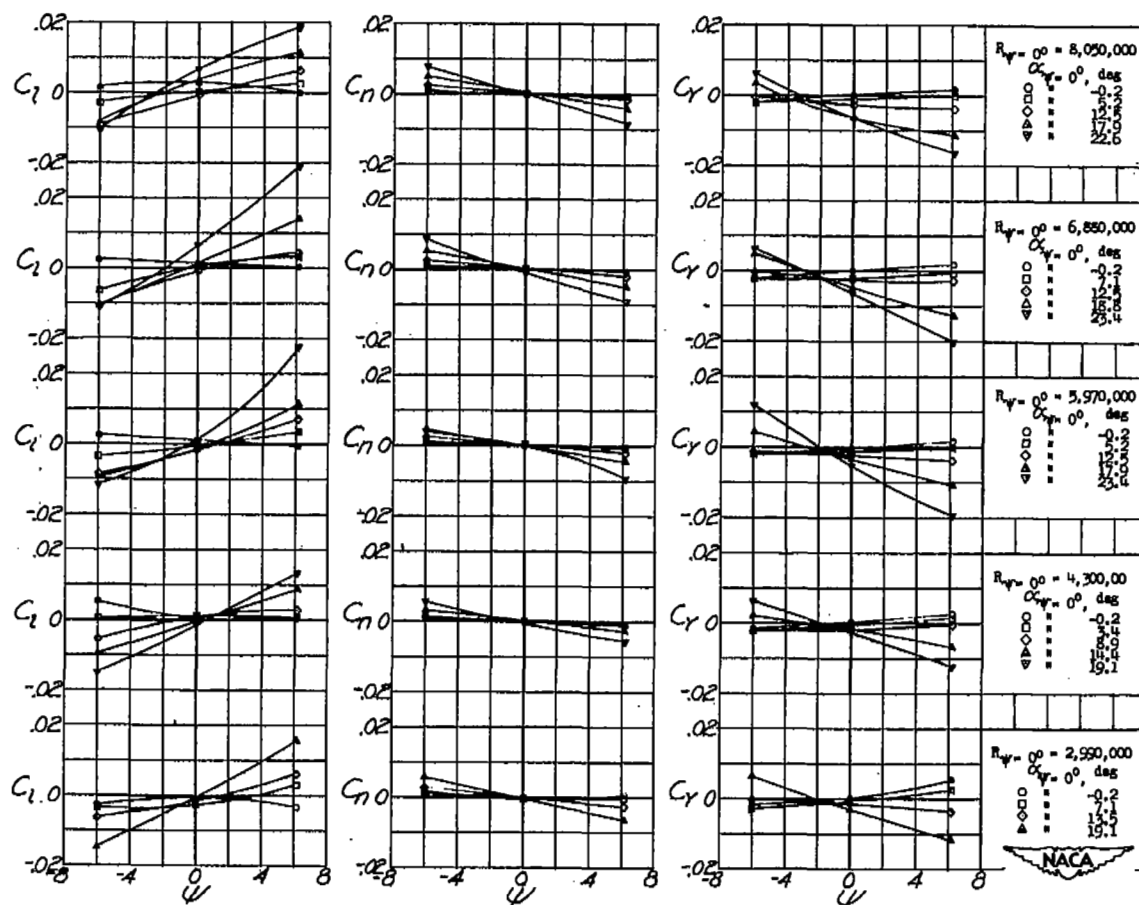
(a) Variation of C_l with ψ. (b) Variation of C_n with ψ. (c) Variation of C_Y with ψ.

Figure 28.- Effect of Reynolds number on the variation of C_l, C_n, and C_Y with ψ of wing with 0.032c round leading edge installed. $\delta_n = 10^0$; $\delta_f = 0^0$.
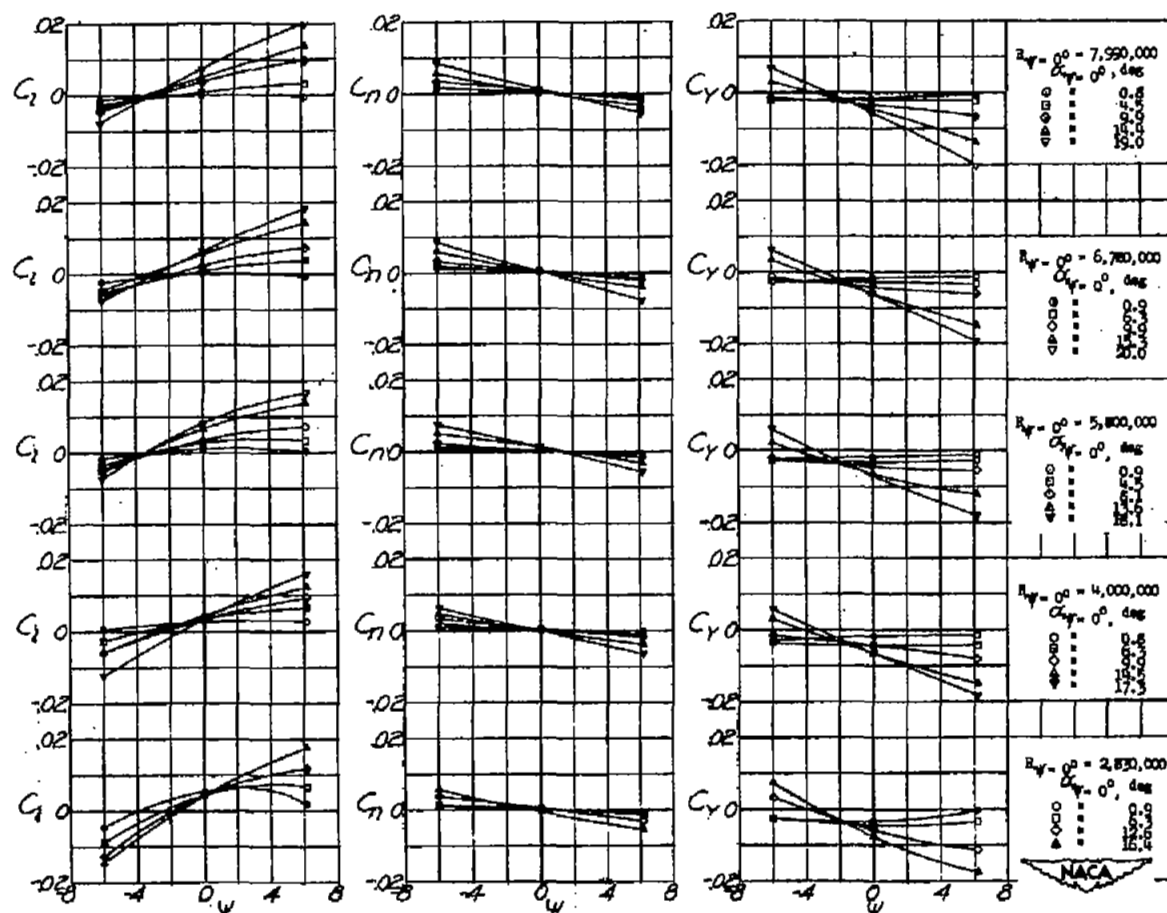
(a) Variation of C_l with ψ. (b) Variation of C_n with ψ. (c) Variation of C_Y with ψ.

Figure 29.- Effect of Reynolds number on the variation of C_l, C_n, and C_Y with ψ of wing with 0.032c round leading edge and half-span split flaps installed. $\delta_n = 10^0$; $\delta_f = 60^0$.

(a) $R_{\psi=0^{\circ}} = 2,890,000.$ (b) $R_{\psi=0^{\circ}} = 4,140,000.$ (c) $R_{\psi=0^{\circ}} = 5,900,000.$
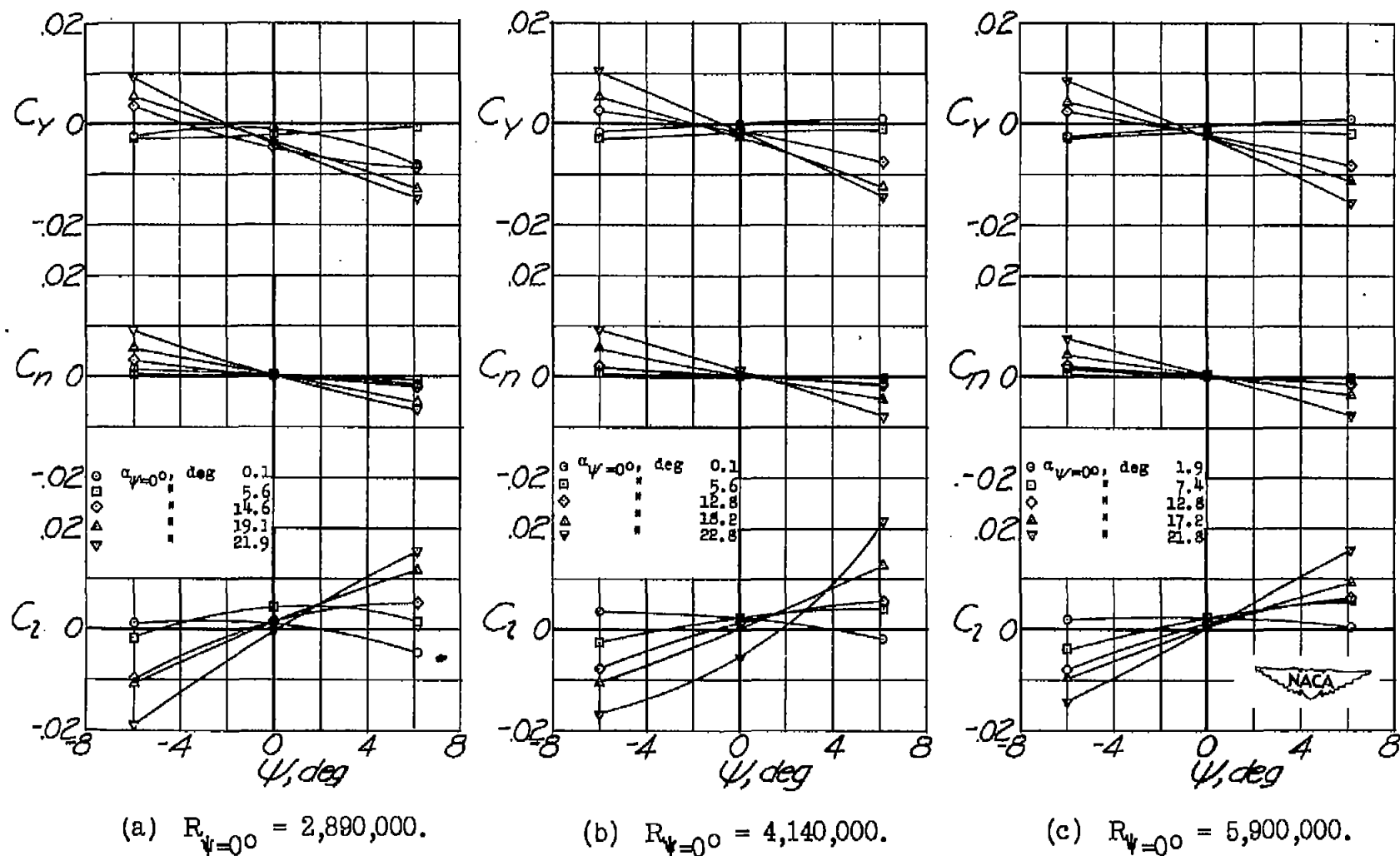
Figure 30.- Effect of Reynolds number on the variation of C_l, C_n, and C_Y with ψ of wing with extensible leading-edge flap installed. $\delta_f = 0^{\circ}$.
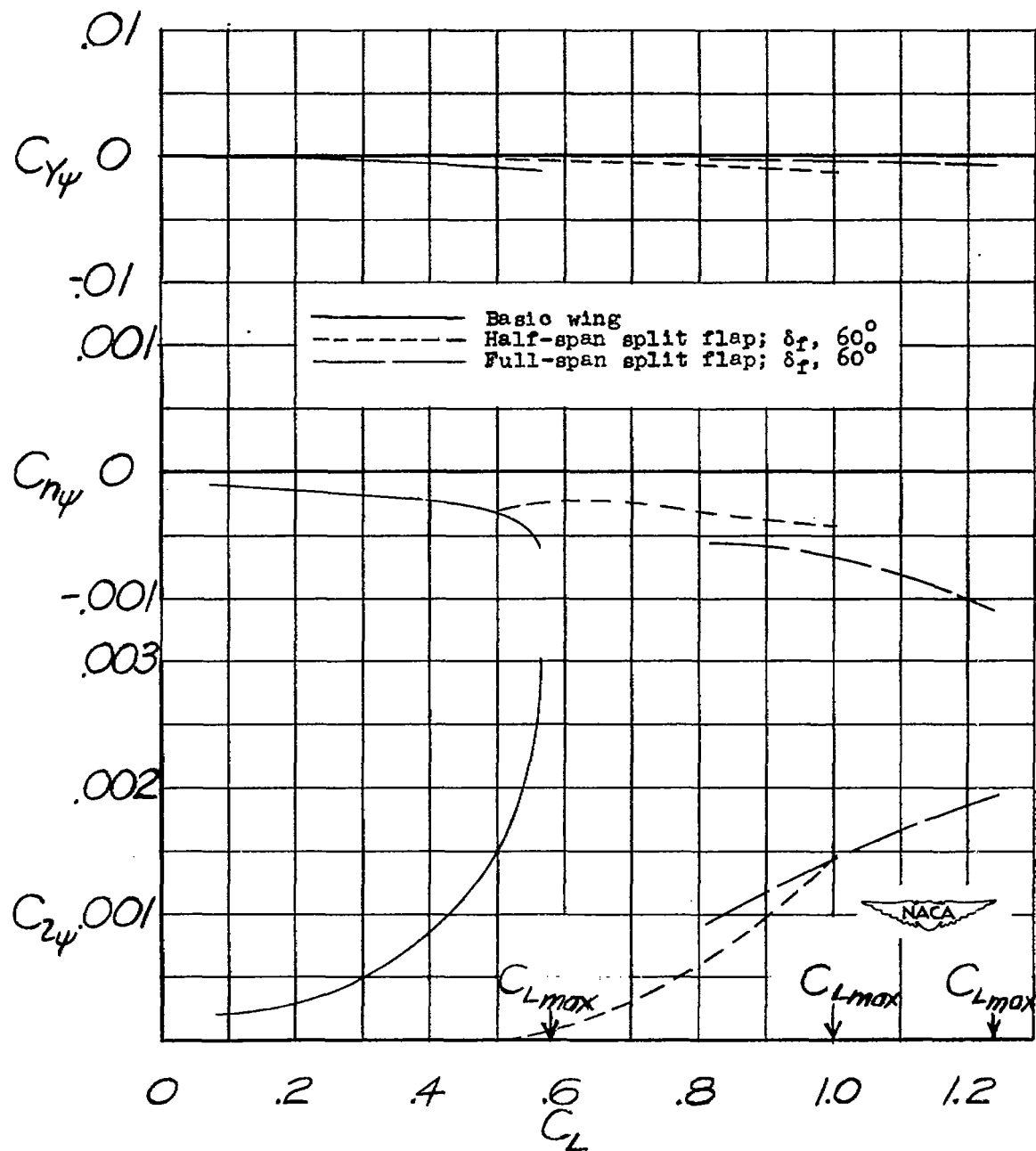
Figure 31.- Effect of split-flap deflection on the lateral characteristics
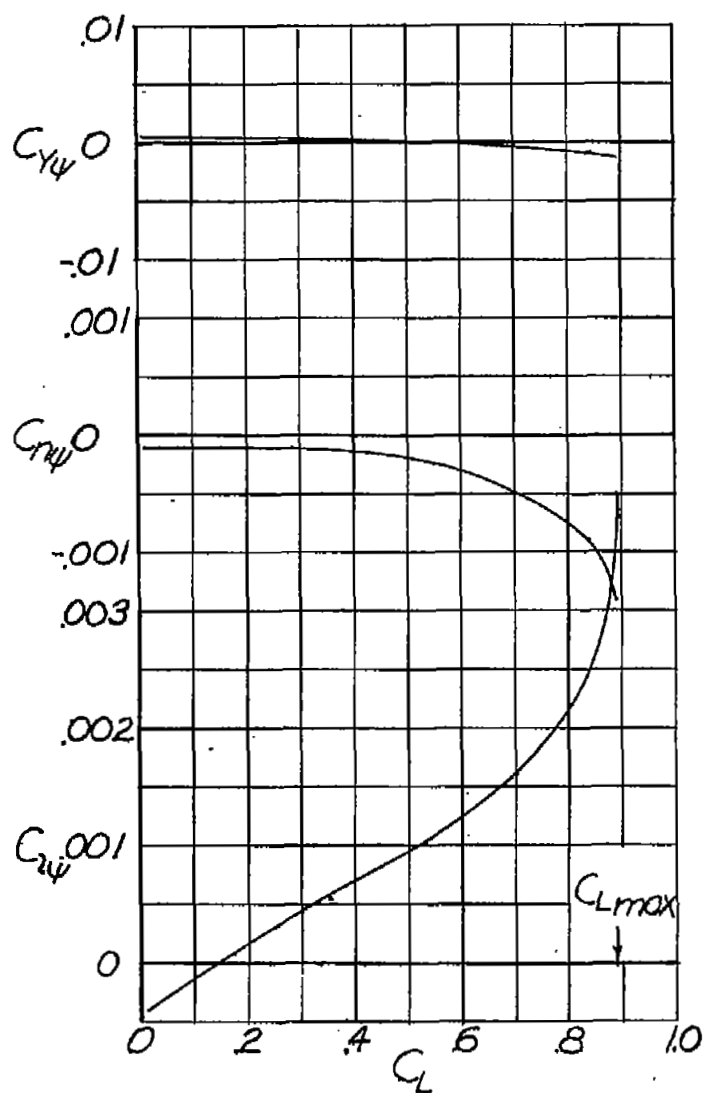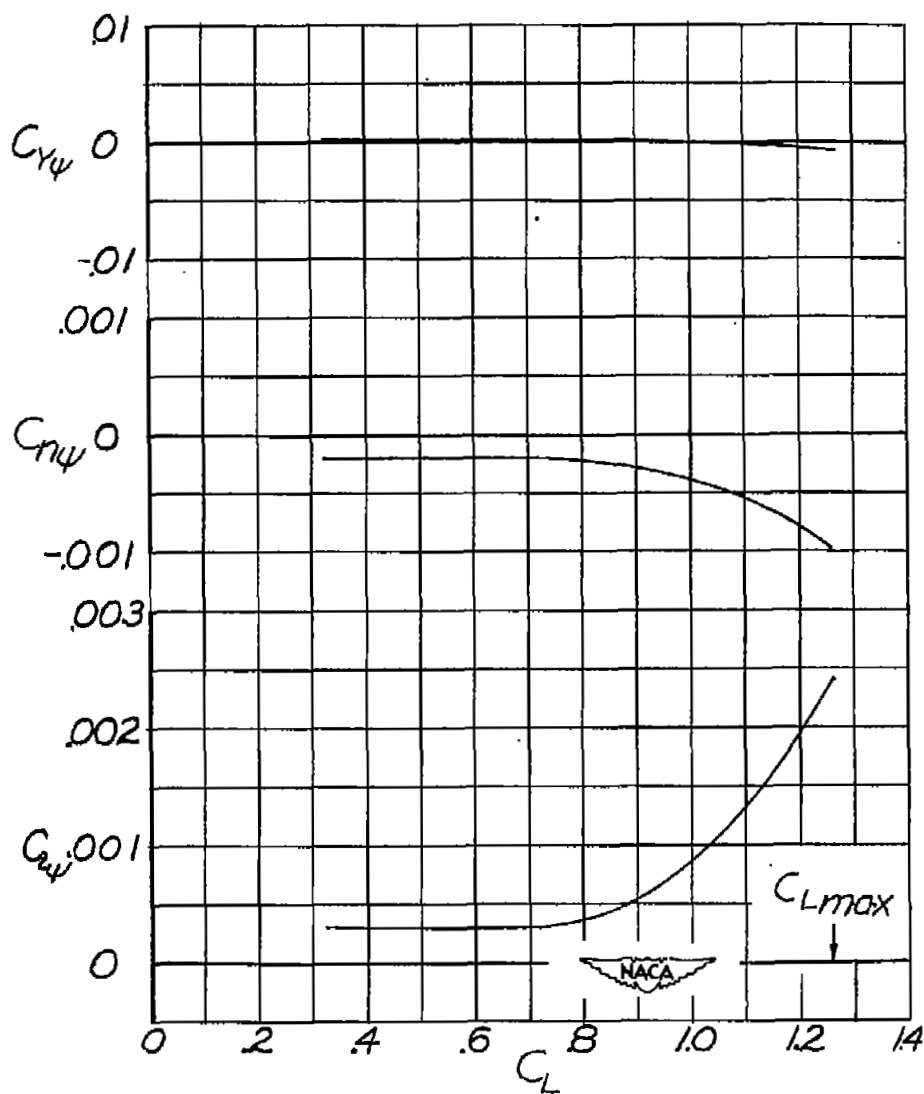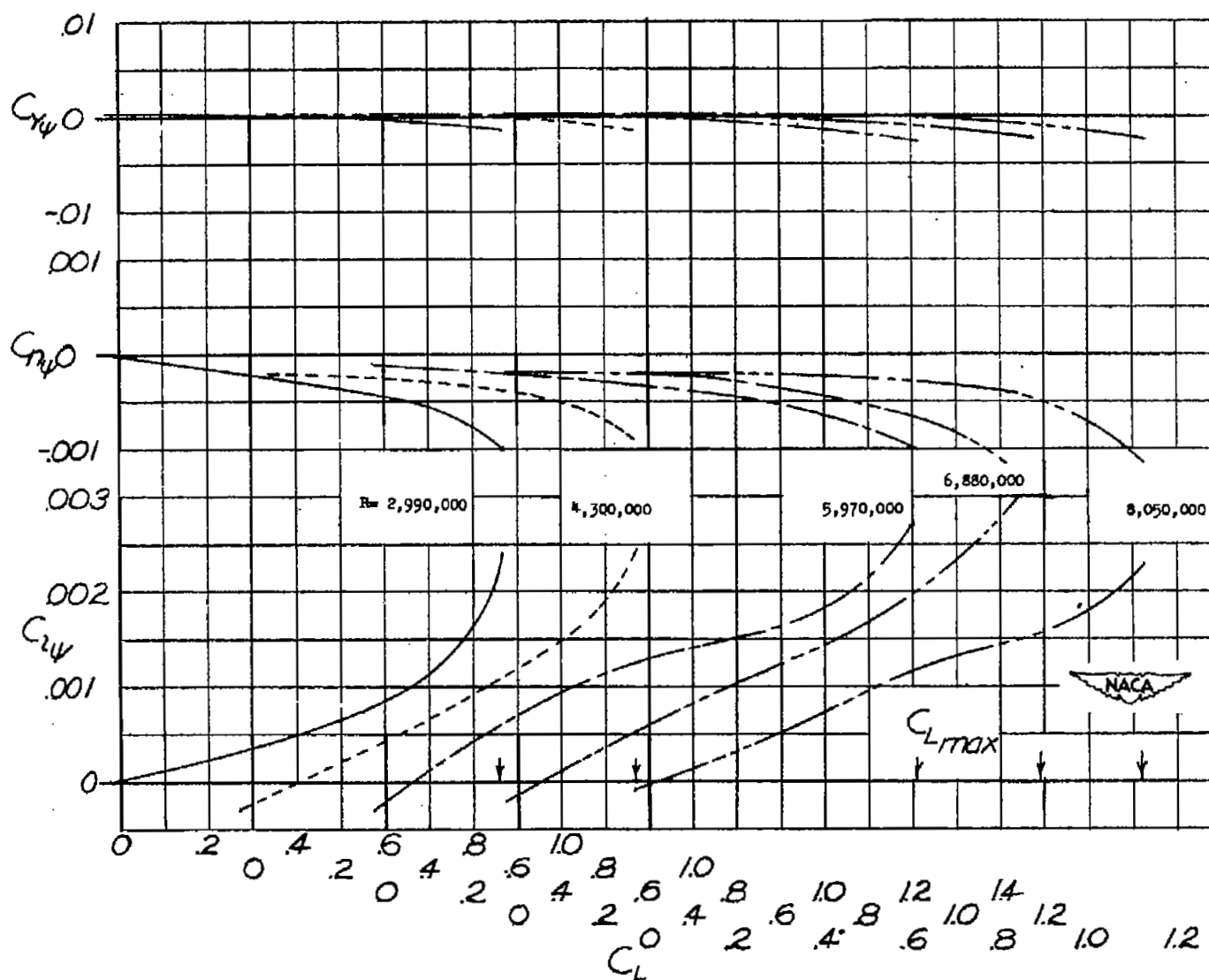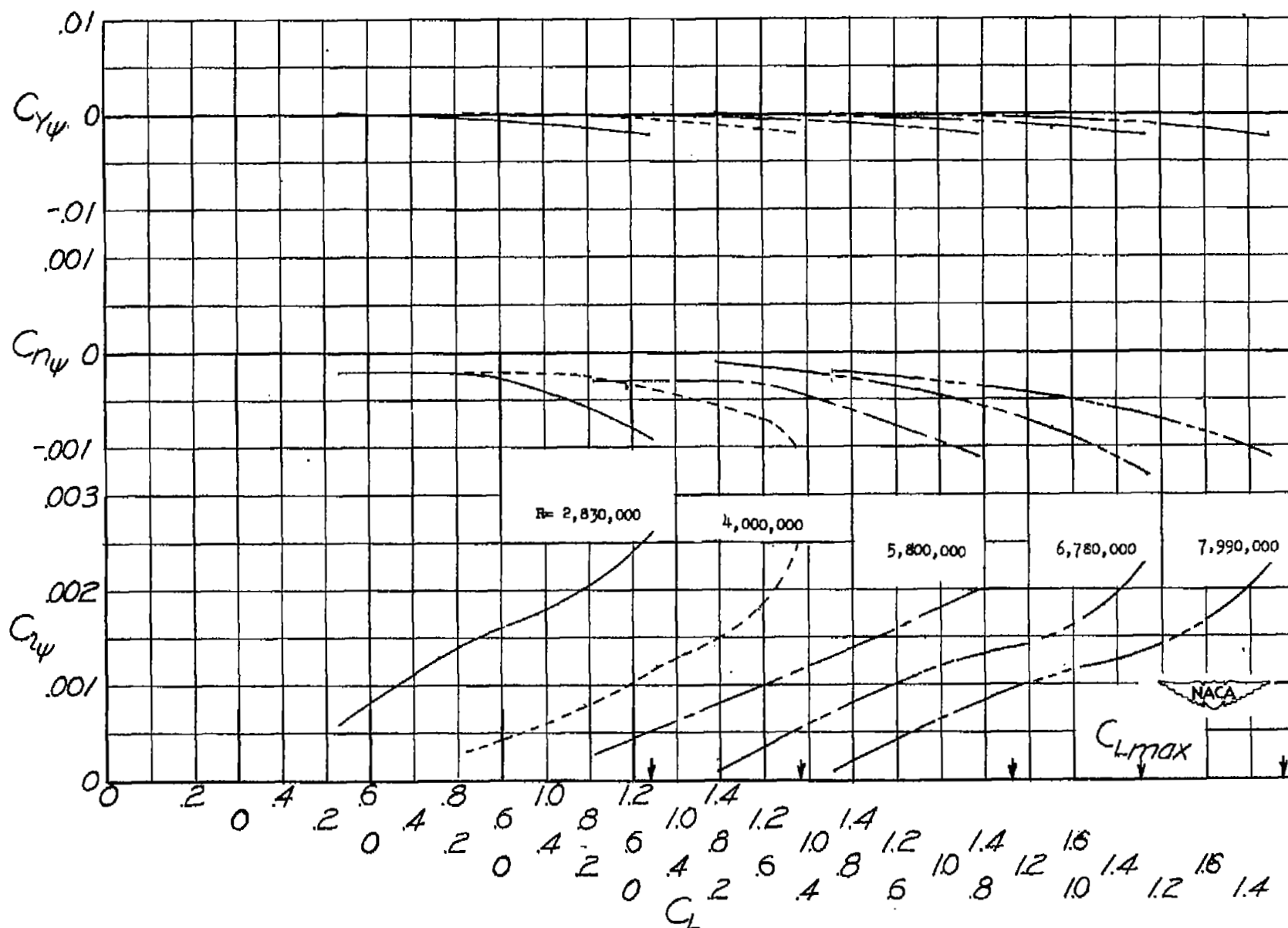of the wing. $\delta_n = 0^\circ$.

(a) $\delta_n = 20^0$; $\delta_f = 0^0$.

(b) $\delta_n = 30^0$; $\delta_f = 60^0$.

Figure 32.- Effect of half-span split-flap deflection on the lateral characteristics of the wing with the drooped-nose flap deflected.

(a) Split flaps removed.

Figure 33.- Effect of Reynolds number on the lateral characteristics of the wing with 0.032c round leading edge installed. $\delta_n = 10^o$.

(b) Half-span split flaps installed. $\delta_f = 60^o$.
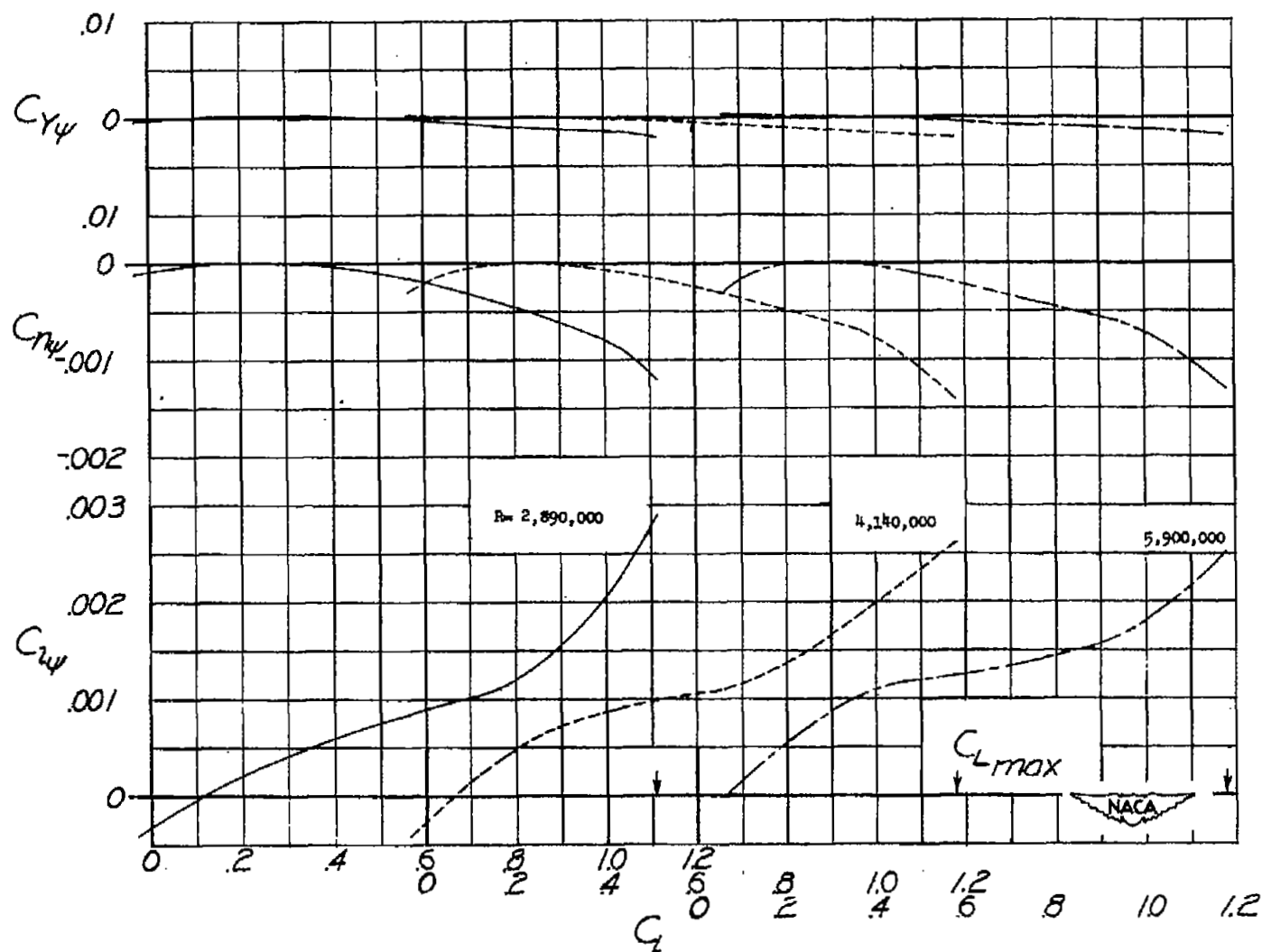
Figure 33.- Concluded.

Figure 34.- Effect of Reynolds number on the lateral characteristics of the wing with extensible leading-edge flap installed. $\delta_f = 0^\circ$.